Determining the wind drag coefficient in hydrodynamic modelling of a shallow, fetch-limited water system:

A case study in Friesland, The Netherlands

MSc Thesis
Stijn Overmeen
April 2021

Preface

Before you lies the Master's thesis "Determining the wind drag coefficient in hydrodynamic modelling of a shallow, fetch-limited water system: A case study in Friesland, The Netherlands". This document is written to fulfill the graduation requirements of the Civil Engineering and Management Program at the University of Twente. I was engaged in researching and writing this thesis from October 2020 to March 2021.

This project was undertaken at the request of Nelen & Schuurmans, where I was able to do an internship. This Master's thesis was formulated together with my supervisors from Nelen & Schuurmans, Nicolette Volp and Thomas Berends, and my supervisors from the University of Twente, Jord Warmink and Anouk Bomers. All of them were always available and willing to answer my questions.

Therefore, I would like to thank my supervisors for their guidance and support during this process. Furthermore, I would like to thank Nynke Vellinga and her colleagues from Wetterskip Fryslân for sharing their data and expertise with me.

I hope you enjoy your reading.

Stijn Overmeen

Utrecht, March 31, 2021

Summary

A well-known effect of high sustained winds from one direction is wind set-up. To accurately represent the wind effects on inland water systems by means of a hydrodynamic model is difficult, especially in fetch-limited water bodies. There is limited information available for practical applications under these conditions. The transmission of momentum between wind and water is generally formulated as a shear stress term, scaled with the wind drag coefficient. This study examined whether, and to what extent, the wind drag coefficient in a shallow, fetch-limited, inland water system varied spatially and/ or with the wind characteristics. Moreover, this study examined whether the wind drag coefficient should vary for these dependencies to improve hydrodynamic model predictions of water levels significantly.

The Frisian bosom, consisting of openly connected lakes through a dense system of canals, served as case study. Different historical wind events, classified based on their wind direction and wind speed, were simulated in the Frisian bosom by means of a 2D hydrodynamic model, which was set up with 3Di software. A calibration method was set up and used to optimize the wind drag coefficient, such that the simulated water levels matched the observations as closely as possible. For each wind class, an optimal wind drag coefficient was retrieved for the whole model domain, as well as for each measurement location separately. The results were analysed to find different wind drag dependencies. Moreover, the results were compared to a reference case to provide an indication of the significance of the improvement in terms of the model accuracy.

This study demonstrated relations between the location in the water system, the wind direction and the optimal wind drag coefficient. The local optimal drag coefficient values varied over the entire search interval of 0.8×10^{-3} to 2.05×10^{-3}. Overall, the drag coefficient was significantly lower at areas with greater fetch-limitations, due to the geometry of the water bodies in-line with the wind direction. These areas with smaller fetches allocated less momentum transmission between the wind and the water as wind shielding had a greater impact.

The overall accuracy of the model with a drag coefficient varying spatially, as well as per wind direction, improved compared to the reference model with approximately 0.18 in terms of the Kling-Gupta Efficiency (KGE), where 44% of the KGE potential was fulfilled. It was found that the model improvements were statistically significant. Based on these results there is good reason to believe that the wind set-up predictions of a hydrodynamic model on a shallow, fetch-limited water system will improve if a spatially and wind direction varying wind drag coefficient is included.

Follow-up research on the wind drag coefficient dependencies can be performed by implementing the opportunity to vary the wind drag coefficient in a hydrodynamic model. This can demonstrate the wind drag dependencies and model improvements explicitly. The results found in this study are approximations, as the wind drag coefficient was not varied spatially or during a simulation for different wind characteristics.

Samenvatting (Dutch: summary)

Hoge, aanhoudende windkrachten kunnen leiden tot windopzet: een verhoogde waterstand aan de benedenwindse zijde van een watersysteem. Het is gecompliceerd om dit effect nauwkeurig te simuleren in een hydrodynamisch model, met name in binnenwatersystemen met beperkte fetches (=strijklengtes). Er is weinig informatie beschikbaar over praktische toepassingen onder deze omstandigheden. De momentum-overdracht van de wind naar het water wordt over het algemeen geformuleerd als een schuifspanning, geschaald met de weerstandscoëfficiënt van de wind. Deze studie onderzocht of, en in welke mate, de weerstandscoëfficiënt binnen een ondiep, fetch-gelimiteerd binnenwatersysteem ruimtelijk varieerde en/ of varieerde met de wind karakteristieken. Bovendien is onderzocht of de modelvoorspelling van de waterstanden significant zouden verbeteren als de weerstandscoëfficiënt ruimtelijk en/of per windrichting zou kunnen variëren, vergeleken met een referentiemodel met een constante weerstandscoëfficiënt.

Het Friese boezemstelsel, bestaande uit meren verbonden door een uitgebreid stelsel van kanalen, diende als casestudy. Een 2D hydrodynamisch model van dit studiegebied is opgezet met 3Di software. Door middel van kalibratie op basis van de waterstanden zijn de optimale weerstandscoëfficiënten gevonden voor verschillende historische wind gebeurtenissen. Deze optimale weerstandscoëfficiënten zijn voor elke windklasse bepaald, op lokale punten in het stelsel, evenals voor de gehele boezem. Aan de hand van deze resultaten zijn de relaties geanalyseerd tussen de locatie, windrichting, windsnelheid en de waarde van de weerstandscoëfficiënt. Ook zijn de resultaten vergeleken met de resultaten van het referentiemodel.

Dit onderzoek demonstreerde verscheidende relaties tussen de locatie binnen het watersysteem, de windrichting en de optimale weerstandscoëfficiënt. Grote verschillen in lokale optimale weerstandscoëfficiënten werden geconstateerd, verspreid over het gehele zoekinterval van 0.8×10^{-3} tot 2.05×10^{-3}. Globaal gezien was de weerstandscoëfficiënt significant lager op locaties waar de fetch beperkt was, door de lokale geometrie in combinatie met de windrichting. Op locaties met kleinere fetches was de windafscherming relatief groter, waardoor de momentum-overdracht lager was.

De gemiddelde nauwkeurigheid van de modelvoorspellingen met een ruimtelijk en per windrichting variërende weerstandscoëfficiënt, vergeleken met het referentiemodel, verbeterde met 0.18 met betrekking tot de Kling-Gupta Efficiency, waarbij gemiddeld 44% van de potentiële verbetering werd benut. Verder werd aangetoond dat deze verbeteringen statisch significant zijn. Gebaseerd op deze resultaten wordt ingeschat dat de windopzet-voorspellingen van een hydrodynamisch model van een binnenwatersysteem significant kunnen verbeteren met een variërende weerstandscoëfficiënt. Vervolgonderzoek, waarin een variërende weerstandscoëfficiënt wordt opgenomen in het model, kan uitwijzen wat de exacte verbeteringen zijn. De resultaten van deze studie zijn een benadering, omdat een variërende weerstandscoëfficiënt niet daadwerkelijk toegepast is.

Contents

List of Figures

List of Tables

List of Acronyms

abl   atmospheric boundary layer

DEM   Digital Elevation Model

IDW   Inverse Distance Weighting

KGE   Kling-Gupta Efficiency

KNMI   Koninklijk Nederlands Meteorologisch Instituut

NSE   Nash Sutcliffe Efficiency

WMO   World Meteorological Organization

Chapter 1

Introduction

Wind. From strong breezes up to storms. From trees swaying in the wind to twigs breaking off. From having difficulties using an umbrella to waking up with the neighbours trampoline in your garden. Everybody is familiar with a strong wind event, and so are water managers from water boards. They are responsible to ensure both water safety, for their inhabitants, as water availability, for shipping. They control the water levels in lakes and canals, while the wind shearing over the water drags the water along to one side of their system. These water managers strongly benefit from an accurate prediction of the water level to optimally control barriers, sluices and pumping stations. Generally, hydrodynamic models are used for this forecast. Nevertheless, modelling the wind effect accurately on inland water systems is difficult, especially in fetch-limited systems. There is limited information available for practical applications under these conditions. This study was initiated to increase the scientific understanding of wind modelling on inland, fetch-limited water systems and the determination of the wind drag coefficient. Concretely, it was initiated to investigate if the wind drag coefficient depends on the wind characteristics (direction and speed) and on the location within a water system. The Frisian bosom (Dutch: boezem) served as a case study. This system consists of openly connected, shallow water bodies and the impact of strong winds on local water levels can be substantial.

The information gap in this theory is introduced in Section 1.1 and the scope in Section 1.2. The objective and the research questions of this thesis are defined based on the information gap and scope, and are provided in Sections 1.3 and 1.4.

Figure 1.1: Illustrative picture of the effects of strong wind (Zegerplas in Alphen (Media-TV, 2020))

1.1 Research gap

Limited information was available on the wind drag coefficient in hydrodynamic models of fetch-limited, inland water systems. The fetch is the length of the water body over which the wind can blow without obstruction. It was known that drag coefficients for different water bodies vary over a wide range. In previous modelling studies of large shallow lakes, the wind drag coefficient was determined based on empirical reference values, or was calibrated based on field data (Cheng et al., 2020). Nevertheless, the theory, which is explained in Chapter 2, suggests that wind drag coefficients vary spatially within a water system and/ or vary with wind direction and wind speed. However, if wind drag coefficients should vary for these dependencies to improve hydrodynamic model predictions of water levels was unknown.

1.2 Scope

This thesis focused on shallow, fetch-limited, inland water systems. Shallow refers to water depths up to 5 m, as defined by Abbasi et al. (2017). Moreover, in this thesis lakes with fetches of up to 10 km were considered. Of the Earth's total number of lakes, 99.9% have an area of less than 10 km^2 (Downing et al., 2006). For the majority of the Earth's lakes, wind shielding and limited wave fields are therefore frequent phenomena. Furthermore, only strong winds were relevant within the scope of this research, as these winds can generate significant set-up. Wind speeds are commonly divided in weak and strong at a threshold of 5 m/s, as stated by Markfort et al. (2010), Wuest and Lorke (2003) and Abbasi et al. (2017). At these water body characteristics and wind speeds, wind set-up and wind shielding are important processes.

1.3 Objective

The objective of this thesis was to determine to what extend the optimal wind drag coefficient in a hydrodynamic model varies spatially, with wind direction and/ or with wind speed on a shallow, fetch-limited water system. This was determined based on a case study analysis. Based on the variation in optimal drag coefficients and its estimated significance on the predicted water levels, an advise was provided. This advise revealed whether the wind set-up predictions of a hydrodynamic model are likely to improve if a drag coefficient is included that varies for any or multiple of its possible dependencies.

Figure 1.2: Lake Tjeukemeer in Fryslân (Barqo, 2018)

1.4 Research questions and hypothesis

The research questions are divided in a main question and several sub-questions.

1.4.1 Main question

Does the optimal wind drag coefficient in a hydrodynamic model vary spatially, with wind direction and/ or with wind speed in a shallow, fetch-limited water system to such an extend that if any or multiple of these dependencies would be integrated in the model, there is good probability that it would significantly improve water level predictions?

1.4.2 Sub-questions

The main question is divided into four sub-questions, which is the basis for reviewing and reflecting on the results in this report. The sub-questions are:

To what extend does the optimal wind drag coefficient in a hydrodynamic model vary spatially on a shallow, fetch-limited water system?

To what extend does the optimal wind drag coefficient in a hydrodynamic model vary with wind direction on a shallow, fetch-limited water system?

To what extend does the optimal wind drag coefficient in a hydrodynamic model vary with wind speed on a shallow, fetch-limited water system?

Is there good reason to believe that the wind set-up predictions of a hydrodynamic model in a shallow, fetch-limited water system will improve if a spatially varying, a wind direction varying and/ or a wind speed varying wind drag coefficient is included?

1.4.3 Hypothesis

It was hypothesised that the optimal wind drag coefficient in hydrodynamic models of inland water systems depends on the roughness of the water surface, the roughness of adjacent terrains and shielding by obstacles. It was hypothesised therefore, that this drag coefficient should vary spatially for better model predictions of water levels. Additionally, it was hypothesised that the wind direction is of significance for the optimal drag coefficient and can yield different optimal values per direction. Furthermore, it was hypothesised that the value of the wind drag coefficient depends on the wind speed, as the water surface becomes rougher with increasing wind speed due to ripple and wave development. It was hypothesised that these three dependencies represented by the wind drag coefficient are significant for accurate water level predictions and should be included in hydrodynamic models to improve water level predictions in future studies and practical applications.

Chapter 2

Theoretical background

This chapter is a general introduction to wind modelling and the wind drag coefficient. It provides the basic information needed to fully understand the hypothesis and later chapters. Section 2.1 explains the physics of the wind in the atmosphere and its interaction with water surfaces. Section 2.2 describes the matter in which the above physics can be modelled and introduces the wind drag coefficient, the main focus of this thesis.

2.1 Wind physics

2.1.1 Wind in the atmosphere

The vertical distribution of horizontal mean wind speeds is often approximated with a logarithmic profile. Close to the Earth's surface the wind is decelerated by friction and at the surface the wind is diminished completely. The atmospheric boundary layer (abl) is the layer where deceleration of the wind by surface friction occurs. The height of the abl is mainly determined by the temperature gradient in the lower atmosphere (stability) and the roughness of the surface. In windy conditions, at wind speeds of 5 m/s and higher, the roughness is most important (Verkaik, 2006). The roughness determines the rate at which the wind speed increases for increasing heights. The vertical wind profile assumed as a logarithmic profile can be computed with (Prandtl, 1935):

$$u_{wind}(z,t) = \frac{u^*}{\kappa} ln\left(\frac{z}{z_0}\right) \tag{2.1}$$

In which: u_{wind} is the wind speed in m/s at level z in m, u^* is the shear velocity in m/s, κ is the dimensionless von Kármán constant and z_0 is the roughness height in m. The roughness height z_0 depends on the local land use. The vertical wind speed profiles for different land uses are illustrated in Figure 2.1, as percentages of the wind speed above the abl. The surface roughness is represented by α in this figure (Recoskie et al., 2017), an exponent that depends on the type of roughness (Plate, 1971). The wind speed is usually measured at the standard reference height of 10 m, as recommended by the World Meteorological Organization (WMO). By combining this measurement and Equation 2.1, the wind speed at the water surface can be approximated.
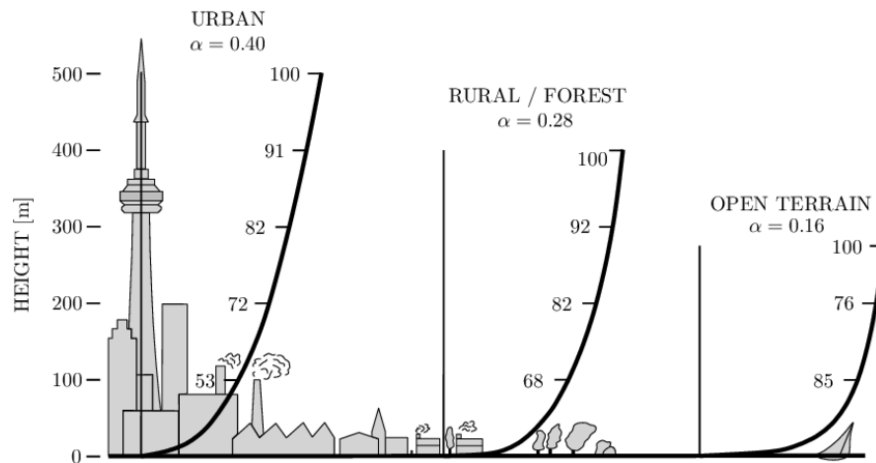
Figure 2.1: Percent gradient wind, surface roughness $\alpha[-]$ and abl height for different land uses (Recoskie et al., 2017)
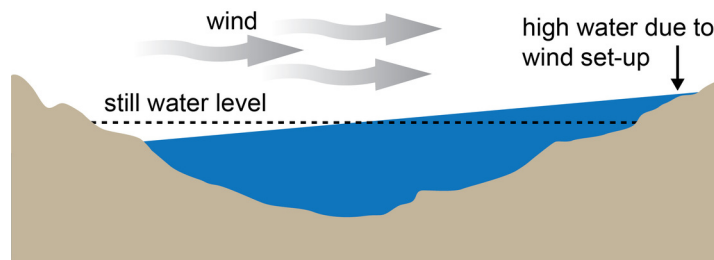
Figure 2.2: Illustration of wind set-up in a lake (Watershed council, 2019)

2.1.2 Wind on water: set-up

A well-known effect of high sustained winds from one direction, within inland water systems, is wind set-up (illustrated in Figure 2.2). Naturally forced displacements of water within an inland water system can be caused by pressure gradients, density gradients and wind stress. Wind stress is the most dominant type of forcing within pure, natural lakes (Lane, 2019). For this reason, the wind can have a major influence on local water levels and currents. Wind moving over the surface of a water body causes a shearing stress which results in a momentum transmission between the wind and the water surface. This momentum generates surface waves, currents and associated turbulence (Liu et al., 2018). Under high sustained winds from one direction the water level in a water body can tilt. The water level is pushed up at one end and consequently drops at the opposite end. Wind set-up is referred to as the positive deviation in the water level, and wind set-down to the negative deviation (van Rinsum, 2015).

The momentum transmission between the wind and the water surface is a complex process that occurs on small scales relative to many practical applications. An example is computing the wind-induced set up in a lake. The impact of wind on water levels and flow velocities can be explained by the force balance of a liquid particle. The pressure gradient is a force that works on the entire volume, whereas the friction and the wind forces work on the surface (Figure 2.3). This indicates that the wind has more impact on a thin layer of water than a deep layer of water. So, the magnitude of the set-up depends upon the dimension of the water body, as well as upon the strength and duration of the forcing mechanism (Lane, 2019). For higher wind speeds, greater fetch lengths and shallower water bodies the wind set-up is higher.
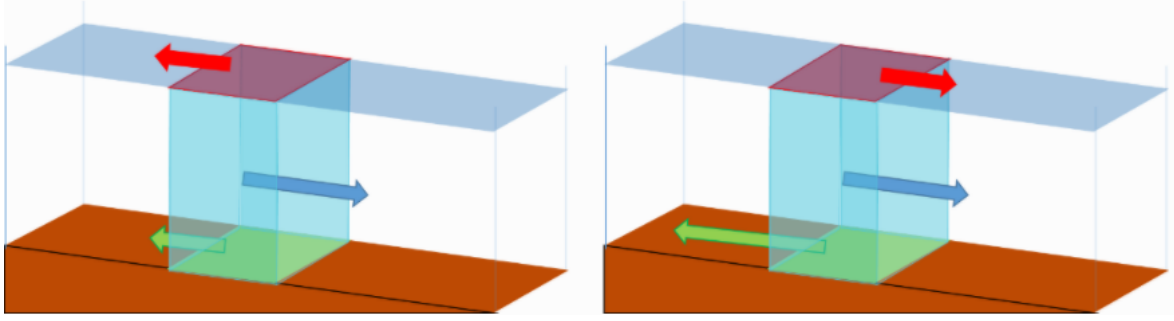
Figure 2.3: Force balance with **pressure gradient**, **friction** and **wind** (Nelen & Schuurmans, 2020)

2.2   Wind modelling

2.2.1   Wind on water: modelling

Water levels are predicted by means of hydrodynamic models. These models compute the flow based on conservation of volume and momentum. 3Di software is an example of such a model (Chapter 3 will explain more on this model). The depth averaged 2D momentum conservation equations in this model are (Nelen & Schuurmans, 2020):

$$\frac{\partial u}{\partial t} + g\frac{\partial \zeta}{\partial x} = -\frac{|u|u}{H_f} + \frac{\rho_{air}}{\rho_{water}V}\iint \chi^2 C_D \left\|\frac{U_{wind}^x}{\chi} - u\right\| \left(\frac{U_{wind}^x}{\chi} - u\right) d\Omega^x \tag{2.2}$$

$$\frac{\partial v}{\partial t} + g\frac{\partial \zeta}{\partial y} = -\frac{|u|v}{H_f} + \frac{\rho_{air}}{\rho_{water}V}\iint \chi^2 C_D \left\|\frac{U_{wind}^y}{\chi} - v\right\| \left(\frac{U_{wind}^y}{\chi} - v\right) d\Omega^y \tag{2.3}$$

In which: u and v are the flow velocities in the x and y direction in m/s, g is the gravitational acceleration in m/s^2, ζ is the water level in m, $|u|$ is the absolute velocity of water in m/s, H_f is the friction depth in m, ρ_{air} is the density of air in kg/m^3, ρ_{water} is the density of water in kg/m^3, χ is a dimensionless limitation factor, C_D is the dimensionless wind drag coefficient, U_{wind}^x and U_{wind}^y are the wind components in x and y direction in m/s and Ω^x and Ω^y are the domains of the impulse balance in x and y direction in m.

To approximate the momentum transmission between the wind and the water surface by means of model equations, the wind measurements provided by the wind gauges must be adapted to local conditions. However, a roughness height is not included in model equations 2.2 and 2.3. In this case, the transmission of momentum is estimated based on the wind velocity and the wind drag coefficient. The wind shear stress can be computed (τ_w) as:

$$\tau_w = -\rho_{air}C_D|u_{wind}|u_{wind} \tag{2.4}$$

With: the relative wind velocity with respect to the water velocity u_{wind}, the wind drag coefficient C_D and the density of air ρ_{air}. In most hydrodynamic models, the momentum transmission is estimated similarly (Wróbel-Niedźwiecka et al., 2019).

2.2.2 Wind drag coefficient

In previous modelling studies of large shallow lakes, the wind drag coefficient in the wind stress equation has been based on empirical reference values, or alternatively, has been calibrated based on field data (Cheng et al., 2020). Measurements of the drag coefficient over inland water systems are relatively scarce, in comparison to seas and oceans. In a literature review by Abbasi et al. (2017) on drag coefficients on lakes, it was found that the values vary over a wide range and are associated with large scatter. The wind drag coefficient on inland water systems typically ranges between 1×10^{-3} and 2×10^{-3}, as was concluded by Wuest and Lorke (2003).

It is widely agreed upon that the wind drag coefficient depends on the mean wind speed, air stratification and wave state (Grachev et al., 1998). Any attempt to properly model the momentum flux as the drag force per unit area at the water surface (surface shear stress, τ_w) takes into account other physical processes responsible for generating turbulence such as air instability and wave breaking (Rieder, Smith, & Weller, 1994). However, usually a neutral drag coefficient (C_{DN10}) is considered (KNMI, 2017). This means that a neutrally stratified momentum flux is considered (Wróbel-Niedźwiecka et al., 2019). The air instability was neglected in this thesis as well, as its significance declines at higher wind speeds (Mehrafar et al., 2018). In literature it was also found that many empirical formulations of drag coefficients considered neutral drag coefficients (Wróbel-Niedźwiecka et al., 2019). Forthcoming, all drag coefficients mentioned in this thesis are neutral drag coefficients.

For strong winds (>5 m/s) the water surface roughness is determined by the height of the gravity waves (Wuest & Lorke, 2003). Commonly, for seas and oceans, the drag coefficient at high wind speeds is based on an empirical relation with the wind speed (KNMI, 2017). However, the wave development in shallow, inland water systems is relatively small. The drag coefficient on these systems strongly depends on local characteristics, which are the following physical aspects:

1. The roughness of the water surface;
2. The roughness of adjacent terrains;
3. The shielding by obstacles and/ or shores;

Not only physical aspects contribute to the variation in the drag coefficient values, another reason is:

4. The lack of information due to the coarse spatial resolution of wind velocity observations.

For these four reasons, the drag coefficient value (or empirical relation) varies spatially and the drag coefficient is often a parameter that is determined by calibrating the hydrodynamic model, in order to approximate the wind set-up as accurately as possible. The origins of these variations are:

1. Firstly, the wind speed profile on the water body depends on the roughness of the water surface, which depends on the wave field (which depends on the wind speed and the state of wave development). A rougher water surface increases turbulence, which strongly enhances the vertical momentum flux between the wind and the water surface (Verkaik, 2006). Local variations in wave development are caused by variations in water depth and fetch lengths. The wave field is typically less developed for smaller fetches and shallower waters (Abbasi et al., 2017).

2. Furthermore, the roughness of adjacent terrains determines the wind speed profile at the water bodies in the system. Significant roughness changes can be observed over short distances, consequently there will also be wind speed differences. However, the height of the abl adapted to the surface roughness change, downwind of this roughness change, can be small (Rao et al., 1974). The surface roughness of the upstream fetch over a considerable distance determines the local wind speed profile.

Figure 2.4: Example of wind shielding on a small lake (Markfort et al., 2010)
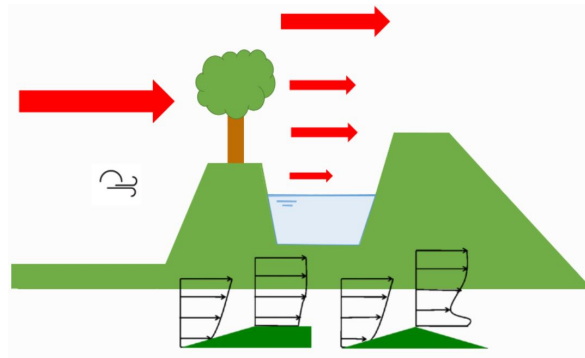
Figure 2.5: Illustration of wind shielding (Nelen & Schuurmans, 2020)

3. Lastly, shielding of the wind has a significant influence on the local wind speed and therefore on the momentum transmission by the wind. Shielding refers to the condition where wind has to pass along or over some obstacle(s), located on the upstream wind side, before meeting the water surface under consideration. For instance, the water surface can be located behind a row of trees, or below the bank level. This local variation of the wind depends on the wind direction with respect to the orientation of the obstacles and the orientation of the water body (Nelen & Schuurmans, 2020).

   That wind shielding can significantly reduce the area of effective fetch, especially on small lakes, is illustrated in Figure 2.4 by the reflection of visible light on surface waves in Holland Lake (area: 0.15 km^2) (Markfort et al., 2010). The total effect of shielding depends on the relative sizes of the obstacles and the water surface. The effect of obstacles extends into the lake anywhere from 10 to 30 times their height, depending on the wind velocity and on the density of the barrier (SailZing, 2018). Figure 2.5 illustrates the differences in the wind speed at the toe of the shore as compared to the crest and the influence of the crest width (Nelen & Schuurmans, 2020). The shore dimensions can therefore influence the wind profile near the water surface considerably.

So, this wind drag coefficient varies on a very small-scale for numerous physical reasons. However, integrating all the small changes in a model, would not be possible without increasing the computational effort beyond practicality. Another aspect of variation in the drag coefficient is introduced due to the course spatial resolution of wind measurements:

4. The wind velocities are generally provided as measurements from wind stations. These velocities are measured at a relatively large spatial resolution, which does not coincide with the small-scale variations in the wind speed profiles. This means that the drag coefficient serves as a scaling factor for the wind stress on locations where the wind speed is not measured within the study area. Even though, this is not an aspect of the official definition of the drag coefficient, this effect is integrated during model calibration. If the hydrodynamic model is linked to a meteorologic model with a very fine computational grid, this effect does not have to be integrated. However, such a model is often not accessible in practice.

Chapter 3

Case study: Wetterskip Fryslân

For centuries, the Dutch have had a relationship with water that is unique in the world. The Netherlands are known for its fascinating landscapes with its iconic windmills, pumping stations, polders, dikes and storm surge barriers. The province of Fryslân is known as thé water province of the Netherlands. Fryslân has 24 lakes (Vakantie Friesland, 2019), located between Lake IJssel and Lauwersmeer (Figure 3.1). The lakes are openly connected through a dense network of canals. To ensure both water safety and water availability, the water levels are regulated under strict supervision by the water board, Wetterskip Fryslân. Their management area consists of the Frisian bosom and the polders that depend on the bosom for supply or drainage of their water (Wetterskip Fryslân, 2014). Additionally, the Frisian Islands Vlieland, Ameland, Terschelling and Schiermonnikoog are governed by Wetterskip Fryslân. An overview of the management area of Wetterskip Fryslân is provided in Figure 3.1.

Lakes

The smallest lake of the Frisian bosom is the Idskenhuistermeer (0.15 km^2) and the largest lake, with an area of 22 km^2, is the Tjeukemeer. The fetch lengths are estimated for different wind directions for a number of lakes as indication in Table 3.1, including the smallest and largest lakes. Lake Fluessen is a long stretched lake situated in the south-west of the bosom area (Figure 3.1 and Figure 3.2). Lake Fluessen is directly connected to Heegermeer and the total fetch length is provided for this reason. The Frisian lakes are not deep, with an average depth of approximately 2 m (Wetterskip Fryslân, 2020).

Table 3.1: A rough estimation of the fetch lengths [km], of various lakes in the Frisian bosom, for various wind directions

		Wind direction			
		N (S)	NE (SE)	E (W)	SE (NW)
Lakes	Tjeukemeer	3.7	6.6	5.5	5.3
	Fluessen and Heegermeer	2.6	10.1	3.5	2.3
	Slotermeer	3.0	4.7	3.8	2.8
	Terhornstermeer	0.5	0.4	0.4	0.6
	Idskenhuistermeer	0.3	0.4	0.5	0.5
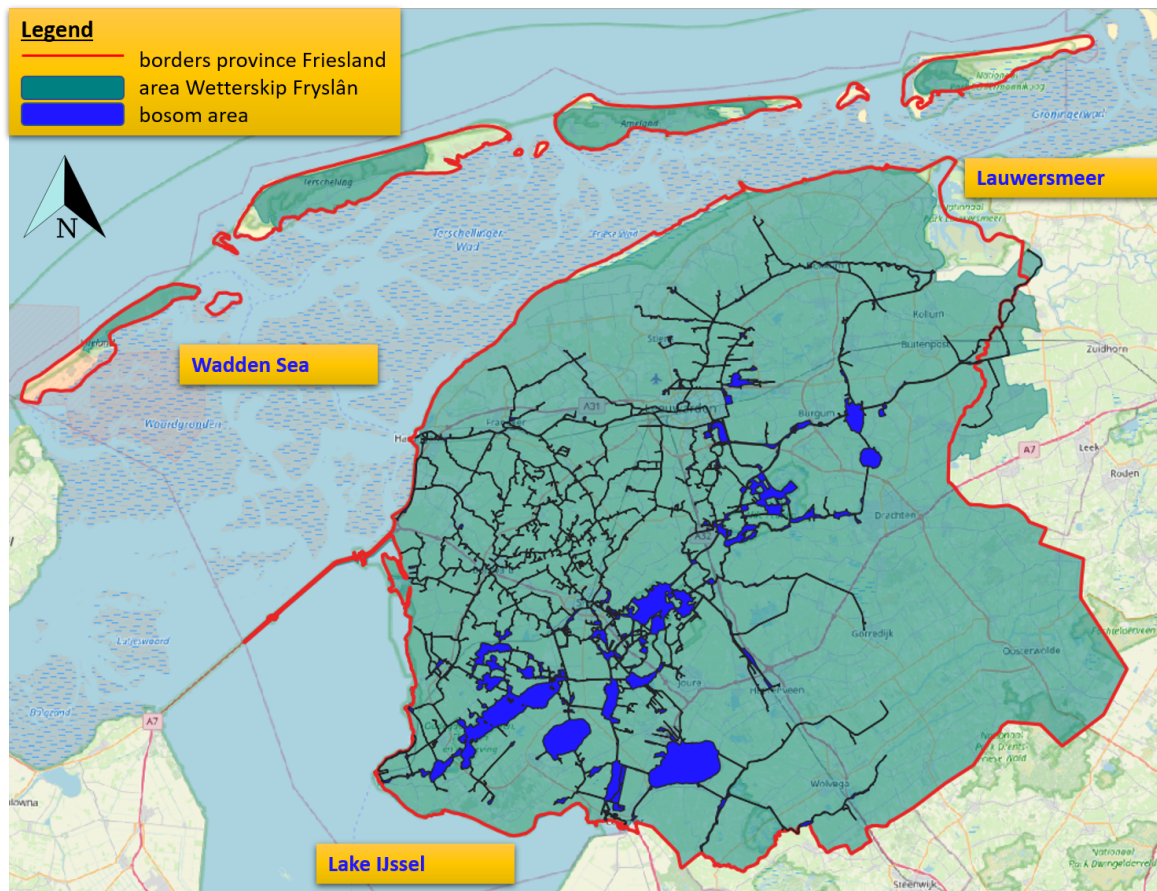
Figure 3.1: Fryslân, with the **management area of Wetterskip Fryslân**, the **borders of the province** and the **bosom area** (Wetterskip Fryslân, 2020)
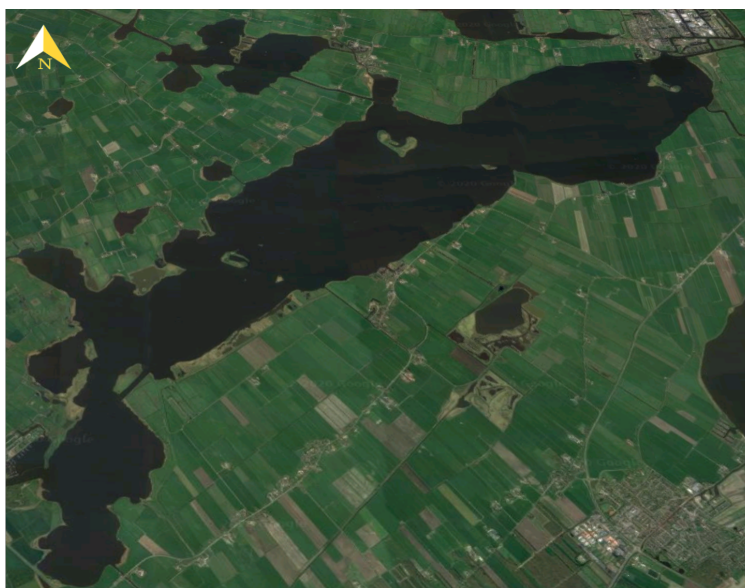
Figure 3.2: The two openly connected lakes Fluessen (lower left) and Heegermeer (top right) (Google, n.d.)

Case study

To investigate the importance of the three described dependencies of the wind drag coefficient, the Frisian bosom (Dutch: boezem) served as a case study. The water bodies within this system all correspond to the dimensions defined in the scope and this system is therefore suitable as study area. The impact of strong winds on local water levels in this system can be substantial. A large accumulation of water can develop at one side of the bosom, as water can flow freely through the system. Especially fierce southwestern wind can cause trouble, as it drives the water from the southwestern to the northeastern part of the system. The southwestern part of the Frisian bosom contains most storage capacity. The accumulated water from the southwest must be collected in a section of the system with a smaller storage area (the northeast) than where the water originated from (Dorst, 2003). This can cause problems, especially in combination with heavy rainfall and set-up of the external water (Wadden Sea), as this limits the natural drainage capacity from the bosom to external water. Additionally, problems may also occur in the southwestern part of the bosom during a strong northeastern wind. However, strong winds from this direction are less frequently experienced.

Modelling the bosom

Currently, the management of the Frisian bosom by the water board is supported by an 1D SOBEK model. SOBEK is an integrated 1D/2D modelling suite by Deltares. However, a new model was developed during this study using 3Di software. 3Di is a process-based, hydrodynamic modelling software for flooding, drainage and other water management related studies (Nelen & Schuurmans, 2020). The 3Di modelling software includes the subgrid method, as well as the opportunity to refine the computational grid using the quad-tree technique. These features allow for fast and accurate simulations. This model was used for the computation of water flow in 2D. This made it possible to integrate the directional effect of wind, which was not possible with the 1D SOBEK model. Nevertheless, currently it is only possible to define a constant wind drag coefficient with 3Di software. The purpose of this study in Fryslân is to find out if the accuracy of wind-related studies will improve if 3Di implements wind drag coefficients that can vary spatially, per wind direction and/ or per wind speed.

Chapter 4

Methodology

To determine if and to what extent the wind drag coefficient depended on the three described dependencies, different historical wind events were simulated in the Frisian bosom. These historical events were classified based on wind speed and wind direction. One event per wind class was used for calibration of its water levels to determine the differences in their optimal wind drag coefficients. Calibration was performed using various types of data and a newly developed 3Di hydrodynamic model. The wind drag coefficient was optimised, based on the water level observations and simulation results, such that the simulated water levels matched the observations as closely as possible.

For each wind class, an optimal wind drag coefficient was retrieved for the whole model domain, as well as for each measurement location separately. This way, the optimal drag coefficient values could be analysed domain-wide as well as locally. After the calibration phase, the optimal drag coefficients were validated using an independent wind event per wind class. Lastly, the results were compared to a reference case. This comparison gives an indication of the significance of the improvement in terms of model accuracy, when integrating the wind drag dependencies in the model. The methodology is broadly illustrated in the flowchart of Figure 4.1.

Subsection 4.1.1 discusses the various types of data that were collected, analysed and filtered, such that it could serve as input for the model or the assessment of model results. Subsection 4.1.2 elaborates on the setting up of the 3Di hydrodynamic model. Section 4.2 describes the calibration method, whereas Section 4.3 describes the validation method. Lastly, Section 4.4 provides information on the reference case and on the in-depth analysis of the wind drag dependencies.
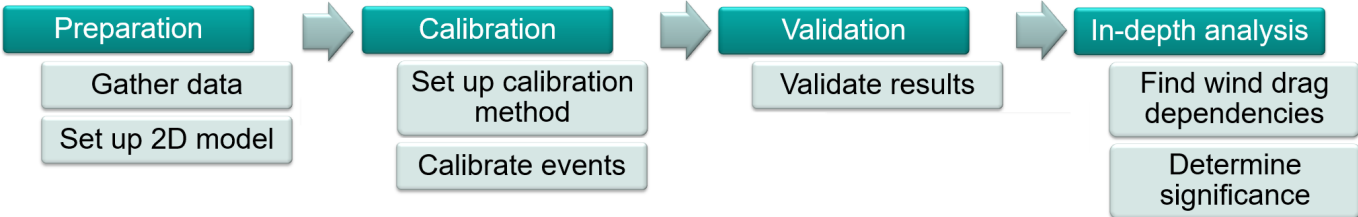
Figure 4.1: An illustration of the methodology

Figure 4.2: The locations of wind stations Stavoren and Leeuwarden (from left to right)

4.1 Preparation

4.1.1 Data collection

Over a period of five years, from 2015-2019, wind measurements were provided by Koninklijk Nederlands Meteorologisch Instituut (KNMI) at two wind stations within the study area. Furthermore, Wetterskip Fryslân provided water level measurements of twenty observation points and discharge measurements of pumping stations, sluices and inlets from and to the external water bodies (Wadden Sea, Lake IJssel and Lauwersmeer, see Figure 3.1). These were provided over the same time period. The locations of the wind stations are presented in Figure 4.2. Moreover, the water level measurement stations are displayed in Figure 4.3, whereas Figure 4.4 provides an overview of the locations of the inlets and outlets.

Wind measurements

The wind stations within this study area are located at Stavoren and Leeuwarden. The locations of these wind stations are presented in Figure 4.2. The average wind speed and direction over these two locations was used as input for the model. The wind data was provided with time steps of 1 hour. The effects of wind gusts are therefore not incorporated. The data was filtered based on wind direction and on wind speed. Wind set-up is experienced in the Frisian bosom, starting at wind forces of 5 Bft (Schaper, 2020). In this analysis wind forces of 6, 7 and 8 Bft were taken into account, which result in more significant water level set-up. Wind events with higher wind forces did not occur in the Frisian bosom during the studied time period.

Figure 4.3: The locations of water level measurement stations

Figure 4.4: The locations of inlets and outlets

Table 4.1: The number of available events per wind class during the study period of 2015-2019

		Wind direction					
		N	E	S	SW	W	NW
	6 Bft	2 events	3 events	3 events	2 events	4 events	4 events
Wind force	**7 Bft**	0 events	0 events	0 events	4 events	5 events	3 events
	8 Bft	0 events	0 events	0 events	1 event	3 events	2 events

The wind speed was divided in three classes:

- 6 Bft (between 10.8 m/s and 13.9 m/s)
- 7 Bft (between 13.9 m/s and 17.2 m/s)
- 8 Bft (between 17.2 m/s and 20.8 m/s)

To determine the effect of wind direction, the wind was split up in eight directions, of 45 degrees, as illustrated in Figure 4.5. However, during the studied time period no relevant wind events of the northeastern and southeastern directions took place, and were therefore not included in this research. The number of available events per wind class are provided in Table 4.1. The requirements on wind speed and direction should have persisted for at least three hours, to ensure that significant wind set-up had occurred. A maximum event length was not determined, instead the duration of the wind event was used. It should be noted that the classified wind events can still differ in wind speed and direction within the intervals. Moreover, the persistence length of the events can differ. However, due the limited available data, classification into finer intervals was not feasible.

Two events per wind class were used in this study, one for calibration and one for validation. These events were named based on their wind properties and a letter A or B. Which event was used for calibration or which for validation was randomly selected. Table 4.2 provides the time and date of the event, as well as the duration. The wind velocity time series of these events are presented in Appendix B. Sometimes a third event was needed as additional validation, these are denoted with the letter C. Further elaboration on this is provided in Appendix E.
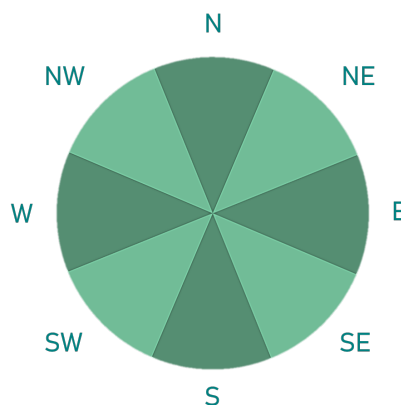
Figure 4.5: An illustration of the eight different wind direction classes, including: N (337.5° to 22.5°), NE (22.5° to 67.5°), E (67.5 to 112.5), SE (112.5 to 157.5°), S (157.5° to 202.5°), SW (202.5° to 247.5°), W (247.5° to 292.5°) and NW (292.5° to 337.5°).

Table 4.2: Overview of the wind events used for calibration and validation

Wind event	Start time	End time	Duration [h]
6 Bft E (event A)	2018-03-15 04:00	2018-03-15 15:00	11
6 Bft E (event B)	2018-03-16 13:00	2018-03-18 18:00	53
6 Bft N (event A)	2019-01-28 00:00	2019-01-28 14:00	14
6 Bft N (event B)	2019-01-01 11:00	2019-01-02 08:00	21
6 Bft NW (event A)	2017-01-03 18:00	2017-01-04 15:00	21
6 Bft NW (event B)	2018-04-05 00:00	2018-04-05 17:00	17
6 Bft NW (event C)	2018-06-21 02:00	2018-06-22 15:00	37
6 Bft S (event A)	2015-02-22 13:00	2015-02-23 06:00	17
6 Bft S (event B)	2016-02-07 07:00	2016-02-08 09:00	26
6 Bft SW (event A)	2015-11-09 08:00	2015-11-10 06:00	22
6 Bft SW (event B)	2016-02-21 05:00	2016-02-22 02:00	22
6 Bft W (event A)	2016-01-07 09:00	2016-01-08 09:00	24
6 Bft W (event B)	2019-03-15 05:00	2019-03-15 18:00	13
7 Bft NW (event A)	2017-01-13 12:00	2017-01-14 06:00	18
7 Bft NW (event B)	2019-01-07 14:00	2019-01-09 01:00	36
7 Bft NW (event C)	2017-10-28 01:00	2017-10-29 10:00	33
7 Bft SW (event A)	2015-06-01 22:00	2015-06-03 00:00	26
7 Bft SW (event B)	2019-08-09 23:00	2019-08-10 22:00	23
7 Bft W (event A)	2015-11-17 20:00	2015-11-19 14:00	42
7 Bft W (event B)	2018-01-04 16:00	2018-01-05 05:00	13
8 Bft NW (event A)	2017-10-05 00:00	2017-10-05 17:00	17
8 Bft NW (event B)	2015-07-25 06:00	2015-07-25 22:00	16
8 Bft SW (event A)	2017-09-10 05:00	2017-09-13 19:00	88
8 Bft W (event A)	2015-03-29 12:00	2015-04-01 03:00	63
8 Bft W (event B)	2017-01-03 00:00	2017-01-03 23:00	23
8 Bft W (event C)	2017-09-12 19:00	2017-09-13 19:00	24

Water level measurements

To simulate, calibrate and validate the wind events, water level observations were gathered to assess simulation results and to use as initial condition. These water level observations are based on a fifteen minute time step. The locations of the twenty measurement stations are presented in Figure 4.3. It was found that locations Burgum and Scharsterbrug were susceptive to measurement noise. Vibrations are observed throughout the entire data set with a magnitude of up to 3 cm. This affects the reliability of the model accuracy assessment increasingly with relatively smaller water level variations. Whether this has impacted the reliability of the model accuracy assessment is discussed in Section 6.1.

Discharge measurements and assumptions

Even though, the dominant forcing is the wind, currents and water levels are influenced by precipitation and discharges from and to external water bodies. Therefore, discharge data was gathered and used as input for the boundary conditions of the model. Only the discharges exchanged between bosom and external water bodies, were available. These are the discharges of five outgoing sluices or pumping stations and six inlets. These discharges served as unsteady boundary conditions, as the entire time series was input for the model. An important side note is that the 'outgoing discharges', the discharges pumped from the bosom into the external water bodies, were not measured. These were computed based on the operating mode, the pump head (Dutch: opvoerhoogte) and revolutions per minute (Dutch: toerentallen) of the pumps. These computed discharges might deviate from the actual unknown discharges (Vellinga, 2020).

The discharges of the circa thousand polder pumping stations, discharging into the bosom, are unknown. Moreover, precipitation data was known, but not used in order to decrease the computational effort by not including rainfall-runoff areas in the model. Instead, the net outgoing discharge was summed and divided over the polder pumping stations. These were used as boundary conditions for the model with a constant incoming discharge. With these boundary conditions the simulations ended up with a net discharge of zero, and no volume was lost. The inflow locations were based on the real locations of the polder pumping stations. However, this method was still a simplification, as the discharge was constant (steady-state) and equally divided. However, the significance of this simplification, also depending on the nature of the precipitation event, was expected to be small.

Bed level measurements

The available bed level measurements within the model domain were provided by the province of Fryslân (Provinsje Fryslân, 2020). The measurements in navigational routes and within the big lakes were extensive. Figure 4.6 displays the available bed level measurements in Slotermeer, to get a better view of the available data within a lake. Nevertheless, not all waterways in the Frisian bosom were measured.
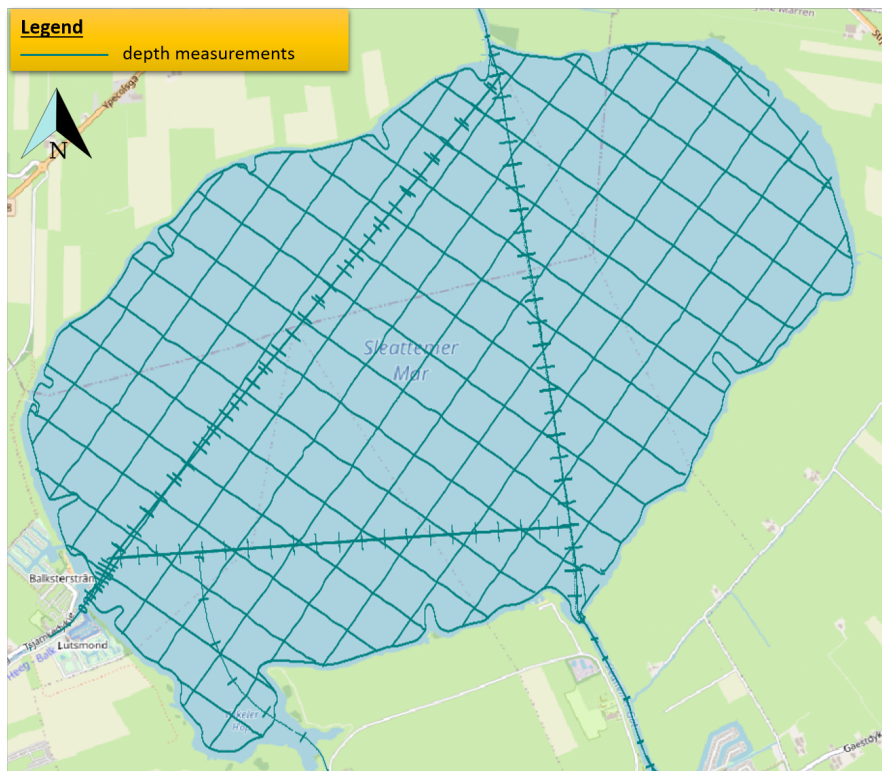
Figure 4.6: The bed level measurements availability in Slotermeer
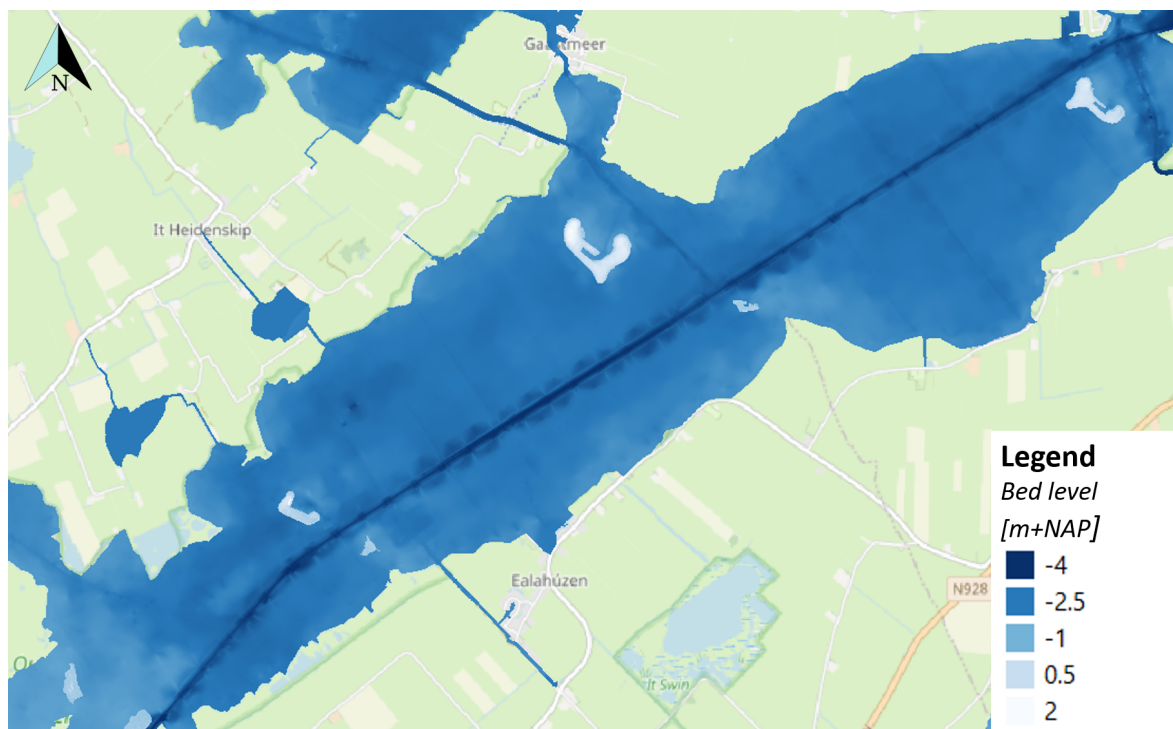
Figure 4.7: The DEM situated at lake Fluessen

4.1.2 Setting up the model

A 3Di model of the Frisian bosom was set up as part of this research and this model was optimised for speed and accuracy. 3Di software enables a Digital Elevation Model (DEM) to be used efficiently for detailed 2D simulations, using the subgrid method (Casulli, 2009) (Stelling, 2012). Such a model consists of a coarse computational grid that can be locally refined by using a quadtree method. This coarse grid is linked to a high resolution subgrid containing all input data, such as the roughness, infiltration rates and bathymetry. The basic idea behind the subgrid method is that water levels vary considerably more gradually than the bathymetry. In hydrodynamic computations, water levels are assumed to be uniform within a computational cell. The subgrid-based approach allows the bathymetry to vary within one computational cell, while the water level remains uniform.

DEM

The DEM was created using QGIS software, by means of combining three layers of the bosom: a layer of ground level measurements of the dry areas, like lake islands, a layer of assumed bed levels and a layer of interpolated bed level measurements. To elaborate, a bed level was assumed for the waterways that were not included in the measurement data. This assumption was based on an average and/ or on extrapolation of surrounding measured bed levels. The three layers were merged, where the interpolated bed levels based on measurements were leading over the assumed bed levels. The Inverse Distance Weighting (IDW) method was used to interpolate. The interpolation search radius was set at 300 m. This radius was large enough to avoid data gaps in the lakes and small enough to keep the process time reasonable. The final DEM resolution was 2 m by 2 m. A part of the DEM, situated at lake Fluessen, is presented in Figure 4.7.

Model schematisation

The model schematisation was also set up using QGIS, by means of SpatiaLite tables. Local grid refinements were applied at smaller water bodies and places where larger water bodies narrow or where an obstacle, like an island, interferes with the flow. To accurately capture the small-scale flow processes, these parts of the bosom were modelled in more detail. Furthermore, the grid resolution and time step were determined based on optimisation of the computational time in combination with the model accuracy. An overview of the model settings is provided in Appendix C. A part of the DEM, situated at Tjeukemeer, with the computational grid cells is presented in Figure 4.8.

Boundary conditions

It was assumed that the bosom area is a closed system, connected to external water bodies and polder systems by means of structures. The actual discharges of these structures exchanged between bosom and external water bodies (Wadden Sea, Lake IJssel and Lauwersmeer, see Figure 3.1) were included in this model. The exchanged discharges between polder systems and the bosom area were simplified as a constant discharge, computed based on actual discharges between bosom and external water and a constant volume in the bosom.
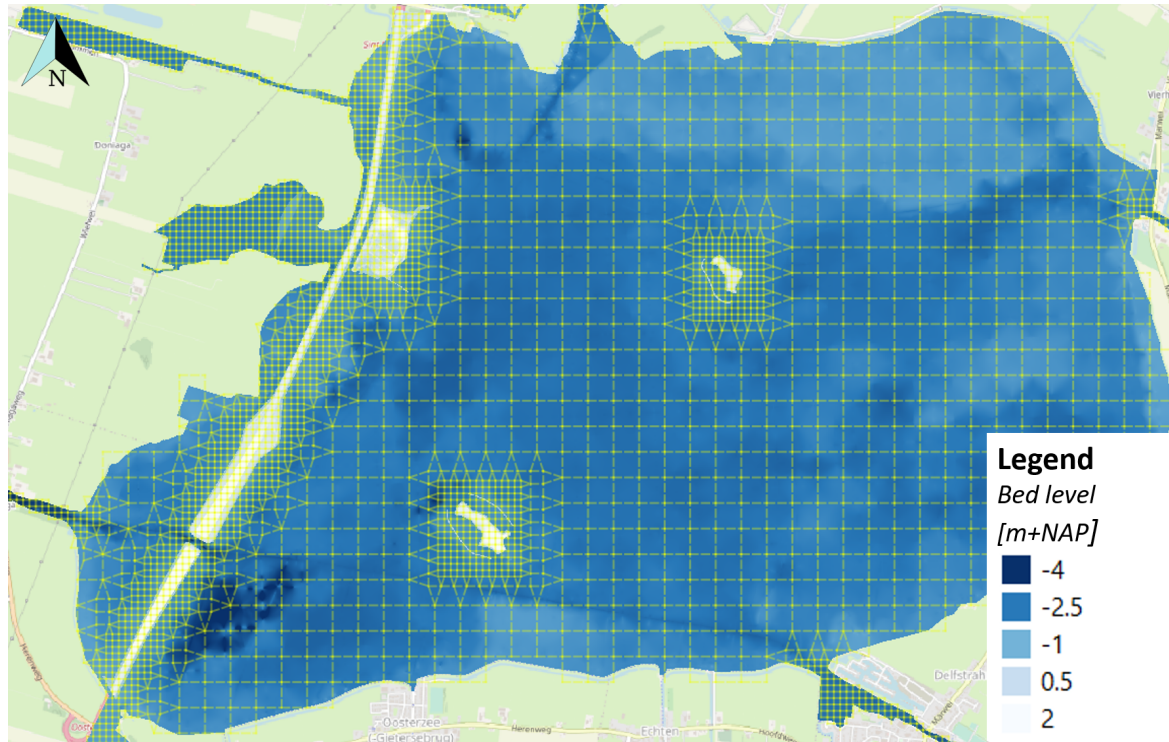
Figure 4.8: The DEM situated at lake Tjeukemeer with the computational grid cells

4.2   Calibration

In this study the wind drag coefficient was fine-tuned to calibrate the model, such that the model output of the water level matched the observations as closely as possible. This was set up as an automatic process, which aimed to maximise the objective function and was implemented as a progressive simulation method with drag coefficient values chosen within an interval. Two simulation stages were implemented, with a reduced interval size in between the stages, based on the two drag coefficients resulting in the highest objective function values.

Twelve wind events (of different classes) were calibrated and the comparison of water levels was made at twenty measurement stations (Figure 4.3). This way, an optimal drag coefficient per wind event was allocated at every measurement location, as well as an average or in other words a domain-wide optimal drag coefficient. The calibration was set up in different phases, these are:

I   ▸   The data collection;

II   ▸   The model initialisation;

III   ▸   The first calibration stage;

IV   ▸   The interim assessment;

V   ▸   The interval refinement;

VI   ▸   The second calibration stage;

VII   ▸   The final assessment.

Table 4.3: KGE values and interpretations

KGE value	Interpretation
KGE < 0.4	Poorly accurate
$0.4 \leq$ KGE < 0.55	Somewhat accurate
$0.55 \leq$ KGE < 0.7	Fairly accurate
$0.7 \leq$ KGE < 0.85	Highly accurate
$0.85 \leq$ KGE ≤ 1	Greatly accurate

Figure 4.9 provides a flowchart of this process, including all these numbered phases. This section will further outline this calibration process. However, first the objective function is described, that was used to objectively assess the accuracy of simulations.

4.2.1 Objective function

During calibration, the differences between the field observations and the model results were quantified using an objective function. The Kling-Gupta Efficiency (KGE) was used, which is a commonly used benchmark over the last decade, as it addresses several perceived shortcomings in the more traditional Nash Sutcliffe Efficiency (NSE) (Knoben et al., 2019). The NSE is based on the mean squared error. The mean squared error between the simulated and observed water levels can be decomposed into the three components mean, variability, and dynamics (Pool et al., 2018). This facilitates analysis of the relative importance of its different components (Gupta et al., 2009). The KGE is based on an improved combination of these three components of the mean squared error (Pool et al., 2018) and can be computed with the following formula (Knoben et al., 2019):

$$KGE = 1 - \sqrt{(r-1)^2 + \left(\frac{\sigma_{sim}}{\sigma_{obs}} - 1\right)^2 + \left(\frac{\overline{\zeta_{sim}}}{\overline{\zeta_{obs}}} - 1\right)^2} \tag{4.1}$$

In which: the first term is the linear correlation between observations and simulations, the second term is a measure of the flow variability error and the last is a bias term. Furthermore, r is the linear correlation coefficient, σ indicates the standard deviation and ζ is the water level at a measurement station in m.

The KGE improves upon the NSE by including the effects of relative movements or trends in the water levels. Moreover, the effects of great differences for a short period of time has more impact (negatively) on the KGE value, due to the variability bias component. And finally, KGE includes the differences between the mean water levels. A technical note on KGE by Knoben et al. (2019) provides more insight in these improvements. The KGE is in line with the paradigm of using multiple objectives for model calibration (Pool et al., 2018). A KGE value of 1, its maximum, means that the model accuracy is optimal. At a KGE value of -0.42 and lower the mean water level is a better predictor. Various authors of previous modelling studies use positive KGE values as indicative of "good" model simulations, whereas negative KGE values are considered "bad". Others consider KGE values lower than 0.5 to be "poor" (Knoben et al., 2019). Further interpretations of KGE values are found to be subjective and no further categorisations are found in literature.

So, the KGE values were categorised, partly based on previous mentioned literature and partly on the author's interpretation, retrieved by analysing the model results. These categories were used to discuss the results and are provided in Table 4.3. During this study the sub-components were also calculated, which allows for more in-depth analysis of the model accuracy.

Furthermore, the interpretation of model improvements were based on the potential for model improvement. The potential is computed as $1 - KGE_{benchmark}$. The improvement is explained by the potential fulfillment (or the skill score), which is the improvement in terms of a percentage of the potential (Knoben et al., 2019):

$$\text{Potential fulfillment} = 100\% \times \frac{KGE_{model} - KGE_{benchmark}}{1 - KGE_{benchmark}} \tag{4.2}$$

4.2.2   Weights

Weights were defined for every measurement location, based on the observed wind set-up (or set-down). This was done to direct the calibration based on locations were wind set-up (or set-down) occurs. These locations weigh heavier in the assessment, as accurate predictions of these locations are meaningful information for water managers. The weights were applied in the computation of the averaged objective function values. The defined weights are provided in Table 4.4.

Table 4.4: The defined assessment weights

Max. observed set-up	Weights
$|\Delta\zeta_{obs}| < 0.1m$	1
$0.1m < |\Delta\zeta_{obs}| < 0.3m$	2
$|\Delta\zeta_{obs}| > 0.3m$	3

4.2.3   Calibration phases

The calibration process and its phases are further explained in this section. Figure 4.9 provides a flowchart of this process.

I ▷ **Data collection**

The input for the automatic calibration script was a definition (the name) of a wind event. This definition was linked to the time and date of the event. In the first step, the data of the measurements, water levels, discharges and wind, were collected. With these measurements the total net outgoing discharge was computed and accordingly the discharge of the polder pumps. Additionally, the weights were computed, based on the observed set-up, which were used in the assessment phases.

II ▷ **Model initialisation**

Thereafter, the initialisation phase started. The model was initialised to provide a more accurate representation of the water levels in the model domain, at the start of the wind event. A period of 24 hours leading up to the wind event was simulated. Input for this simulation was the average observed bosom water level. This water level was computed, based on the observed water level at different locations within the bosom:

$$\zeta_{bosom} = 0.09(\zeta_{Burgum}) + 0.06(\zeta_{Leeuwarden}) + 0.13(\zeta_{Nesserzijl}) + 0.19(\zeta_{Scharsterbrug})$$
$$+0.14(\zeta_{Sneek}) + 0.13(\zeta_{Woudsend}) + 0.26(\zeta_{Elahuizen}) \tag{4.3}$$

This formula is recommended and used by the Frisian water board (Vellinga, 2020). The corresponding wind and discharge series were additional input for this simulation. These settings were sent to the 3Di calculation server. After the simulation was finished, a saved state was pulled from this server. This saved state was input for all the simulations in the calibration process.
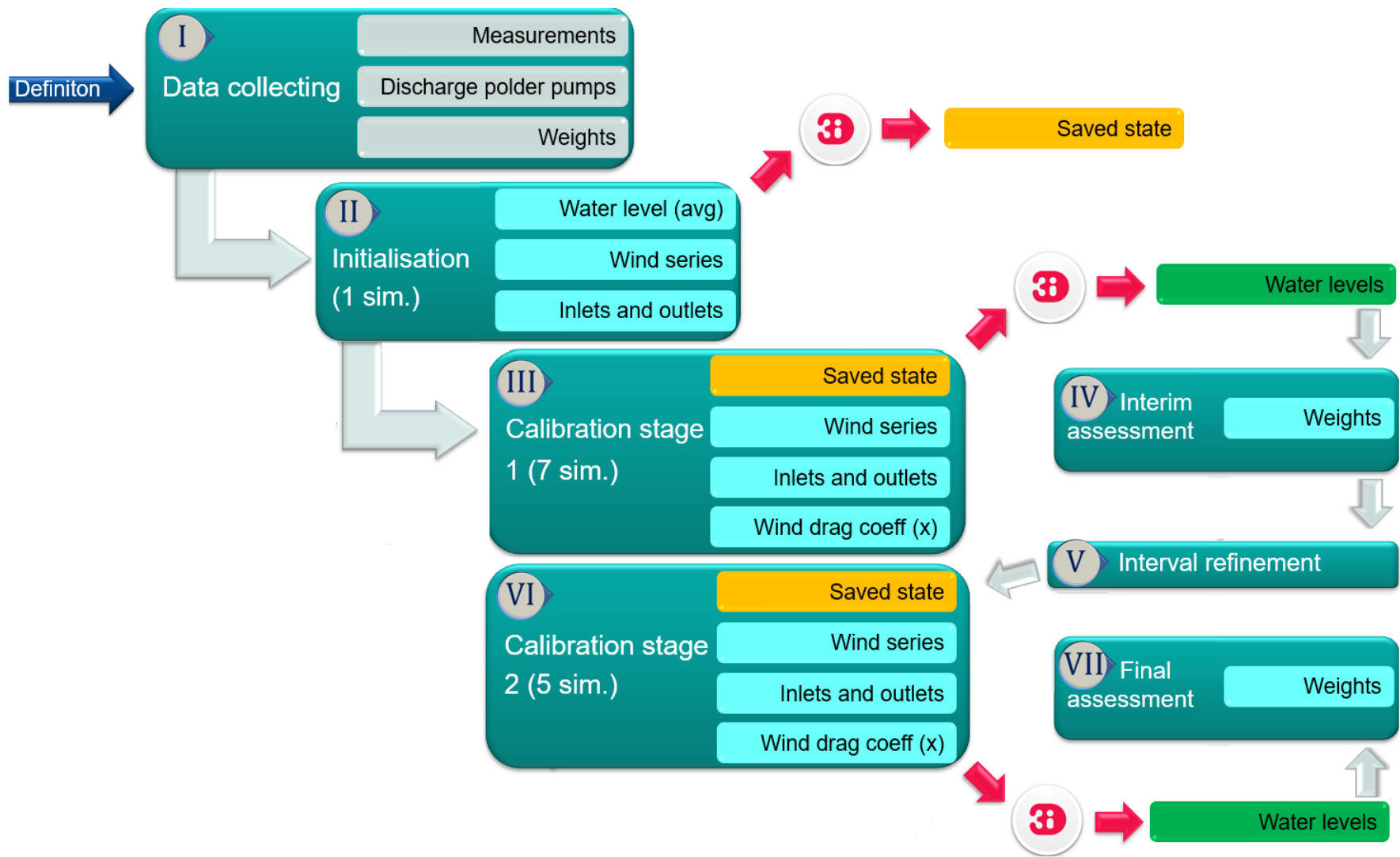
Figure 4.9: The flowchart of the automatic calibration process

Table 4.5: An example of the calibration stages, with the corresponding wind drag coefficient values
of the simulations

	Wind drag coefficient C_D [10^{-3}]						
Stage 1	0.80	1.00	1.20	1.40	1.60	1.80	2.00
Stage 2	1.35	(1.40)	1.45	1.50	1.55	(1.60)	1.65

(III) Calibration stage 1

After the model was initialised, calibration stage 1 started. The saved state formed the initial state
for the simulations. The wind and discharge series during the wind event and a wind drag coefficient
were additional input. The wind drag coefficient is presented in Figure 4.9 as a function of x, indicating
that its value changed every simulation. However, during the simulation the wind drag coefficient did
not vary over time or over space. This is a preliminary study to see if it is significant to implement a
varying drag coefficient in hydrodynamic models.

The drag coefficient varies within a certain interval during the simulations of calibration stage 1. In
Subsection 2.2.2 it was indicated that the typically range of the wind drag coefficient is between
1×10^{-3} and 2×10^{-3}. However, the first interval was taken somewhat wider, based on the results of
a few trial runs. The first range was adjusted to 0.8×10^{-3} and 2×10^{-3}. The first stage required seven
simulations, varying the drag coefficient with steps of 0.2×10^{-3}. These settings were sent to the
3Di calculation server and after the simulations were finished, the water levels at the computational
nodes, corresponding to the locations of the measurement stations, were retrieved.

(IV) Interim assessment

The following phase was the interim assessment. The objective function values were computed per
simulation per measurement location. The weights were applied in the computation of the averaged
(domain-wide) objective function values. Additionally, the four locations with the lowest objective
function value were not included in this computation. This was done to exclude locations that might
never have aligned with the observations, regardless of the wind drag coefficient value. This could be
due to a number of uncertainties, like measurement or model insecurities, further discussed in Sec-
tion 6.1. By excluding these locations, these uncertainties did not influence the interval refinement
(phase V).

(V) Interval refinement

The two highest averaged objective function values, corresponding to two drag coefficient values,
were determined from the interim assessment. The original interval was redefined, based on these
drag coefficient values. An example is presented in Table 4.5. In this table the maximum objective
function values during stage 1 were derived with a C_D of 1.4×10^{-3} and 1.6×10^{-3}. The refined
interval was taken somewhat wider than this, as the relation between the momentum transmission
and the water level set-up is non-linear.

(VI) Calibration stage 2

The refined interval was input for the second calibration stage. The other settings, regarding wind
and discharge series, remained unaltered. Five simulations were performed during this stage, as
two of the seven drag coefficients of stage 2 were previously simulated in stage 1. The achieved
precision of the C_D value was 5×10^{-5}, with which a simulated water level precision of lower than 1
cm was achieved.

(VII) **Final assessment**

Thereafter, a final assessment took place and the wind drag coefficient value with the highest objective function value was determined. The output of this calibration script were the simulated water levels, a table with values of the KGE and its sub-components, graphs of the wind series and the simulated and observed water levels. Additional output of the script were the discarded locations such that a pattern in the faulty locations could possibly be found.

4.3 Validation

In order to determine whether the calibrated model was sufficiently accurate in predicting water levels, it was validated. The matter in which the calibrated model was able to reproduce observations from an independent data set was examined (van Waveren et al., 1999). For each wind class a second independent wind event was simulated. This is the wind event that is not used for calibration, provided in Table 4.2. The optimal wind drag coefficient value was used as input for this simulation. The assessment of the validation results is based on the KGE once more. The validation required further investigation, if the KGE deviated considerably from the calibration outcome. To determine the origin of this difference, the wind events were examined on comparability. Sometimes an additional wind event was available for a particular wind class and this event was used to validate. This method is further elaborated in Appendix E.

4.4 In-depth analysis

In what manner the results of the different dependencies of the wind drag coefficient, aligning with the sub research questions (Section 1.4), were analysed is described in this section. The method of this in-depth analysis is described for every dependency of the wind drag coefficient. A combination of dependencies was also analysed.

Moreover, the matter in which the significance of the results was determined is also provided. The significance of these dependencies were demonstrated by means of comparing optimised results to a reference case. To set up this reference case, all wind classes were simulated with an uniform wind drag coefficient. This wind drag coefficient was the average of all domain-wide optimal drag coefficient values of all wind classes. This is referred to as the reference case, since this drag coefficient would have been applied if the wind drag dependencies were not accounted for. Comparison between the reference case and the calibration results can give an indication of the significance of varying the wind drag coefficient per wind class and per location.

This comparison was based upon deviations in water level predictions, in terms of objective function values. The potential $1 - KGE_{benchmark}$ for model improvement is provided and subsequently, the potential fulfillment. Moreover, to determine the statistical significance of the improvement in KGE values a paired samples t-test was performed. The null hypothesis H_0, that there was no improvement, was tested at a 5% significance level. Additionally, graphical representations of the time series of simulations versus the observations were provided, to represent the improvement expressed in water level predictions.

Spatial dependency

The spatial dependency was analysed based on the local optimal drag coefficients (averaged over all wind classes). To effectively capture the spatial dependency, an overview of the Frisian bosom with the optimal drag coefficient per location was composed. The value of these drag coefficients was expressed in the size of a circle. The significance of a varying wind drag coefficient per location was approximated by comparing the reference case to the case including:

- The local optimal drag coefficients (averaged over all wind classes)

This comparison was performed at one location and was not extended into other locations.

Wind directional dependency

The wind directional dependency was examined based on the domain-wide optimal drag coefficients per wind direction (averaged over all locations). This information was provided in a wind rose-like plot. The value of these drag coefficients per wind directions was expressed as the size of a triangle and the model accuracy as the fill color. The significance of a varying wind drag coefficient per wind class was retrieved comparing the reference case to the case including:

- The domain-wide optimal drag coefficient per wind class (averaged over all locations)

This comparison has been done for all twelve wind classes.

Wind speed dependency

The wind speed dependency was examined supported with a bar graph, for three wind directions. Wind events from other directions only occurred at a maximum wind speed of 6 Bft. In order to single out the wind speed dependency only wind events from the same wind direction were compared, such that the wind directional dependency could not interfere with the results.

Spatial and wind directional dependency

To examine a combination of the spatial and wind directional dependency, an overview of the Frisian bosom was set up once more. This overview included the local optimal drag coefficients per wind direction. This information was provided in wind rose-like plots, scattered over the study area. Moreover, these results were averaged over all locations, to give an indication of how accurate the model can predict water levels per wind direction, in a model including spatial variability. In the same line of thought, these results were averaged over the wind directions, to give an indication of how accurate the model can predict water levels per location, in a model which also includes wind directional variability.

The significance of a drag coefficient varying spatially, as well as per wind class was approximated by comparing the reference case to the case including:

- The local optimal drag coefficient values per wind class

This comparison has been done at all twenty locations and all twelve wind classes.

Chapter 5

Results

This chapter provides the results of this research on the wind drag coefficient. The arrangement of this chapter is equivalent to that of the Methodology (Chapter 4), first the calibration results are briefly presented in Section 5.1, followed by the validation results in Section 5.2. Furthermore, the results of one wind event are highlighted in Appendix D. If the reader is interested in a detailed example of the calibration process, reading this Appendix is recommended. The results are described for every step along the calibration process, this might help with the interpretation of the overall results. The interpretation of the results are provided in Section 5.3, as the in-depth analysis.

5.1 Calibration

The results of the calibration process involve:

- The assessment weights;
- The discarded measurement locations;
- The optimal wind drag coefficient values of every wind class, per measurement location as well as domain-wide;
- The corresponding KGE values.

The tabular results are presented and discussed in Appendix A. These results serve as the basis for the in-depth analysis. The domain-wide optimal drag coefficients with the corresponding KGE per wind class are presented in Table 5.1.

5.2 Validation

In order to assess the reliability of the calibration results, validation was applied. Only validated results were included in the analysis. Validation was applied by simulating an independent wind event per wind class. Table 5.1 bundles the results of the calibration and the validation and provides the domain-wide optimal drag coefficient with the KGE values. For event 8 Bft SW no validation event was available, therefore this row is empty.

Table 5.1: The bundled results of calibration and validation: the domain-wide optimal drag coefficient with the KGE values

	Calibration		Validation
Wind event	$C_D \times 10^{-3}$	**KGE**	**KGE**
6 Bft E	1.60	0.56	0.39
6 Bft N	1.25	0.48	0.65
6 Bft NW	0.95	0.64	0.54
6 Bft S	1.85	0.69	0.73
6 Bft SW	1.25	0.82	0.71
6 Bft W	1.55	0.53	0.54
7 Bft NW	1.00	0.74	0.62
7 Bft SW	1.10	0.69	0.64
7 Bft W	1.10	0.61	0.57
8 Bft NW	1.30	0.54	0.36
8 Bft SW	1.45	0.72	-
8 Bft W	1.50	0.67	0.60
Avg	**1.33**	**0.64**	**0.58**

The model accuracy of some wind classes decreased with the validation event relative to the calibration event. Wind classes 6 Bft E and 8 Bft NW decreased with at least 0.15 in terms of the KGE. The optimal wind drag coefficient for these wind classes remains quite uncertain for this reason. However, it cannot be expected that the simulation accuracy of wind events within a wind class are exactly identical. The wind event can differ in length and in wind speed and direction within the classification interval. Moreover, the initial state of water levels (initial gradient) in the model domain can be quite different as well, due to the effects of precipitation and discharges of inlets and outlets. For these reasons all calibration results were used in the analysis. However, the results of these wind classes were considered with more caution. The KGE value of wind class 6 Bft N increased for its validation event relative to its calibration event. The same reasoning as for the accuracy decrease applies here.

5.3   In-depth analysis

The results of the different dependencies of the wind drag coefficient, aligning with the sub research questions (Section 1.4), are provided in this section. The significance of the dependencies was analysed by comparison of the reference case and the calibration results. This provided an indication of the significance of varying the wind drag coefficient per wind class and/ or per location. Therefore, all wind events were simulated once more with a uniform wind drag coefficient of 1.25×10^{-3}, which is the average of all domain-wide optimal drag coefficient values. The results were analysed based on each dependency individually or as a combination of multiple dependencies, as described in the Methodology (Section 4.4).

Table 5.2: Comparison of a case with the local optimal drag coefficient and the reference case, at measurement station Stavoren

		Wind event
		6E	6N	6NW	6S	6SW	6W	7NW	7SW	7W	8NW	8SW	8W	Avg
Loc. case	C_D	1.59	1.59	1.59	1.59	1.59	1.59	1.59	1.59	1.59	1.59	1.59	1.59	
	KGE	0.61	0.90	0.77	0.62	0.86	0.82	0.67	0.92	0.72	0.59	0.79	0.76	**0.75**
Ref. case	C_D	1.25	1.25	1.25	1.25	1.25	1.25	1.25	1.25	1.25	1.25	1.25	1.25	
	KGE	0.45	0.80	0.84	0.29	0.85	0.96	0.79	0.63	0.41	0.60	0.49	0.36	**0.62**

Spatial dependency

The spatial dependency was analysed based on the local optimal drag coefficients (averaged over all wind classes). The spatial dependency of the optimal wind drag coefficients can be derived from Table A.2. Based on this table, an overview of the Frisian bosom with the optimal drag coefficient per location was composed and is presented on the next page. The value of the averaged optimal drag coefficient is expressed in the size of the circle.

This overview reveals a pattern of higher local optimal drag coefficient values in the south compared to a lower drag coefficient in the north of the bosom. The southern part consists of larger water bodies and the northern part consists of a dense system of small canals. Shielding by shores and objects is therefore more effective in the northern part, explaining the lower drag coefficient values. Moreover, another effect which might enhance the gradient in optimal wind drag coefficients is the coarse spatial resolution of wind measurements. Wind speeds, close to the sea, can be higher than wind speeds, further inland, due to roughness effects. As the wind slows down as it moves further inland, less momentum is transferred as well. This was not captured in the model forcing, as wind was a spatially constant input.

The significance of a spatially varying drag coefficient can be approximated by comparing the model output of all wind classes for two cases: a case with the local optimal drag coefficient (average of all wind classes (Table A.2)) and the reference case. An example of this comparison is provided in Table 5.2, at measurement station Stavoren. For this location the average improvement in terms of KGE is 0.13, as the average KGE increased from 0.62 to 0.75. Moreover, the potential for improvement is 0.38 and this is fulfilled with 34%. Also, the null hypothesis, that there is no improvement at a significance level of 5% can be rejected, as $t_{stat} = 2.33 > t_{crit} = 1.80$, and subsequently $P(T \leq t; H_0) = P(T(11) \leq 2.33) = 0.02 < 0.05$.

Local optimal wind drag coefficients (x0.001)
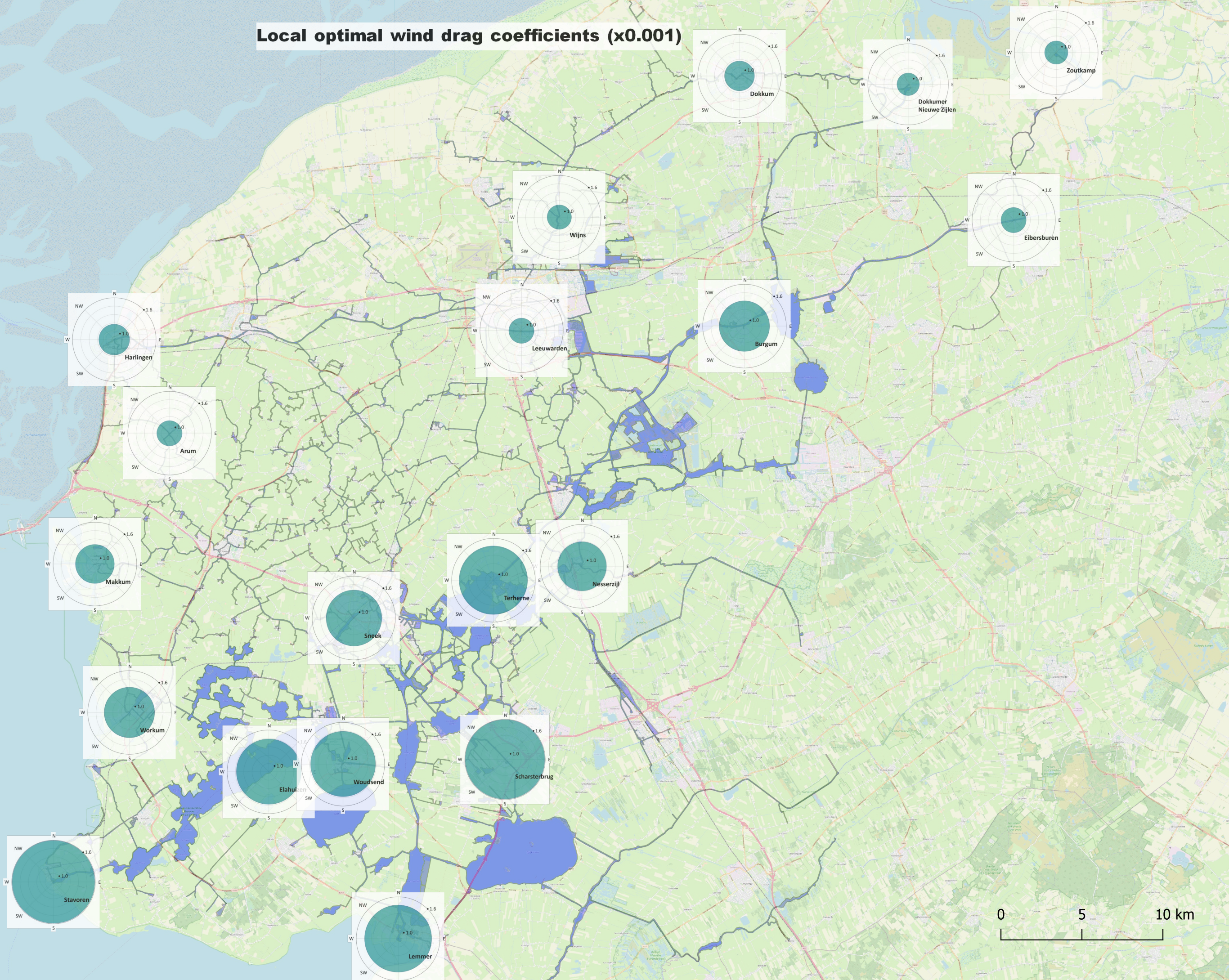
Domain-wide optimal C_D $[\times 10^{-3}]$ per wind direction
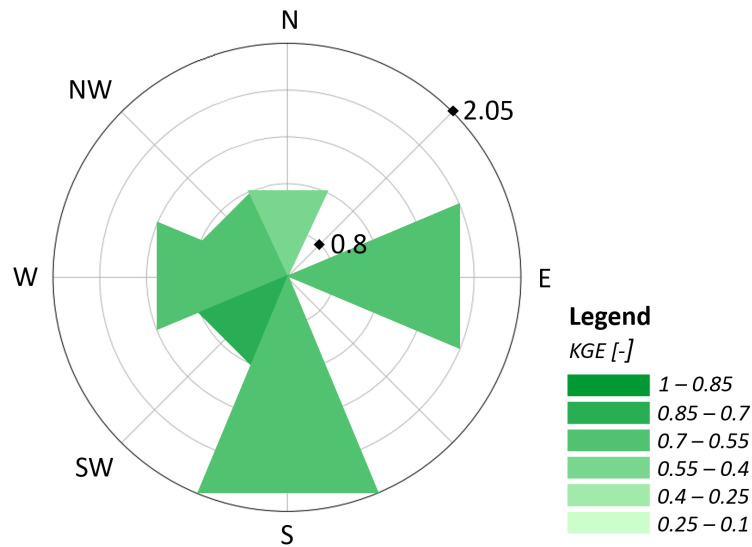
Figure 5.1: Domain-wide optimal $C_D[\times 10^{-3}]$ per wind direction expressed as size of the triangle, with corresponding KGE values expressed as fill color. For wind classes W, NW and SW the average values are displayed

Wind directional dependency

The wind directional dependency was examined based on the domain-wide optimal drag coefficients per wind direction (averaged over all locations). Figure 5.1 provides an overview of the wind directional dependency by providing the domain-wide optimal wind drag coefficients in a wind rose-like plot. The drag coefficients $C_D[-]$ are expressed in the size of the triangle. The lowest values are retrieved for northwestern directions. This can be explained by the dimensions of lakes and canals in line with the wind direction. A northwestern wind direction is perpendicular to this pattern of lakes beginning at the southwestern part of the bosom and going towards a northeastern direction. The fetches are small and wind shielding is more effective. Subsequently, relatively high optimal C_D values are retrieved for eastern and southern directions. The KGE values are also presented, as the fill color, as this gives an indication of the reliability of the results. In case of the directions SW, W and NW three events were calibrated (for different wind speeds). Their average C_D and KGE values are displayed for this reason. That multiple events were calibrated for these directions improves the certainty that exposed patterns in these results exist.

To examine the significance of the improvement, Table 5.3 is provided. This table presents the results of the calibration cases and the reference case per wind class. It provides the domain-wide optimal KGE values per wind class, compared to the KGE values acquired with the reference drag coefficient. This indicates the significance of varying the drag coefficient per wind class. It reveals a small average improvement of the objective function value of 0.04. The potential fulfillment is $+10\%$. Moreover, the null hypothesis, that there is no improvement at a significance level of 5% can be rejected, as $t_{stat} = 3.83 > t_{crit} = 1.80$, and subsequently $P(T \leq t; H_0) = P(T(11) \leq 3.83) = 0.001 < 0.05$. The most significant improvements were found for wind classes 6 Bft E and 6 Bft S, due to the greater differences between their optimal drag coefficient value and the reference drag coefficient.

Table 5.3: The results of the calibration cases and the reference case per wind class: the domain-wide optimal drag coefficient per wind direction with the KGE values and the reference drag coefficient with the KGE values

Wind event	Wind class specific optimal C_D case		Reference case		Potential	Fulfillment
	$C_D \times 10^{-3}$	KGE	$C_D \times 10^{-3}$	KGE		
6 Bft E	1.60	0.56	1.25	0.47	0.53	17%
6 Bft N	1.25	0.48	1.25	0.48	0.52	0%
6 Bft NW	0.95	0.64	1.25	0.58	0.42	14%
6 Bft S	1.85	0.69	1.25	0.57	0.43	28%
6 Bft SW	1.25	0.82	1.25	0.82	0.18	0%
6 Bft W	1.55	0.53	1.25	0.50	0.50	6%
7 Bft NW	1.00	0.74	1.25	0.69	0.31	16%
7 Bft SW	1.10	0.69	1.25	0.67	0.33	6%
7 Bft W	1.10	0.61	1.25	0.57	0.43	9%
8 Bft NW	1.30	0.54	1.25	0.53	0.47	2%
8 Bft SW	1.45	0.72	1.25	0.70	0.30	7%
8 Bft W	1.50	0.67	1.25	0.63	0.37	11%
Avg		**0.64**		**0.60**		**10%**

Wind speed dependency

The wind speed dependency was examined supported with a bar graph, see Figure 5.2. Only for three wind directions the wind speed dependency was examined. Wind events from other directions only occurred at a maximum wind speed of 6 Bft. In order to single out the wind speed dependency only wind events from the same wind direction were compared, such that the wind directional dependency could not interfere with the results. The hypothesised trend, that the wind drag coefficient increases with wind force, was only retrieved for northwestern wind directions. The average of these wind directions decreases between wind forces 6 and 7 Bft, which deviates from the expected trend. However, it increases between wind forces 6 and 8 Bft and 7 and 8 Bft. Nevertheless, the results were inconclusive and the data sample was too small to substantiate the wind speed dependency and to test the statistical significance of a possible trend. The improvements retrieved with a varying drag coefficient per wind class were therefore attributed to the wind directional dependency.

Spatial and wind directional dependency

To examine a combination of the spatial and wind directional dependency, an overview of the Frisian bosom was composed. This overview includes the local optimal drag coefficients per wind direction and is presented on page 34. The local optimal drag coefficients $C_D[-]$ are provided per wind direction and the values are expressed in the size of the triangle. Also, the fill color corresponds to the KGE value of the simulation(s) and for directions SW, W and NW the results are averaged.

A large spatial variation in optimal wind drag coefficient values and per wind direction can be observed. This is due to great differences in water body dimensions, in surrounding objects (causing wind shielding) and/ or in the local surface roughness.
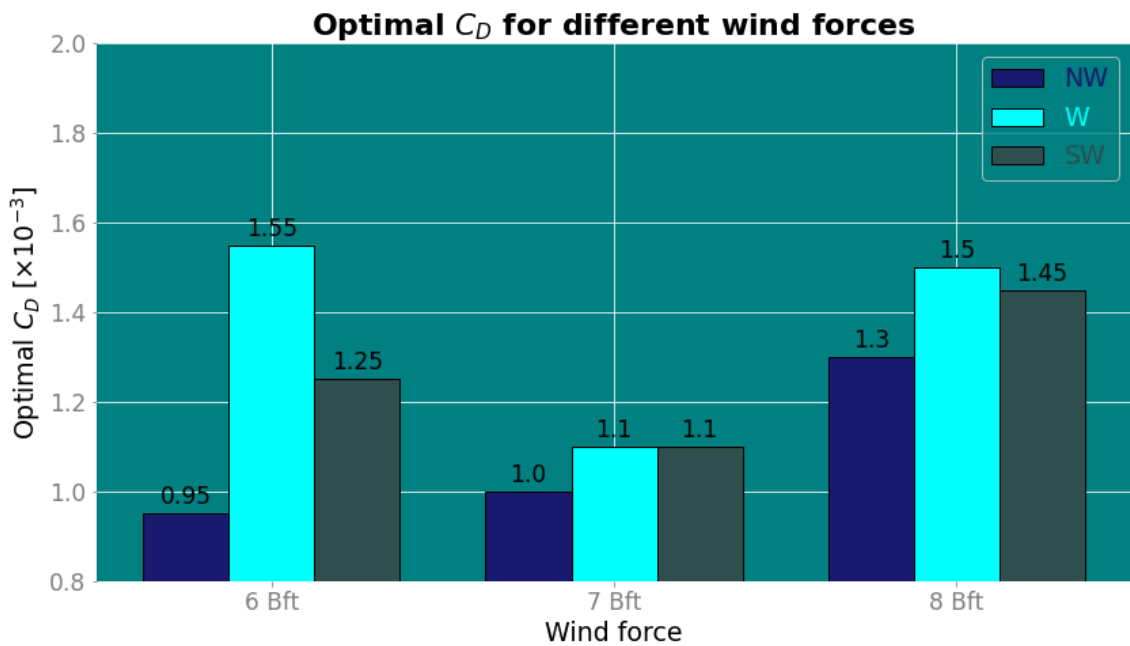
Figure 5.2: The optimal $C_D \times 10^{-3}$ for the wind directions NW, W and SW for different wind forces

Table 5.4: All local optimal drag coefficient values per wind direction averaged over all locations such that an optimal per wind direction is retrieved, with corresponding KGE values

Wind direction	Spatially and wind class varying optimal C_D averaged over all locations	
	$C_D \; [\times 10^{-3}]$	KGE
W	1.24	0.74
NW	1.02	0.68
N	1.32	0.78
E	1.46	0.72
S	1.51	0.87
SW	1.31	0.84

Averaged over all locations

All local optimal drag coefficient values per wind direction, with corresponding KGE values were averaged over all locations, such that the results per wind direction could be examined. This gives an indication of the model's potential to predict water levels per wind direction, if spatially varying wind drag coefficients are included. This information is provided in Table 5.4. Once more, it was found that the lowest C_D values were retrieved for a northwestern wind direction and the highest for eastern and southern directions. It was also found that southern and southwestern directions were more accurately modelled than the other directions and that wind events from the northwestern directed wind classes are the least accurately represented by the model. This might also be explained by the smaller fetches in line with this wind direction, relatively increasing the effect of wind shielding, complicating the model's ability to accurately represent the wind effects.

Local optimal wind drag coefficients per wind direction (x0.001) [-]

Legend

KGE [-]

- 1 − 0.85
- 0.85 − 0.7
- 0.7 − 0.55
- 0.55 − 0.4
- 0.4 − 0.25

0   5   10 km
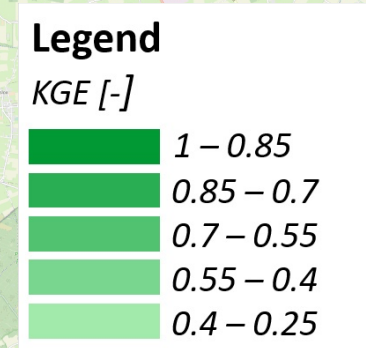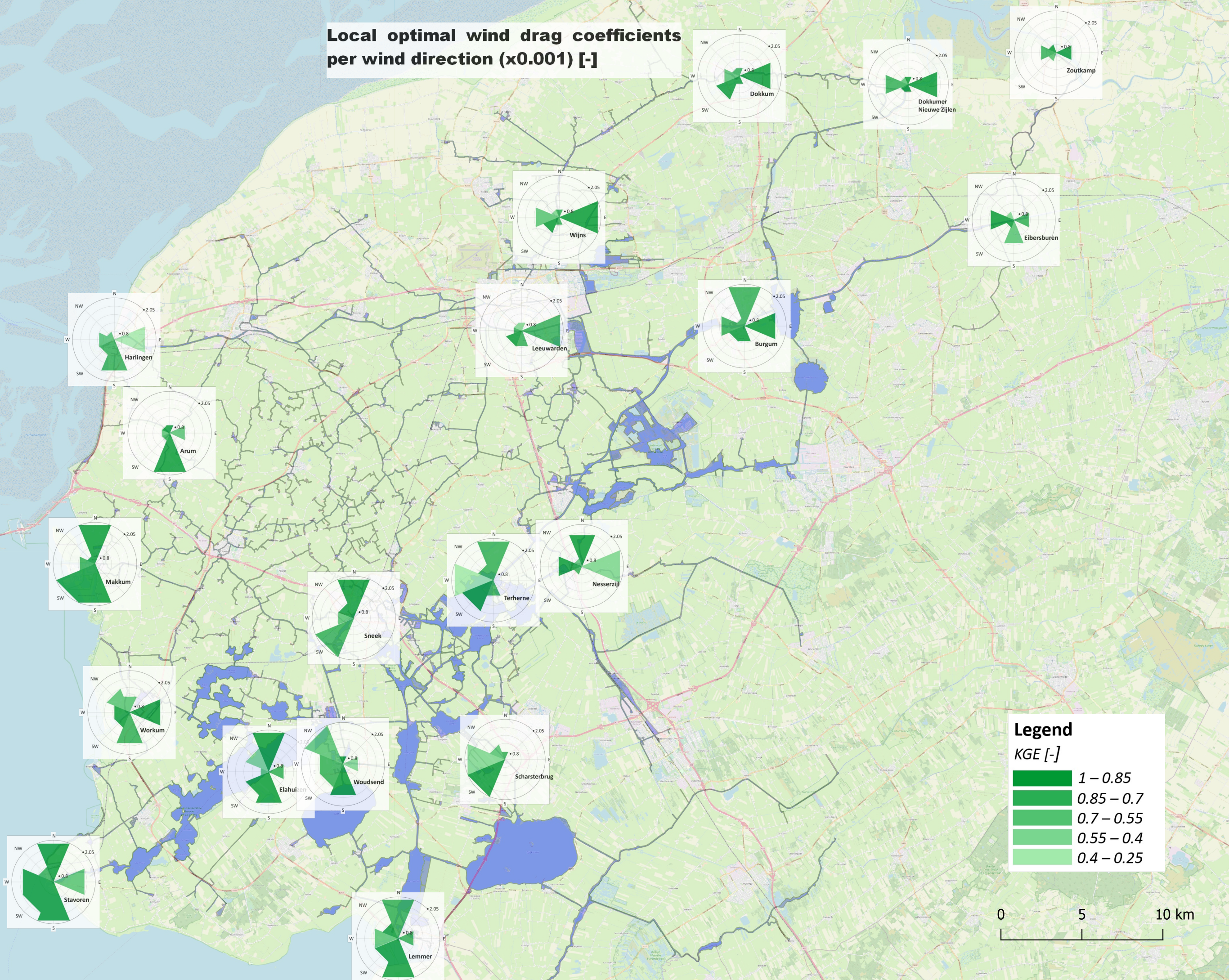
Table 5.5: All local optimal drag coefficient values per wind direction averaged over all wind classes such that an optimal per location is retrieved, with corresponding KGE values

Location	Spatially and wind class varying optimal C_D averaged over all wind classes	
	C_D $[\times 10^{-3}]$	KGE
Scharsterbrug	1.59	0.67
Stavoren	1.59	0.85
Terherne	1.46	0.75
Lemmer	1.45	0.83
Elahuizen	1.44	0.78
Woudsend	1.44	0.73
Sneek	1.34	0.78
Burgum	1.30	0.81
Workum	1.30	0.86
Nesserzijl	1.29	0.74
Makkum	1.20	0.86
Harlingen	1.12	0.65
Tacozijl	1.12	0.79
Dokkum	1.11	0.81
Arum	1.08	0.72
Eibersburen	1.08	0.75
Leeuwarden	1.08	0.68
Wijns	1.07	0.69
Dokkumer NZ	1.06	0.75
Zoutkamp	1.06	0.73

Averaged over all wind directions

All local optimal drag coefficient values per wind direction averaged over all wind classes such that a local optimal is retrieved, with corresponding KGE values, are provided in Table 5.5. This gives an indication of the model's potential to predict water levels per location, if wind directional varying drag coefficients are included. These KGE values are significantly higher than the KGE values in Table 5.1 with domain-wide wind drag coefficients.

Furthermore, it was found that the most accurately simulated locations were Makkum, Workum, Stavoren and Lemmer. These are all located at the boundaries of the southwestern part of the bosom. Most wind events used during this study orientate from a western direction (W, NW and SW). At these locations the most significant wind set-down occurs. This effect was found to be captured accurately by the model, with means of calibration of the wind drag coefficient.

The significance of a drag coefficient varying spatially, as well as per wind class, can be approximated by comparing the model output of two cases: a case combining all local optimal drag coefficient values per wind class and the reference case with the most reference drag coefficient. An example of this comparison is provided in Table 5.6, at measurement station Stavoren. For this location the KGE improves overall with 0.23.

Table 5.6: Comparison of a case combining all local optimal drag coefficient values per wind class and the reference case, at measurement station Stavoren

		Wind event
		6E	**6N**	**6NW**	**6S**	**6SW**	**6W**	**7NW**	**7SW**	**7W**	**8NW**	**8SW**	**8W**	**Avg**
Loc. case	C_D	1.60	2.00	1.10	2.05	1.4	1.35	1.00	1.80	1.80	1.40	1.80	1.80	**1.59**
	KGE	0.61	0.97	0.85	0.88	0.95	0.95	0.87	0.93	0.77	0.60	0.90	0.88	**0.85**
Ref. case	C_D	1.25	1.25	1.25	1.25	1.25	1.25	1.25	1.25	1.25	1.25	1.25	1.25	**1.25**
	KGE	0.45	0.80	0.84	0.29	0.85	0.94	0.79	0.63	0.41	0.60	0.49	0.36	**0.62**

This comparison has been extended for the significance at all measurement stations. These comparisons are summarised in Figure 5.3, where the average values are provided. Examining the differences between the average of these average KGE values provides information on the overall improvement. The overall improvement of this model with a drag coefficient varying spatially, as well as per wind class, is approximated at 0.18 in terms of the KGE, from 0.58 to 0.76. The null hypothesis, that there is no improvement at a significance level of 5% can be rejected, as $t_{stat} = 14.42 > t_{crit} = 1.73$, and subsequently $P(T \leq t; H_0) = P(T(19) \leq 14.42) = (<< 0.001) < 0.05$. Moreover, the average potential fulfillment is $+44\%$, indicating that the model accuracy increased significantly.
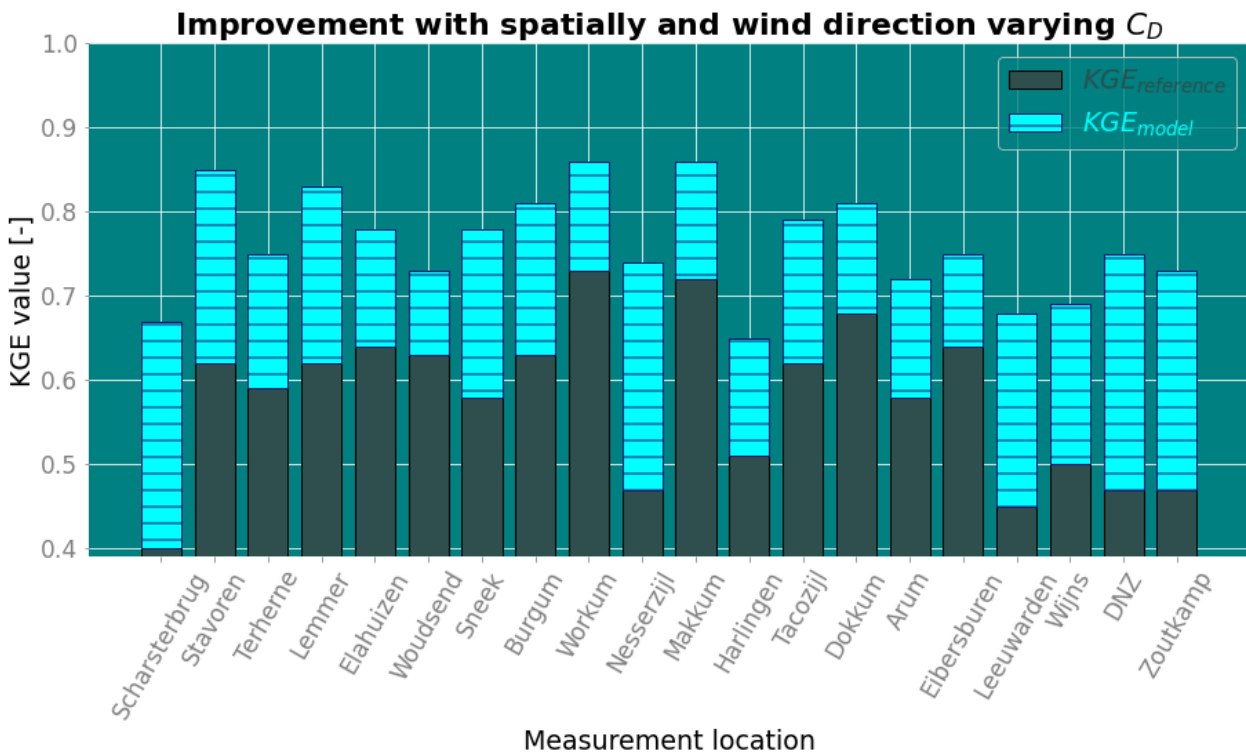
Figure 5.3: The model improvement with spatial and wind directional variability of the drag coefficient as compared to the reference case, in terms of KGE

Table 5.7: A rough summary of the significance of the wind drag dependencies

		Relation found?	Significance determined?	Overall KGE increase	Overall potential fulfilment	Statistically significant?
Dependency	Spatial	Yes	No			
	Direction	Yes	Yes	0.04	10%	Yes
	Direction & spatial	Yes	Yes	0.18	44%	Yes
	Speed	No	No			

Furthermore, some graphical representations of the improved water level predictions are provided:

- Figure 5.4 presents the water levels at Stavoren during wind event 6 Bft S (B) at the local optimal drag coefficient for this wind class and the reference drag coefficient. The reference case deviates up to 25 cm from the observations, while the simulation with the local optimal drag coefficient for this wind class stays within a margin of 10 cm from the observations.

- Figure 5.5 presents the water levels at Lemmer during wind event 8 Bft SW (A) at the local optimal drag coefficient for this wind class and the reference drag coefficient. The reference case and the simulation with the local optimal drag coefficient for this wind class deviate up to 3 cm compared to each other. Both simulations stay within a margin of 10 cm from the observations.

- Figure 5.6 presents the water levels at Stavoren during wind event 8 Bft W (A) at the local optimal drag coefficient for this wind class and the reference drag coefficient. The reference case deviates up to 30 cm from the observations, while the the simulation with the local optimal drag coefficient for this wind class stays within a margin of 20 cm from the observations.

So, the magnitude of the improvement varies highly per wind event. It depends on the magnitude of the wind set-up, as well as on the relative difference between values of the optimal wind drag coefficients and the reference drag coefficients. More graphical representations of these improvements are provided at various locations at various wind classes in Appendix B.

Will the set-up predictions improve with a varying wind drag coefficient?

The results of this study are summarised in Table 5.7. Based on these results there is good reason to believe that the wind set-up predictions of a hydrodynamic model on a shallow, fetch-limited water system will improve if a spatially and/ or wind direction varying wind drag coefficient is included. It was found that the model improvements were statistically significant.

Wind: 6 Bft S (event B) with a C_D of 2.05e-03 and 1.25e-03
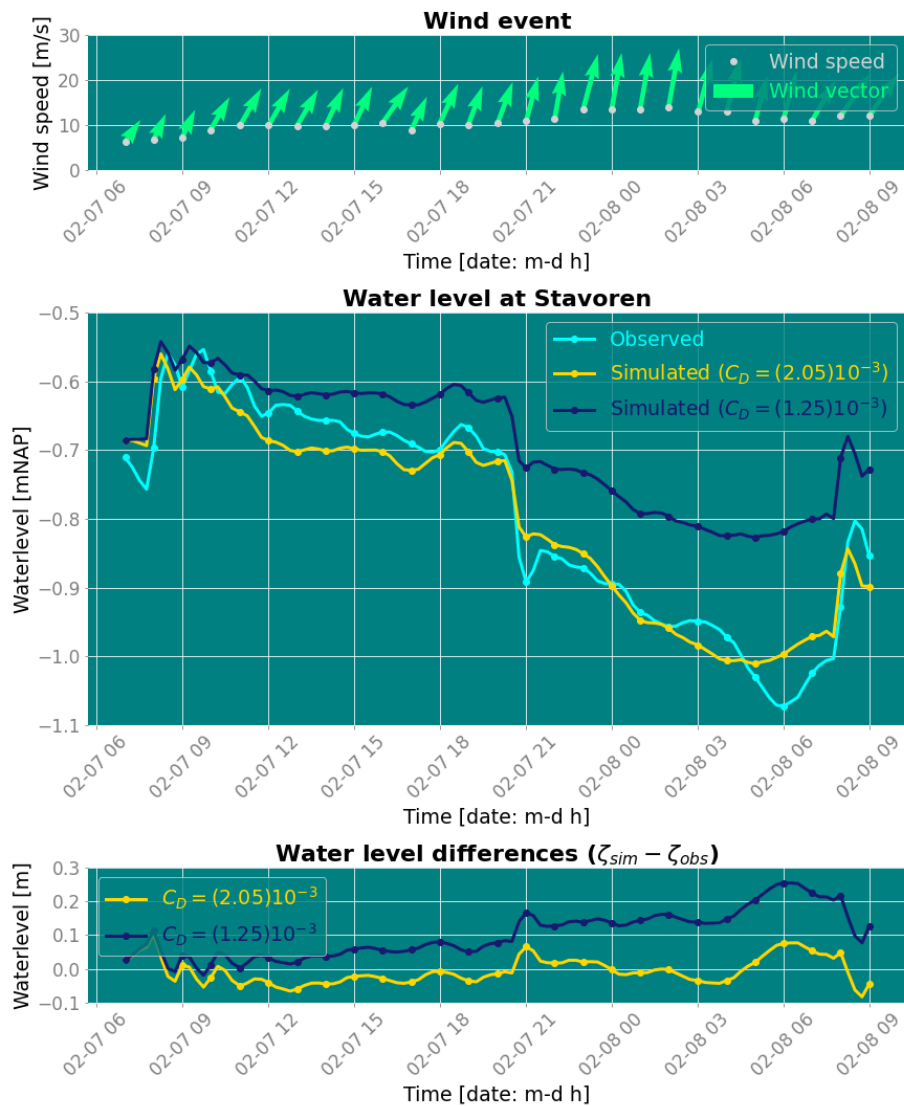
Figure 5.4: Water levels at Stavoren during event 6 Bft S (B) at a local optimal C_D of $2.05 \times 10^{-3}[-]$ (KGE$= 0.88$) in comparison to the uniform optimal C_D of $1.25 \times 10^{-3}[-]$ (KGE$= 0.29$)
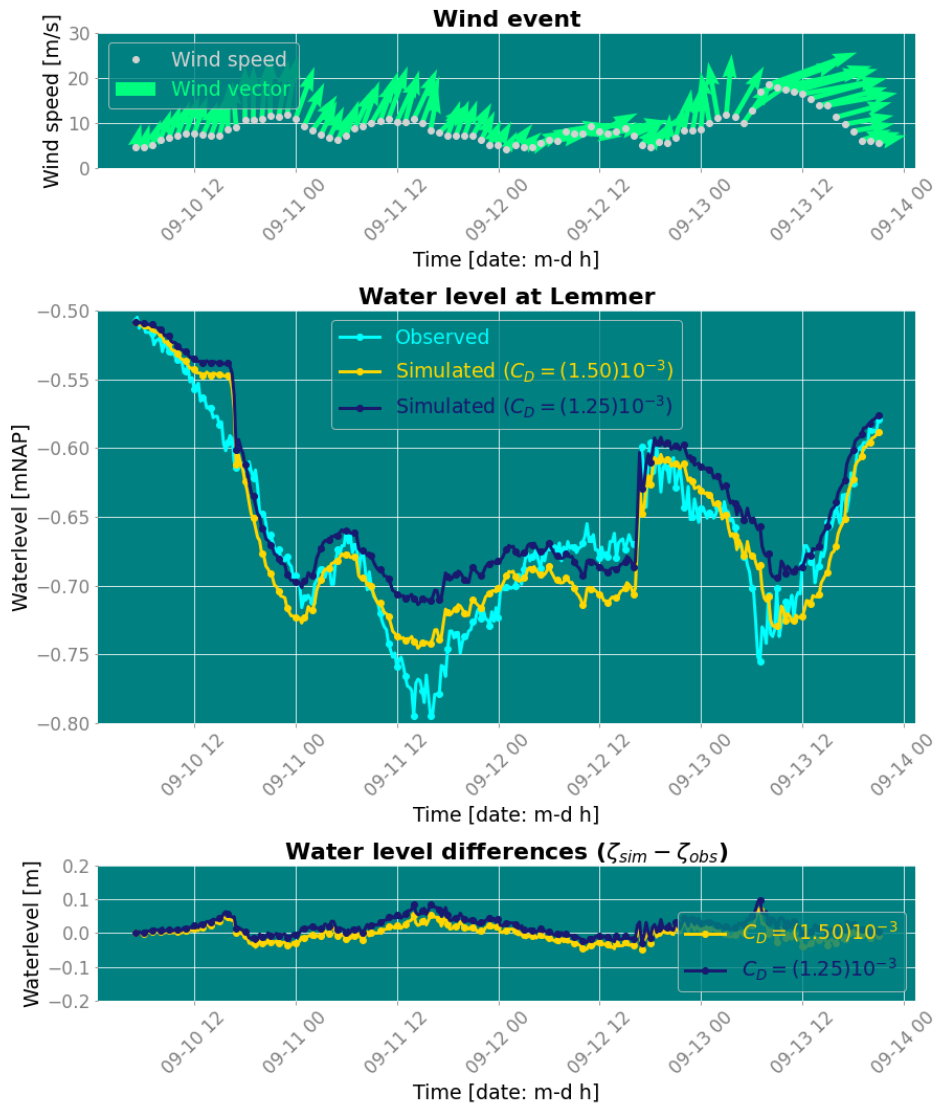
Figure 5.5: Water levels at Lemmer during event 6 Bft S (B) at a local optimal C_D of $1.50 \times 10^{-3}[-]$ (KGE$= 0.94$) in comparison to the uniform optimal C_D of $1.25 \times 10^{-3}[-]$ (KGE$= 0.88$)

Wind: 8 Bft W (event A) with a C_D of 1.80e-03 and 1.25e-03
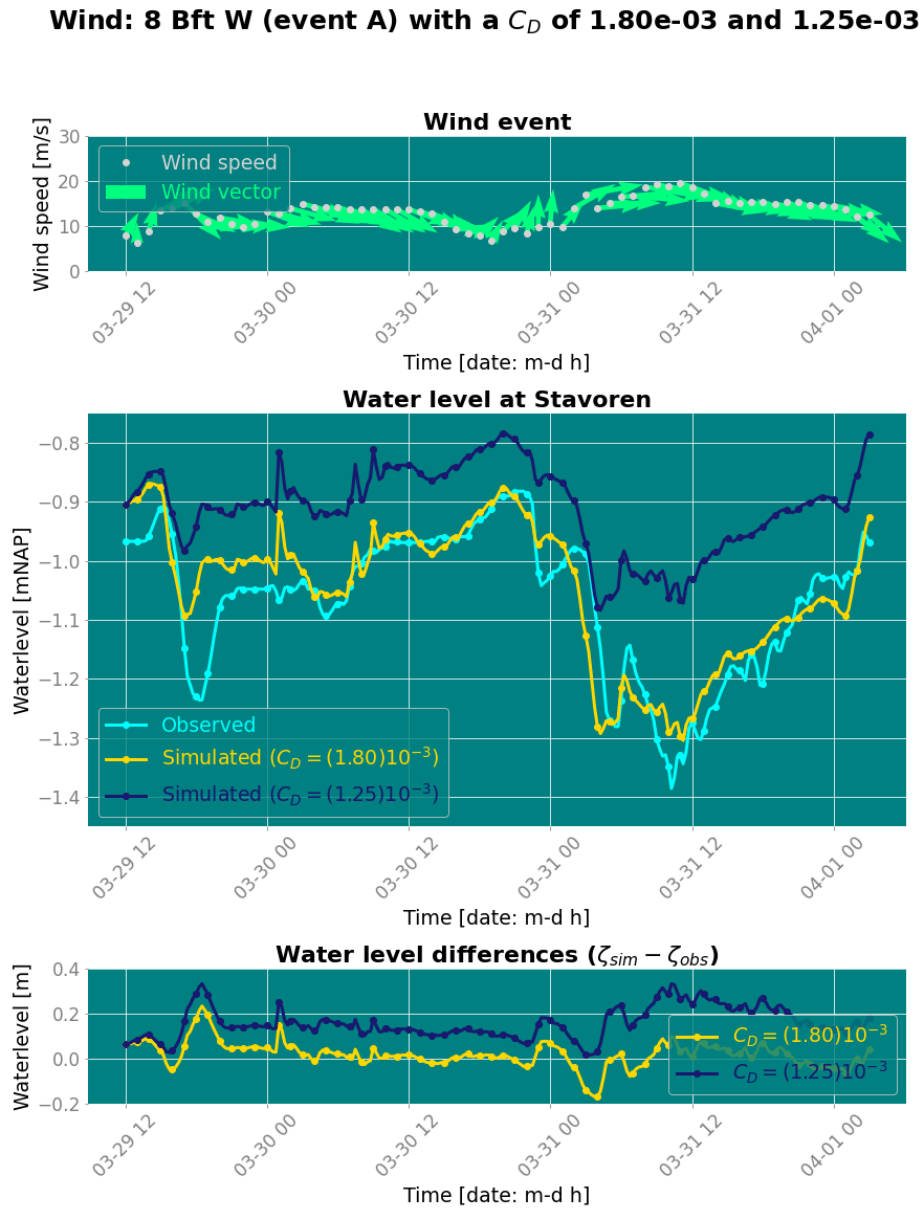
Figure 5.6: Water levels at Stavoren during event 8 Bft W (A) at a local optimal C_D of $1.80 \times 10^{-3}[-]$ (KGE= 0.88) in comparison to the uniform optimal C_D of $1.25 \times 10^{-3}[-]$ (KGE= 0.36)

Chapter 6

Discussion

Limited information was available on the wind drag coefficient in hydrodynamic models of fetch-limited, inland water systems. This study examined whether, and to what extent, the wind drag coefficient in a shallow, fetch-limited, inland water system varied spatially and/ or with the wind direction and wind speed. Moreover, this study examined whether the wind drag coefficient in models should vary for these dependencies to improve model predictions of water levels. The implications of this study are discussed in this chapter. Section 6.1 discusses the implication of the methodology, where strong features, limitations and uncertainties are reviewed. Furthermore, Section 6.2 discusses the implications of the results and Section 6.3 provides recommendations for follow-up research.

6.1 Implications of the methodology

To determine if and to what extent the wind drag coefficient depended on the three described dependencies, different historical wind events were simulated in the Frisian bosom by means of a 3Di hydrodynamic 2D model. Calibration was performed to determine differences in optimal wind drag coefficients. This section reviews the implication of the conducted methodology, as the selected research method can influence the results and consequently, the conclusions drawn from the study.

6.1.1 Data and hydrodynamic model

A hydrodynamic 2D model was set up with 3Di and QGIS software. Strong features of this model were the fine computational grid cells, the relatively short simulation time and the inclusion of the bathymetry at a fine resolution of 2 m by 2 m. Moreover, boundary conditions were based upon observed discharge time series at a fifteen minute time step, which is a relatively small time step, enabling more accurate results.

Every hydrodynamic model is associated with uncertainties. In this specific case, the uncertainty of modelling wind effects on inland water systems are the small-scale variations in the wind profile. Furtermore, the uncertainties of this study were:

1. Possible model inaccuracies in the bathymetry and bottom friction. The bathymetry was realised based upon interpolation of measurement data at a coarse resolution and a large number of small waterways was not included in the depth measurements. Furthermore, no information on the bottom friction could be provided for this study site by experts. The coefficient was specified based on a quick analysis of a number of model results with varying Manning values.

41

2. Limitations to the number of wind events that could be analysed. More wind events could not be analysed, because the water level and discharge measurements were provided at a limited time period of five years. Strong sustaining wind events were relatively scarce and classification into finer wind classes was not feasible. Moreover, as a results of this data limitation, it was not feasible to calibrate multiple wind events per wind class.

3. Possible inaccuracies in the measurement data:
   - The wind velocities were provided at a very coarse spatial resolution, and additionally, at a relatively coarse time step of an hour. Spatial variation in wind speeds and the effects of wind gusts were therefore not incorporated.
   - It was found that a few locations were susceptive to noise in their water level measurements. This affected the reliability of the model accuracy assessment at one location.
   - The outgoing discharges from the bosom to external water bodies were based on computations and might deviate from the actual unknown discharges (Vellinga, 2020).

6.1.2 Calibration method

A calibration method was set up and used to optimise the wind drag coefficient. Strong features of this calibration method were the increased efficiency due to the automated procedure and the reduced interval size in between stages and the precision of the derived optimal drag coefficient. The precision of the C_D value was 5×10^{-5}, with which a simulated water level precision of approximately 1 cm was achieved.

An uncertainty in this calibration method was the model initialisation, as at various wind events an offset was displayed between the simulated and the observed water levels at the start of the event. Nevertheless, the impact of the initialisation error on the derived optimal drag coefficient was minimised by using the KGE objective function, as it included the trend in water levels in its assessment. If this model is deployed for water level predictions, it can be updated by means of error correction to diminish initialisation errors. Therefore, it is important to capture the trend in water levels.

Furthermore, during the assessments the average objective function values were computed as a weighted average. These weights were defined for every measurement location, based on the observed wind set-up (or set-down). This was done to direct the calibration of domain-wide drag coefficients based on locations were wind set-up (or set-down) occurs, as accurate predictions of these locations are meaningful information for water managers. The implication of these weights can be derived from Table A.2, displaying an increase in domain-wide drag coefficient values for most wind classes and slightly increasing the variations. However in hindsight, the results following from this study are not much affected by the choice to apply weights. Additionally, the four locations with the lowest objective function value were excluded from the assessment. Arguably, this was justified, as it was found that the simulated water level at some measurement locations never aligned with the observations, regardless of the wind drag coefficient value.

6.2 Implications of the results

This study is the first to demonstrate the significance of wind drag dependencies in a fetch-limited, inland water system. The results can be used as a first stepping stone to improve hydrodynamic modelling of wind effects. It can also clarify inaccuracies in current hydrodynamic models of inland water systems.

However, the results are accompanied with some uncertainties. The model improvements, retrieved with the varying wind drag coefficients for different dependencies, are approximations. The coefficient was not actually varied spatially during the simulation, and changing the drag coefficient at a single location can effect the flow throughout the entire system. Moreover, the wind drag coefficient was also stationary for varying wind directions during the simulations.

Another uncertainty was that the significance of the spatial dependency could only be approximated for one measurement location. Therefore, the significance of a spatially varying drag coefficient was not substantiated. Nevertheless, there is a high likeability that this improvement would have been found for other locations, based on the results of the 'spatial and wind directional dependency'.

6.3 Recommendations for follow-up research

In this section recommendations for follow-up research are provided, with in Subsection 6.3.1 general recommendations and in Subsection 6.3.2 recommendations for further research on wind set-up on the Frisian bosom.

6.3.1 General research on wind set-up

The findings in this study gave a good indication of the wind drag coefficient value on inland water systems. It was found in literature that the wind drag coefficient on inland water systems typically ranges between 1×10^{-3} and 2×10^{-3} (Wuest & Lorke, 2003). During this study a larger interval, between 0.8×10^{-3} and 2.05×10^{-3}, was found. However, there were indications that with a wider initial search interval the variations in the retrieved optimal drag coefficient values would be slightly increased. Nevertheless, this did not affect the conclusions drawn from this research. However, it is recommended for follow-up researches to apply a wider initial search interval.

A wind drag coefficient varying spatially and/ or with wind direction should be generally beneficial for the model accuracy of hydrodynamic models of all study areas within the scope of this study. However, follow-up research is needed to validate if these results on wind set-up can be reproduced for another inland water system. In practice, the spatial and directional dependencies can be found in a similar matter as in this study, by calibrating different wind events at different measurement locations. However, it is also possible to implement the opportunity to vary the wind drag coefficient in a hydrodynamic model. Calibration of such a model can demonstrate the wind drag dependencies and model improvements explicitly.

Furthermore, such a study can possibly provide parameterisations of the relation between water body geometry, shielding, wind characteristics and the momentum transmission (drag coefficient). Moreover, such a research with a varying wind drag coefficient can substantiate if wind speed affects the C_D value and for what conditions. However, this can likely only be substantiated on a study area where (small) waves are common.

The significance of the model improvement, by including the spatial and directional dependencies, will vary based on the study area characteristics. Naturally, for study areas where wind set-up is a more significant phenomenon, the model improvements will be greater. This will be the case for study areas of greater size and a smaller water depth. Furthermore, the spatial and directional fluctuations of the drag coefficient will be greater for study areas with varying fetch sizes, different types of wind shielding and roughness changes.

6.3.2 Research on wind set-up in the Frisian bosom

Follow-up research on the wind drag coefficient dependencies in the Frisian bosom can be performed by implementing a varying wind drag coefficient in the 3Di software. Such a study can demonstrate the accuracy of the model improvement approximations found in this study. During follow-up researches part of the problem associated with the limited observational data can be overcome with a cross-validation method. The advantages of this method are: it results in a better estimate of the model accuracy and it is more efficient as the data of every wind event is used for both calibrating and validating. This method is further introduced in Appendix E. Furthermore, in order to improve the hydrodynamic model more insight on the bottom friction can be derived by means of field measurements or calibration. Additionally, more bed level measurements can improve the DEM.

Chapter 7

Conclusion

Limited information was available on the wind drag coefficient in hydrodynamic models of shallow, fetch-limited, inland water systems. This study examined whether, and to what extent, the wind drag coefficient in a shallow, fetch-limited, inland water system varied spatially and/ or with the wind characteristics. Moreover, this study examined whether the wind drag coefficient should vary for these dependencies to improve hydrodynamic model predictions of water levels. The sub-questions of this research were:

To what extend does the optimal wind drag coefficient in a hydrodynamic model vary spatially on a shallow, fetch-limited water system?

To what extend does the optimal wind drag coefficient in a hydrodynamic model vary with wind direction on a shallow, fetch-limited water system?

To what extend does the optimal wind drag coefficient in a hydrodynamic model vary with wind speed on a shallow, fetch-limited water system?

Is there good reason to believe that the wind set-up predictions of a hydrodynamic model on a shallow, fetch-limited water system will improve if a spatially varying, a wind direction varying and/ or a wind speed varying wind drag coefficient is included?

Spatial dependency

This study demonstrated a relation between the location in the water system and the optimal wind drag coefficient. The local optimal drag coefficient values varied over the entire search interval of 0.8×10^{-3} to 2.05×10^{-3}. Overall, the drag coefficient was significantly higher for areas with larger water bodies. These areas with wide and long fetches allocated more momentum transmission between the water and the wind as shielding is less impactful. The significance of a spatially varying drag coefficient was approximated at a single location in the bosom area, Stavoren. For this location the average improvement was 0.13 in terms of the KGE, where 34% of the KGE potential was fulfilled. Moreover, the statistical significance of this improvement was demonstrated.

Wind directional dependency

A relation between the wind direction and the domain-wide optimal wind drag coefficient was demonstrated. It was found that for small fetches, due to the geometry of the water bodies in-line with the wind direction, the wind shielding was more effective and optimal drag coefficient values were smaller. The local optimal drag coefficient values varied between 1.08×10^{-3} to 1.85×10^{-3}. Nevertheless, the significance of this improvement was found to be small. The average improvement for all wind classes was 0.04 in terms of the KGE, where 10% of the KGE potential was fulfilled. The statistical significance of this improvement was demonstrated. The most significant improvements were found for wind classes with greater differences between their optimal drag coefficient value and the reference drag coefficient.

Spatial and wind directional dependency

This study demonstrated a relation between the location in the water system, the wind direction and the local optimal wind drag coefficient. The local optimal drag coefficient values per wind direction varied over the entire search interval. The overall accuracy of the model improved with a drag coefficient varying spatially, as well as per wind direction, with approximately 0.18 in terms of the KGE, where 44% of the KGE potential was fulfilled. It was found that the model improvements were statistically significant.

Wind speed dependency

The results on the speed dependency of the wind drag coefficient were inconclusive. The data sample was too small to substantiate the wind speed dependency and to test the statistical significance of a possible trend.

Will the set-up predictions improve with a varying wind drag coefficient?

It was found that there is good reason to believe that the wind set-up predictions of a hydrodynamic model on a shallow, fetch-limited water system will improve if a spatially and/ or wind direction varying wind drag coefficient is included. Follow-up research on the wind drag coefficient dependencies can be performed by implementing the opportunity to vary the wind drag coefficient in a hydrodynamic model. This can demonstrate the wind drag dependencies and model improvements explicitly. The results found in this study are approximations, as the wind drag coefficient was not varied spatially or during a simulation for different wind characteristics.

References

Abbasi, A., Annor, F. O., & van de Giesen, N. (2017, December). A framework to simulate small shallow inland water bodies in semi-arid regions. *Advanced in Water Resources*, *110*, 77–96. Retrieved 10-09-2020, from `https://doi.org/10.1016/j.advwatres.2017.09.023`

Barqo. (2018). *Een dag varen op het tjeukemeer.* Retrieved 28-02-2021, from `https://barqo.co/blog/community/dag-varen-op-tjeukemeer`

Casulli, V. (2009). A high-resolution wetting and drying algorithm for free-surface hydrodynamics. *International Journal for Numerical Methods in Fluids*, *60*, 391–408. Retrieved 10-02-2021, from `https://doi.org/10.1002/fld.1896`

Cheng, F., Zang, C., Brett, M. T., & Nielsen, J. M. (2020, September). The importance of the wind-drag coefficient parameterization for hydrodynamic modeling of a large shallow lake. *Ecological Informatics*, *59*. Retrieved 09-09-2020, from `https://doi.org/10.1016/j.ecoinf.2020.101106`

Dorst, L. (2003). *Het friese boezemstelsel onder extreme condities* (Master's thesis, Technische Universiteit Delft). Retrieved 28-07-2020, from `https://repository.tudelft.nl/islandora/object/uuid%3Ad1224d85-d8f0-4cf8-b595-40d7d7dfc695`

Downing, J. A., Prairie, Y. T., Cole, J. J., Duarte, C. M., Tranvik, L. J., Striegl, R. G., ... Middelburg, J. J. (2006, September). The global abundance and size distribution of lakes, ponds, and impoundments. *Limnology and Oceanography*, *51*(5), 2388–2397. Retrieved 10-09-2020, from `https://doi-org.ezproxy2.utwente.nl/10.4319/lo.2006.51.5.2388`

Engineering ToolBox. (2004). *Manning's roughness coefficients.* Retrieved 24-12-2020, from `https://www.engineeringtoolbox.com/mannings-roughness-d_799.html`

Google. (n.d.). *3d satellite view of lakes fluessen and heegermeer.* Retrieved 18-01-2021, from `https://www.google.com/maps/@52.850518,5.5272851,10851a,35y,37.87t/data=!3m1!1e3`

Grachev, A. A., Fairall, C. V., & Larsen, S. E. (1998). On the determination of the neutral drag coefficient in the convective boundary layer. *Boundary-Layer Meteorology*, *86*, 257–278. Retrieved 25-08-2020, from `https://doi-org.ezproxy2.utwente.nl/10.1023/A:1000617300732`

Gupta, H. V., Kling, H., Yilmaz, K. K., & Martinez, G. F. (2009, October). Decomposition of the mean squared error and nse performance criteria: Implications for improving hydrological modelling. *Journal of Hydrology*, *377*(1-2), 80–91. Retrieved 12-01-2021, from `https://doi.org/10.1016/j.jhydrol.2009.08.003`

Holmes, J. (2015). *Wind loading of structures* (3rd ed.). CRC Press.

KNMI. (2017, July). *Drag at high wind velocities - a review* (Tech. Rep.). RWS-VWL. Retrieved 07-08-2020, from `http://projects.knmi.nl/publications/fulltexts/sterl_review_drag_tr361_2017.pdf`

Knoben, W. J. M., Freer, J. E., & Woods, R. A. (2019). Technical note: Inherent benchmark or not? comparing nash–sutcliffe and kling–gupta efficiency scores. *Hydrol. Earth Syst. Sci.*, *23*, 4323—4331. Retrieved 27-08-2020, from `https://doi.org/10.5194/hess-23-4323-2019`

Lane, R. (2019). Lake. *Encyclopædia Britannica, inc.* Retrieved 03-08-2020, from `https://www.britannica.com/science/lake`

Liu, S., Ye, Q., Wu, S., & Stive, M. (2018, June). Horizontal circulation patterns in a large shallow lake: Taihu lake, china. *Water*, *10*(792). Retrieved 04-08-2020, from `https://www.mdpi.com/2073-4441/10/6/792/htm`

Markfort, C. D., Perez, A. L. S., Thill, J. W., Jaster, D. A., Porté-Agel, F., & Stefan, H. G. (2010, March). Wind sheltering of a lake by a tree canopy or bluff topography. *Water Resources*

Research, *46*(3). Retrieved 10-09-2020, from `https://doi-org.ezproxy2.utwente.nl/10` `.1029/2009WR007759`

Media-TV. (2020). Lees terug: Storm ciara aan de kust: Honderden meldingen, geen gewonden. *Omroep West*. Retrieved 15-01-2021, from `https://www.omroepwest.nl/nieuws/3995131/` `LEES-TERUG-Storm-Ciara-aan-de-kust-Honderden-meldingen-geen-gewonden`

Mehrafar, H., Azad, M. T., Pasand, M. M., & Raeisi, A. (2018). Calculation of sea surface drag coefficient and wind stress in the gorgan bay. *Research in Marine Sciences*, *3*(4), 379–389. Retrieved 10-08-2020, from `https://www.researchgate.net/publication/330039826` `_Calculation_of_sea_surface_drag_coefficient_and_wind_stress_in_the_Gorgan_Bay`

Nelen & Schuurmans. (2020). *5. wind effects.* Retrieved 08-08-2020, from `https://docs.3di` `.lizard.net/b_wind.html`

Plate, E. J. (1971, January). *Aerodynamic characteristics of atmospheric boundary layers.* (Tech. Rep.). Argonne National Lab., Ill. Karlsruhe Univ. (West Germany). Retrieved 11-01-2021, from `https://doi-org.ezproxy2.utwente.nl/10.2172/4053705`

Pool, S., Vis, M., & Seibert, J. (2018, December). Evaluating model performance: towards a non-parametric variant of the kling-gupta efficiency. *Hydrological Sciences Journal*, *63*, 13–14. Retrieved 12-01-2021, from `https://doi.org/10.1080/02626667.2018.1552002`

Prandtl, L. (1935). *The mechanics of viscous fluids*. Berlin: Aerodynamic Theory III.

Provinsje Fryslân. (2020). *Waterdieptekaart.* Retrieved 18-08-2020, from `https://www.fryslan` `.frl/home/kaarten_3208/item/waterdieptekaart_718.html`

Rao, K. S., Wyngaard, J. C., & Coté, O. R. (1974, April). The structure of the two-dimensional internal boundary layer over a sudden change of surface roughness. *J. Atmos. Sci.*, *31*(3), 738–746. Retrieved 19-08-2020, from `https://doi.org/10.1175/1520-0469(1974)031<0738:TSOTTD>` `2.0.CO;2`

Recoskie, S., Lanteigne, E., & Gueaieb, W. (2017). A high-fidelity energy efficient path planner for unmanned airships. *Robotics*, *6*(28). Retrieved 18-08-2020, from `https://doi.org/10.3390/` `robotics6040028`

Rieder, K., Smith, J., & Weller, R. (1994). Observed directional characteristics of the wind, wind stress, and surface waves on the open ocean. *J. Geophys. Res. - Oceans*, *C11*, 589–596. Retrieved 11-01-2021, from `10.1029/94JC02215`

SailZing. (2018). *Light air on lakes: More wind near the shore?* Retrieved 20-08-2020, from `https://sailzing.com/light-air-on-lakes-more-wind-near-the-shore/`

Schaper, P. (2020, October). personal communication.

Stelling, G. S. (2012). Quadtree flood simulations with sub-grid digital elevation models. *Water Management*, *165*, 567-–580. Retrieved 14-01-2021, from `http://dx.doi.org/10.1680/wama` `.12.00018`

Vakantie Friesland. (2019). *Alles wat je wilt weten over de friese meren.* Retrieved 28-07-2020, from `https://www.vakantiefriesland.com/blog/alles-wat-je-wilt-weten-over-de-friese` `-meren/#:~:text=Friesland%20telt%2024%20offici%C3%ABle%20meren,voor%20kleine%` `20en%20grote%20zeilsport.`

van Rinsum, G. (2015). *Accuracy wind set-up formula for irregularly shaped lakes with a strong varying water depth* (Bachelor's Thesis, TU Delft). Retrieved 05-08-2020, from `https://repository.tudelft.nl/islandora/object/uuid%3Adf28cafb-ffb2` `-4561-90d6-943bfc9dd9f1`

van Waveren, H., Groot, S., Scholten, H., & van Geer, F. C. (1999). *Good modelling practice handbook*. STOWA/RWS-RIZA.

Vellinga, N. (2020, December). personal communication.

Verkaik, J. W. (2006). *On wind and roughness over land* (Doctoral dissertation, Wageningen Universiteit). Retrieved 19-08-2020, from `https://edepot.wur.nl/121786`

Watershed council. (2019). *Seiches.* Retrieved 28-08-2020, from `https://www.watershedcouncil.org/seiches.html#`

Wetterskip Fryslân. (2014, November). *Veiligheidsplan ii eindconcept onderzoeksrapport* (Tech. Rep.). Arcadis. Retrieved 28-07-2020, from `https://www.wetterskipfryslan.nl/documenten-catalogus/algemeen/calamiteiten/veiligheidsplan-ii.pdf`

Wetterskip Fryslân. (2020). *Over ons.* Retrieved 27-07-2020, from `https://www.wetterskipfryslan.nl/over-ons/over-wetterskip`

Wróbel-Niedźwiecka, I., Drozdowska, V., & Piskozub, J. (2019). Effect of drag coefficient formula choice on wind stress climatology in the north atlantic and the european arctic. *Oceanologia*, *61*(3), 291–299. Retrieved 09-08-2020, from `https://doi.org/10.1016/j.oceano.2019.02.002`

Wuest, A., & Lorke, A. (2003). Small-scale hydrodynamics in lakes. *Annu. Rev. Fluid Mech.*, *35*, 373–412. Retrieved 10-09-2020, from `10.1146/annurev.fluid.35.101101.161220`

Appendix A

Tables

Assessment weights and discarded measurement locations

The domain-wide drag coefficient value was computed with weights based on the observed wind set-up. Table A.1 provides an overview of the applied weights, and is ordered based on the sum of the weights. The open spots are discarded locations, with the lowest maximum KGE values for all simulations during calibration stage 1. From this table it is derived that the highest sum of weights are found for the measurement locations (Figure 4.3) at the boundaries of the bosom, as the accumulation effect of wind set-up on the water levels is naturally the largest. Zoutkamp is one of those locations, as the wind set-up was higher than 30 cm for various wind events. Nevertheless, this location has a relatively low sum of weights due to the fact that this location is discarded five out of the twelve times. The discarded locations can also be derived from Table A.1 as the absence of a weight appliance.

One of the five times that Zoutkamp was discarded was due to unavailability of measurement data. Still, with four times left, this is one of the locations with the most inaccurate model performance. Zoutkamp is located at the northeastern boundary of the bosom. This is a location where currents flow towards and accumulation occurs. Wind set-up seems to be easily overestimated at this location. The rate at which this occurs is influenced by the bottom friction and the amount by the momentum transmission (drag coefficient), but also by the bathymetry. These were factors of uncertainty in the model, which is further described in Section 6.1.

The water levels at Scharsterbrug were even harder to accurately represent by the model, as this location is discarded six out of twelve times. This was mainly caused by the vibrations in the measurement data, as mentioned in Section 4.1.1, in combination with low set-up effects, relatively increasing the effects of the vibrations on the KGE value. Event 6NW is an example of this, see Figure B.27. The initialisation of this event had a small offset of 3 cm, but this simulation captured the trend in water level increase quite good. Nevertheless, the KGE was low due to the noise in the measurement data and this location was discarded during the assessment. As mentioned, another location that is susceptive to measurement noise is Burgum. The noise is of the same magnitude of a couple centimeters, but was less noticeable due to the more significant water level variations. Consequently, this location was never discarded.

Table A.1: Weights applied to locations, vertically sorted based on the sum of weights

Location	Wind event												Sum
	6E	6N	6NW	6S	6SW	6W	7NW	7SW	7W	8NW	8SW	8W	
Stavoren	2	2	1	3	2	2	2	3	3	2	3	3	**28**
Dokkumer Nieuwe Zijlen	2	2	1	2	1	2	1	2	2	1	2	3	**21**
Lemmer	1	2	2	2	1	1	2	2	2	2	2	2	**21**
Harlingen	2		1	1	1	2	2	1	2	2	2	3	**19**
Workum	2		1	1	1	2	2	1	2	2	2	3	**19**
Burgum	2	1	1	1	1	2	1	2	1	1	2	2	**17**
Eibersburen	2		1	1	2	2	1	2		2	2	2	**17**
Makkum		1	1	1		2	2	1	2	2	2	3	**17**
Tacozijl	1	2	2	2	1	1	2	2	2		2		**17**
Zoutkamp	3					2	2	2	3		2	3	**17**
Dokkum	2	1	1	1	1		2	2	2		2	2	**16**
Arum	1	1		1		1	2		2	2	2	2	**14**
Wijns	2	1	1	1	1		1	1	1	1		2	**12**
Woudsend	1	1	1	1	1	1		1	2		2	1	**12**
Nesserzijl	2	1			1	2		1		1	1	2	**11**
Leeuwarden	2	1	1	1	1		1	1	1	1			**10**
Elahuizen	1	1	1	1	1	1			1	1			**8**
Scharsterbrug		1			1	1				1	2	2	**8**
Sneek		1	1				1		1	1	2	1	**8**
Terherne		1	1	1	1	1	1	1		1			**8**

Optimal wind drag coefficients

The optimal wind drag coefficient is the drag coefficient for which the simulation resulted in the highest KGE value. Table A.2 gives an overview of these values. The table is horizontally ordered based on wind speed and vertically based on the location with the highest local optimal drag coefficients. The average of the optimal drag coefficient per location is presented in the column on the right. The lowest two rows contain the average optimal drag coefficients per wind event, where the upper row contains the averages without weights and the lowest row contains the weighted averages.

Table 5.1 provides the domain-wide optimal drag coefficients with the KGE values retrieved during calibration. A wide variety in objective function values is noticeable. This can indicate a number of things. That some events were modelled better than others can be explained by the fact that some events were more accurately represented with a domain-wide optimal drag coefficient than others. This indicates that some wind classes will benefit more from a spatially varying wind drag coefficient than other wind classes. However, that some events were modelled better than others might also be partly due to a variety of uncertainties, which is elaborated on in Section 6.1.

Table A.3 provides the optimal wind drag coefficient for all locations bundled per wind direction and includes an average per wind direction. Only the wind directions NW, SW and W were included, as for the other wind directions only one event was simulated and these results can be directly derived from Table A.2. These results are graphically represented and are further elaborated on in the in-depth analysis of the wind drag dependencies (Section 5.3).

Table A.2: The optimal $C_D \times 10^{-3}$ values, with: the local optimal values per wind class in the mid-section, the local optimal values in the columns on the right and the the domain-wide optimal (weighted) values in the bottom rows

Location	6E	6N	6NW	6S	6SW	6W	7NW	7SW	7W	8NW	8SW	8W	Local avg	Local avg (weighted)
Scharsterbrug		0.80			1.60	2.00				1.15	2.00	2.00	**1.59**	
Stavoren	1.60	2.00	1.10	2.05	1.4	1.25	1.00	1.80	1.80	1.40	1.80	1.80	**1.59**	
Terherne		2.00	0.80	1.20	1.45	2.00	1.10	1.80		1.35			**1.46**	
Lemmer	1.20	2.00	1.00	2.00	1.20	1.00	0.80	1.40	1.25	2.00	1.50	2.00	**1.45**	
Elahuizen	1.20	2.00	0.80	1.60	1.30	1.00			1.00	2.00			**1.44**	
Woudsend	1.20	1.00	1.80	1.60	1.00	1.45		1.25	1.25		2.00	1.80	**1.44**	
Sneek		2.00	0.95				1.10		0.95	1.15	2.00	1.20	**1.34**	
Burgum	1.70	1.80	0.80	1.20	1.30	1.80	0.80	1.10	0.80	1.25	1.20	1.80	**1.30**	
Workum	1.20		1.40	1.60	0.80	0.80	1.80	1.00	1.25	1.35	1.55	1.50	**1.30**	
Nesserzijl	2.00	1.70			1.00	1.20		0.80		0.80	1.20	1.60	**1.29**	
Makkum		1.80	0.95	1.90		1.00	1.15	0.80	1.15	1.00	1.00	1.20	**1.20**	
Harlingen	1.75		0.80	1.60	1.20	0.80	0.80	0.80	1.40	0.80	1.35	1.00	**1.12**	
Tacozijl	1.00	0.80	0.95	2.05	1.00	0.80	0.80	1.15	1.15		1.50		**1.12**	
Dokkum	1.55	0.80	0.80	1.00	1.25		0.80	1.15	0.80		1.55	1.35	**1.11**	
Arum	1.20	1.00		2.05		0.80	1.05		1.15	0.80	0.80	0.80	**1.08**	
Eibersburen	1.20		0.95	1.40	1.20	1.60	0.80	0.80		0.80	0.80	1.20	**1.08**	
Leeuwarden	2.00	0.80	0.80	1.20	1.15		0.80	1.40	0.80	0.80			**1.08**	
Wijns	1.80	0.80	0.80	1.00	1.15		0.80	0.95	0.80	0.80		1.80	**1.07**	
Dokkumer NZ	1.55	0.80	0.80	1.00	1.15	2.00	0.80	1.00	0.80	0.80	0.80	1.35	**1.06**	
Zoutkamp	1.20					1.35	0.80	0.80	0.80		1.00	1.45	**1.06**	
Domain-wide avg	**1.46**	**1.41**	**0.97**	**1.53**	**1.20**	**1.31**	**0.95**	**1.13**	**1.07**	**1.14**	**1.38**	**1.49**	**1.25**	
Domain-wide avg (weighted)	**1.60**	**1.25**	**0.95**	**1.85**	**1.25**	**1.55**	**1.00**	**1.10**	**1.10**	**1.30**	**1.45**	**1.50**		**1.33**

Table A.3: Local optimal C_D values sorted by wind direction, for the directions NW, SW and W

	Wind class											
	NorthWest				SouthWest				West			
Location	6NW	7NW	8NW	Avg	6SW	7SW	8SW	Avg	6W	7W	8W	Avg
Scharsterbrug			1.15	1.15	1.60		2.00	1.80	2.00		2.00	2.00
Stavoren	1.10	1.00	1.40	1.17	1.40	1.80	1.80	1.67	1.25	1.80	1.80	1.62
Terherne	0.80	1.10	1.35	1.08	1.45	1.80		1.63	2.00			2.00
Lemmer	1.00	0.80	2.00	1.27	1.20	1.40	1.50	1.37	1.00	1.25	2.00	1.42
Elahuizen	0.80		2.00	1.40	1.30			1.30	1.00	1.00		1.00
Woudsend	1.80			1.80	1.00	1.25	2.00	1.42	1.45	1.25	1.80	1.50
Sneek	0.95	1.10	1.15	1.07			2.00	2.00		0.95	1.20	1.08
Burgum	0.80	0.80	1.25	0.95	1.30	1.10	1.20	1.20	1.80	0.80	1.80	1.47
Workum	1.40	1.80	1.35	1.52	0.80	1.00	1.50	1.12	0.80	1.25	1.50	1.18
Nesserzijl			0.80	0.80	1.00	0.80	1.20	1.00	1.20		1.60	1.40
Makkum	0.95	1.15	1.00	1.03		0.80	1.00	0.90	1.00	1.15	1.20	1.12
Harlingen	0.80	0.80	0.80	0.80	1.20	0.80	1.35	1.12	0.80	1.40	1.00	1.07
Tacozijl	0.95	0.80		0.88	1.00	1.15	1.50	1.22	0.80	1.15		0.98
Dokkum	0.80	0.80		0.80	1.25	1.15	1.55	1.32		0.80	1.35	1.08
Arum		1.05	0.80	0.93			0.80	0.80	0.80	1.15	0.80	0.92
Eibersburen	0.95	0.80	0.80	0.85	1.20	0.80	0.80	0.93	1.60		1.20	1.40
Leeuwarden	0.80	0.80	0.80	0.80	1.15	1.40		1.28		0.80		0.80
Wijns	0.80	0.80	0.80	0.80	1.15	0.95		1.05		0.80	1.80	1.30
Dokkumer Nieuwe Zijlen	0.80	0.80	0.80	0.80	1.15	1.00	0.80	0.98	2.00	0.80	1.35	1.38
Zoutkamp		0.80		0.80		0.80	1.00	0.90	1.35	0.80	1.45	1.20
Avg	**0.97**	**0.95**	**1.14**	**1.03**	**1.20**	**1.13**	**1.38**	**1.25**	**1.31**	**1.07**	**1.49**	**1.30**
Weighted avg	**0.95**	**1.00**	**1.30**	**1.08**	**1.25**	**1.10**	**1.45**	**1.27**	**1.55**	**1.10**	**1.50**	**1.38**

Appendix B

Graphs

This appendix provides additional graphs, which are referred to in the report or serve as background information. Section B provides the wind velocity time series of all wind events and Section B provides a collection of water level time series.

Wind events

Subsection 4.1.1 elaborates by what method wind data was collected and by what means the wind events were categorized. Table 4.1 defines the wind events that were used for calibration and validation of the hydrodynamic model. However, the actual course of the individual wind events was not further specified. This section includes the wind velocity time series of each event. This provides a good overview of the course of the event and their differences in length, wind direction and wind speed. Figure B.1 to Figure B.26 represent these wind events, where the dots indicate the wind speed and the arrows the wind velocity vectors (direction and magnitude).

Water level simulations

Location Scharsterbrug

The water levels at Scharsterbrug were hard to accurate represent by the model. This was mainly caused by vibrations in the measurement data in combination with low set-up effects, relatively increasing the effects of the vibrations on the KGE value. The time series of event 6NW, an example of this, are provided in Figure B.27. Important note: the y-axis is scaled to the wind set-up, so the differences are actually quite small. The initialisation of this event is slightly off, with a small offset of 3 cm. But this simulation captured the trend in water level increase quite good. Nevertheless, the KGE was low due to the noise in the measurement data.

Improvements in comparison to the reference case

This subsection provides graphical representations of the improvement of the model with a drag coefficient varying spatially, as well as per wind class at various locations at various wind classes. The following wind classes are included: 6 Bft S, 6 Bft W, 7 Bft SW, 8 Bft SW and 8 Bft W, at the following measurement stations: Stavoren, Lemmer, Makkum, Burgum and Dokkum. The graphs (Figure B.28 to Figure B.48) are categorised based on the wind class.
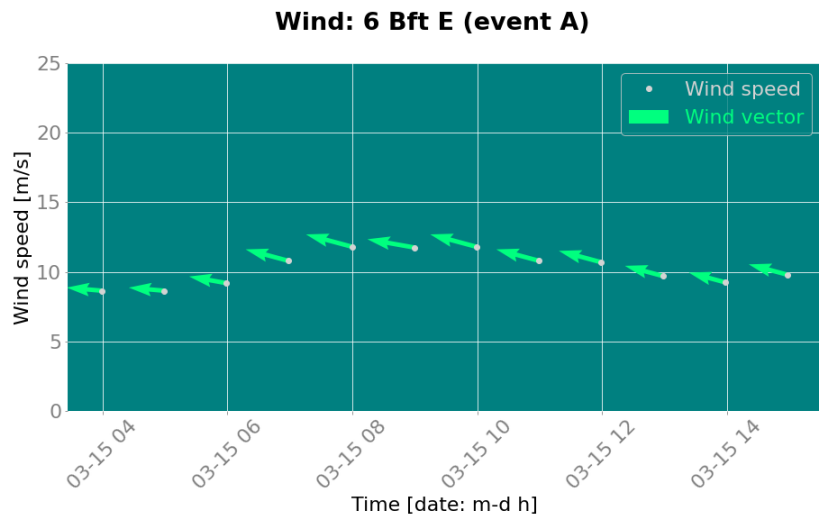
Wind: 6 Bft E (event A)

Figure B.1: Wind velocity time series: 6 Bft E (event A)

Wind: 6 Bft E (event B)
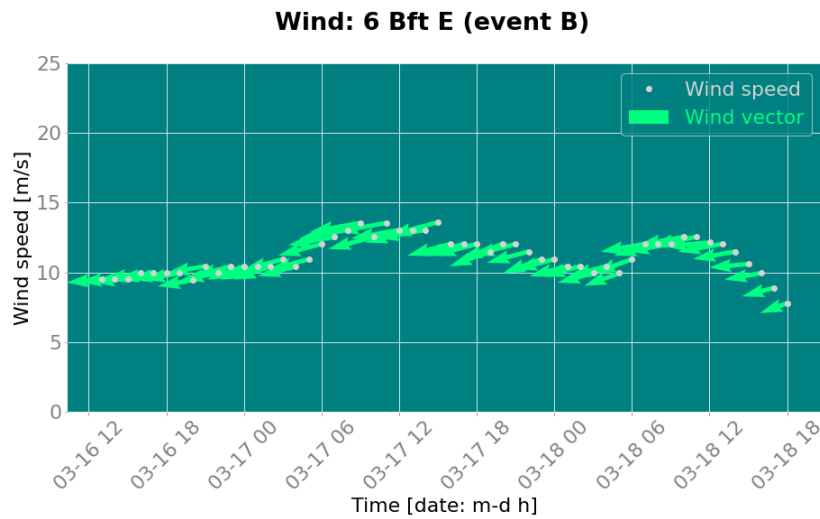
Figure B.2: Wind velocity time series: 6 Bft B (event A)
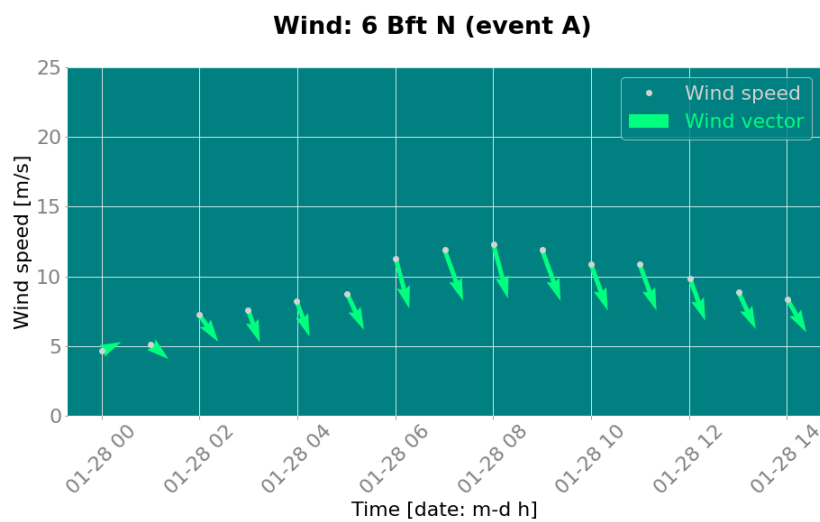
Wind: 6 Bft N (event A)

Figure B.3: Wind velocity time series: 6 Bft N (event A)
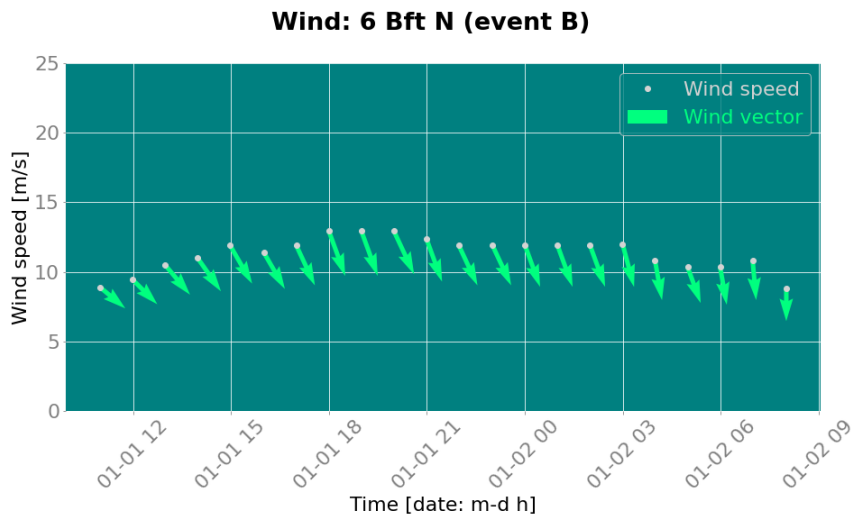
Wind: 6 Bft N (event B)

Figure B.4: Wind velocity time series: 6 Bft N (event B)
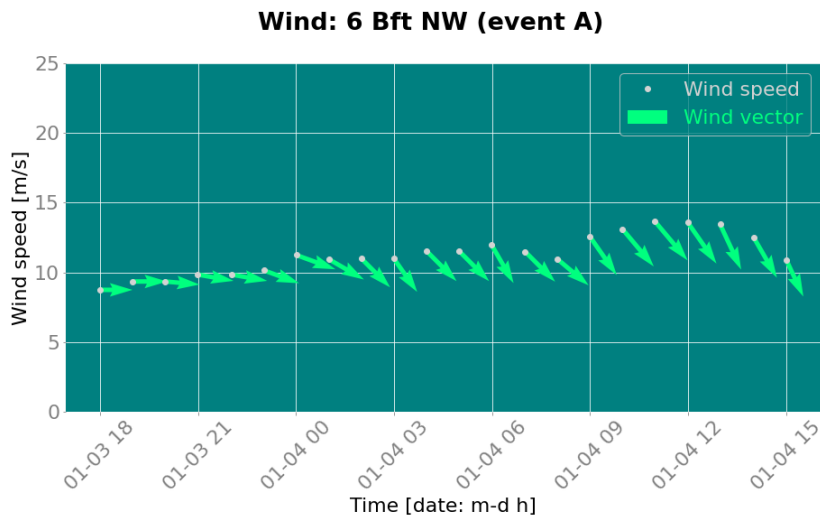
Wind: 6 Bft NW (event A)

Figure B.5: Wind velocity time series: 6 Bft NW (event A)
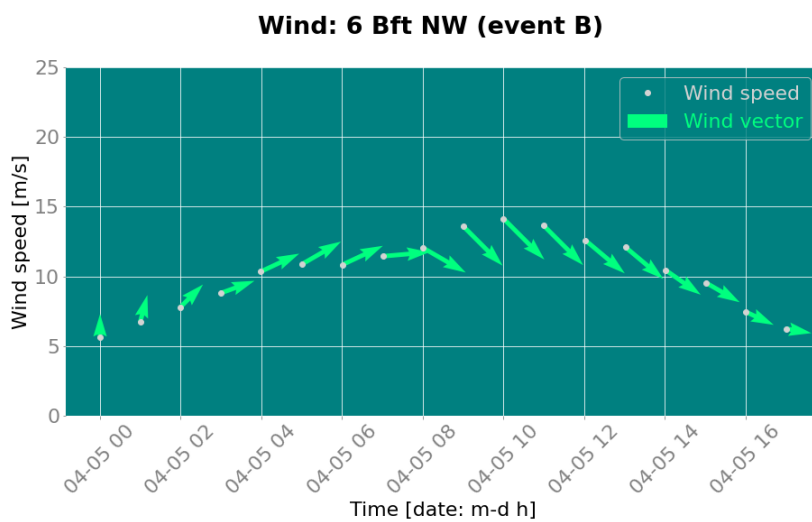
Wind: 6 Bft NW (event B)

Figure B.6: Wind velocity time series: 6 Bft NW (event B)
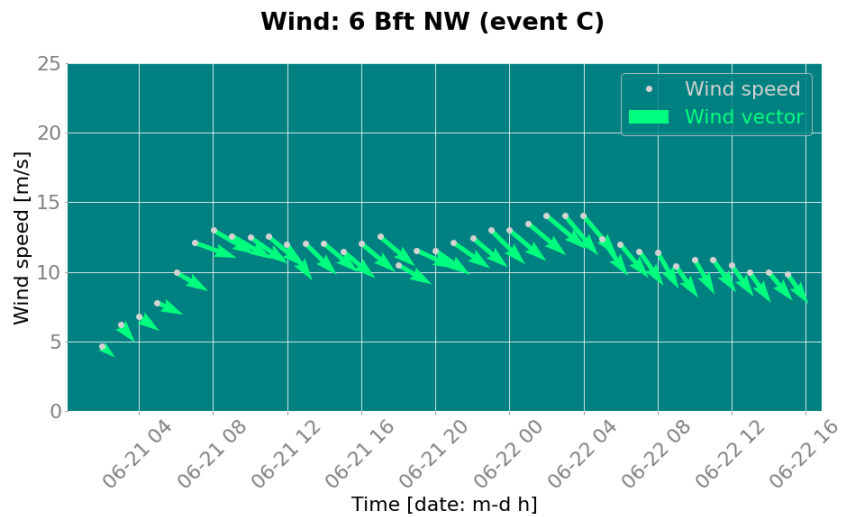
Wind: 6 Bft NW (event C)

Figure B.7: Wind velocity time series: 6 Bft NW (event C)
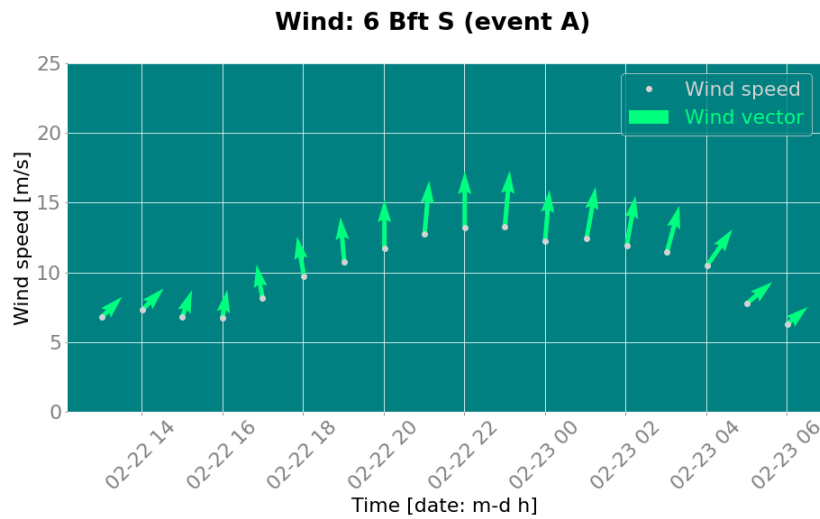
Wind: 6 Bft S (event A)

Figure B.8: Wind velocity time series: 6 Bft S (event A)
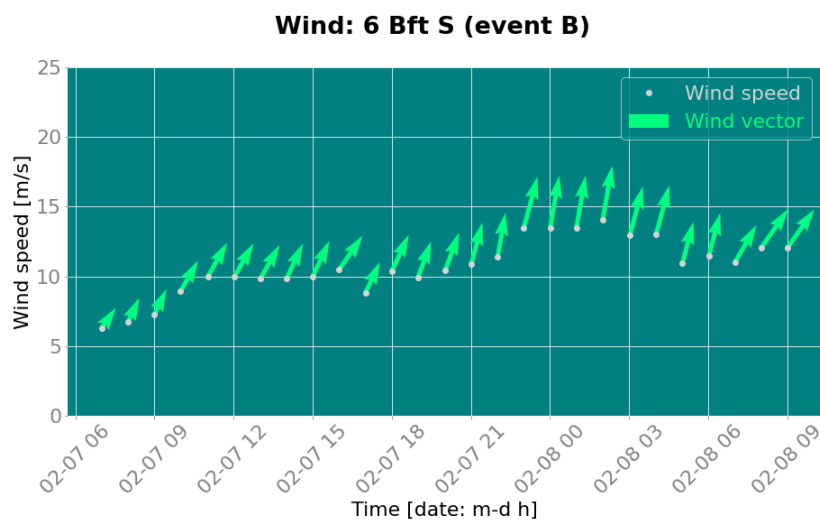
Wind: 6 Bft S (event B)

Figure B.9: Wind velocity time series: 6 Bft S (event B)
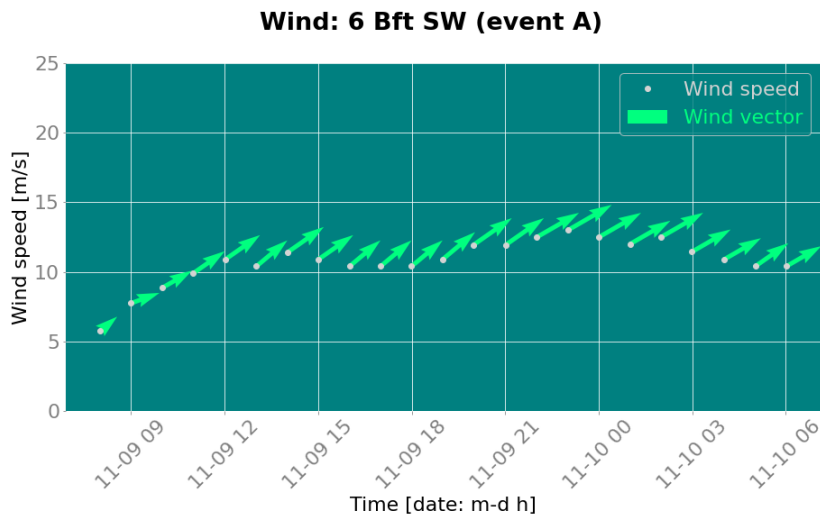
Wind: 6 Bft SW (event A)

Figure B.10: Wind velocity time series: 6 Bft SW (event A)
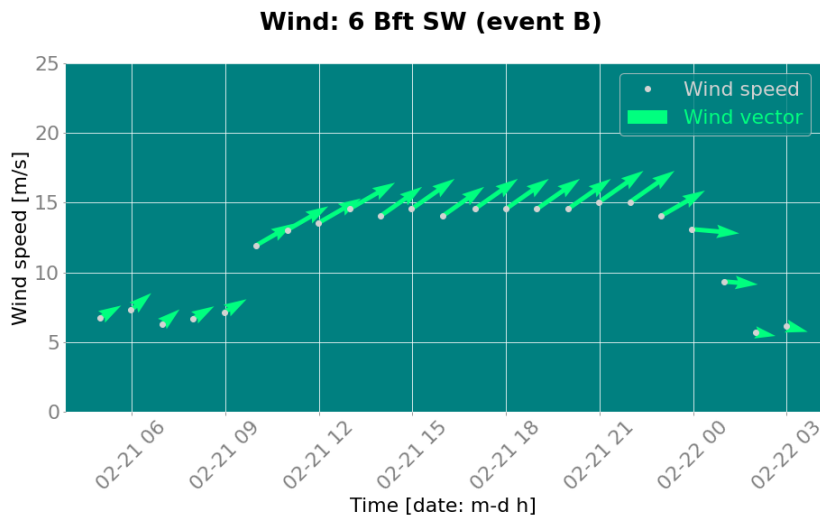
Wind: 6 Bft SW (event B)

Figure B.11: Wind velocity time series: 6 Bft SW (event B)
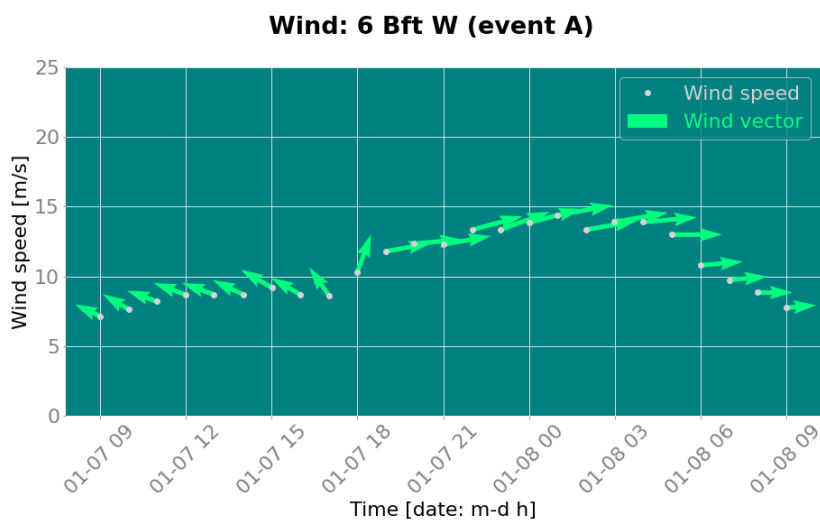
Wind: 6 Bft W (event A)

Figure B.12: Wind velocity time series: 6 Bft W (event A)
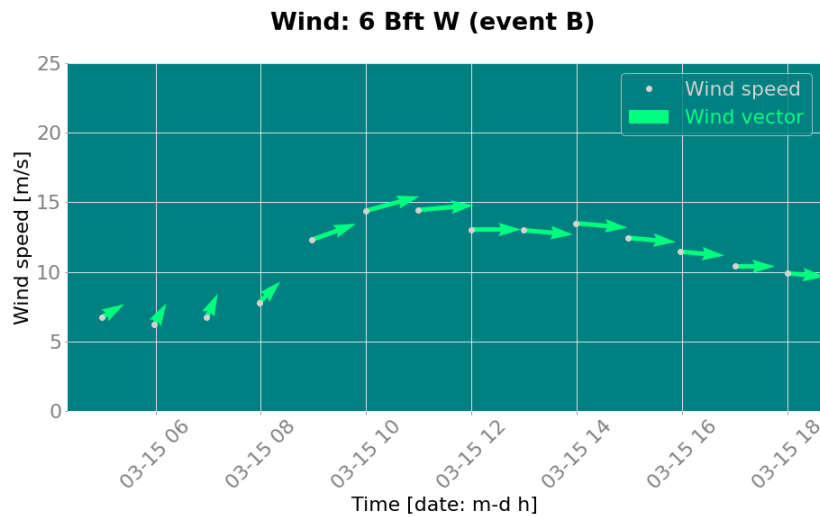
Wind: 6 Bft W (event B)

Figure B.13: Wind velocity time series: 6 Bft W (event B)
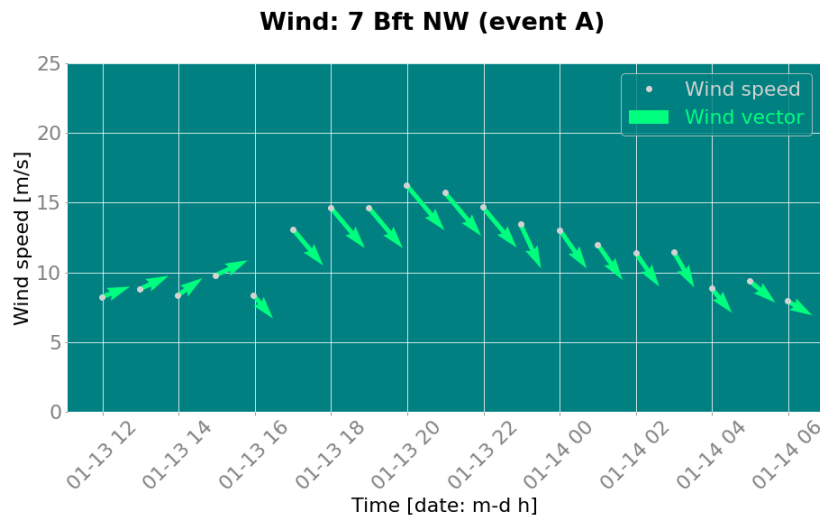
Wind: 7 Bft NW (event A)

Figure B.14: Wind velocity time series: 7 Bft NW (event A)
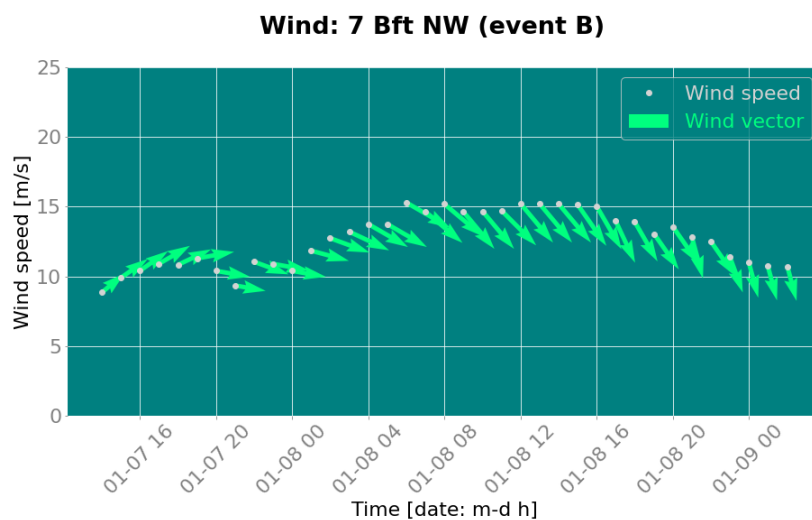
Wind: 7 Bft NW (event B)

Figure B.15: Wind velocity time series: 7 Bft NW (event B)
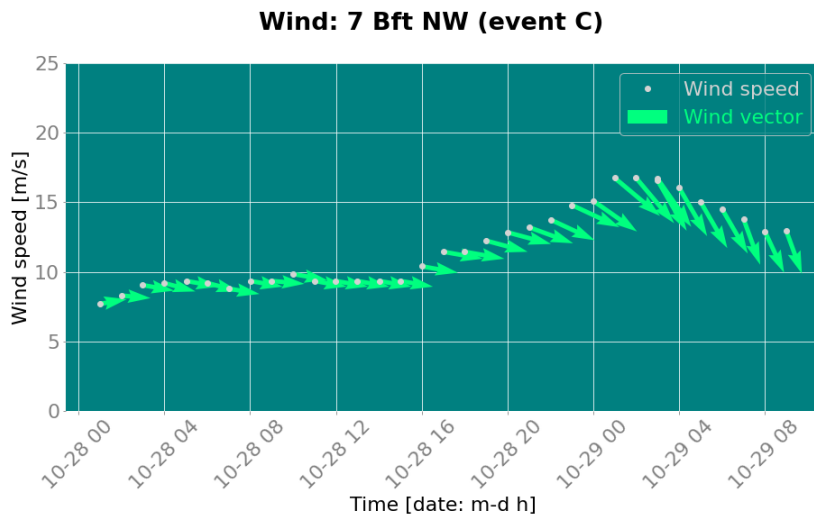
Wind: 7 Bft NW (event C)

Figure B.16: Wind velocity time series: 7 Bft NW (event C)
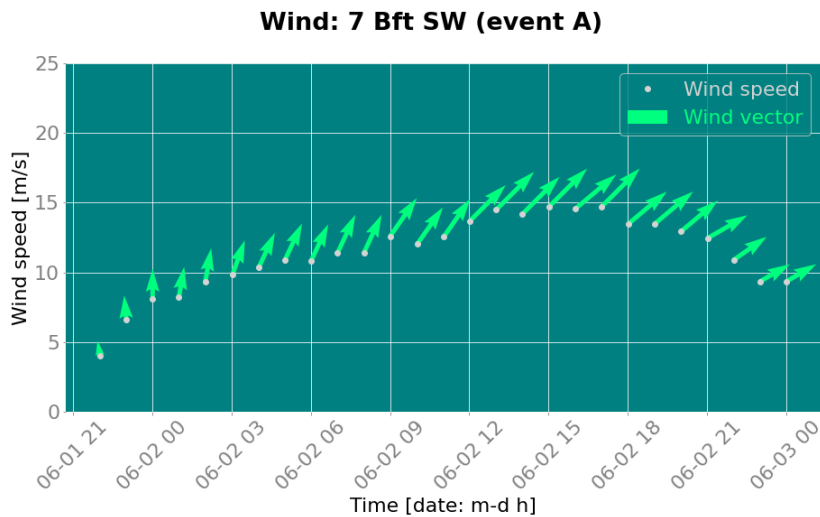
Wind: 7 Bft SW (event A)

Figure B.17: Wind velocity time series: 7 Bft SW (event A)

Wind: 7 Bft SW (event B)

Figure B.18: Wind velocity time series: 7 Bft SW (event B)
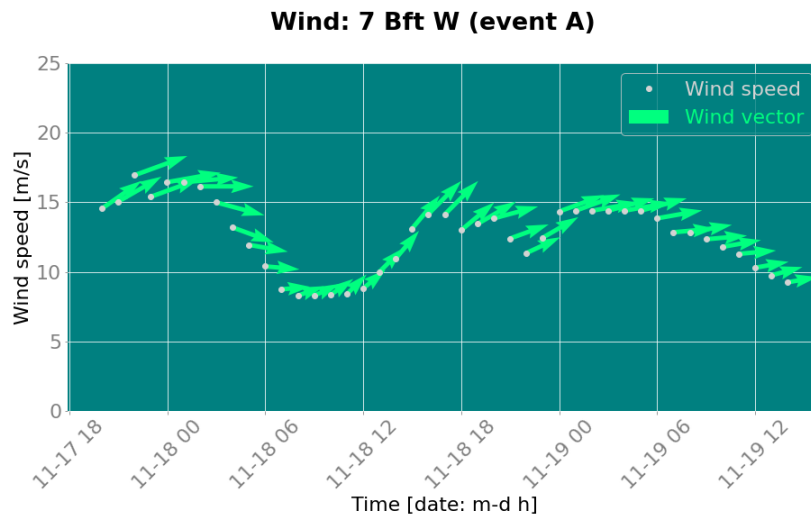
Wind: 7 Bft W (event A)

Figure B.19: Wind velocity time series: 7 Bft W (event A)

Wind: 7 Bft W (event B)

Figure B.20: Wind velocity time series: 7 Bft W (event B)
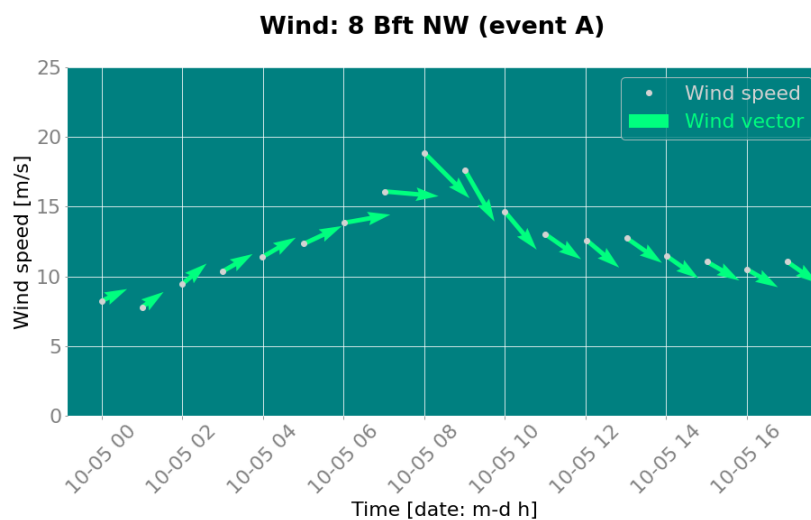
Wind: 8 Bft NW (event A)

Figure B.21: Wind velocity time series: 8 Bft NW (event A)
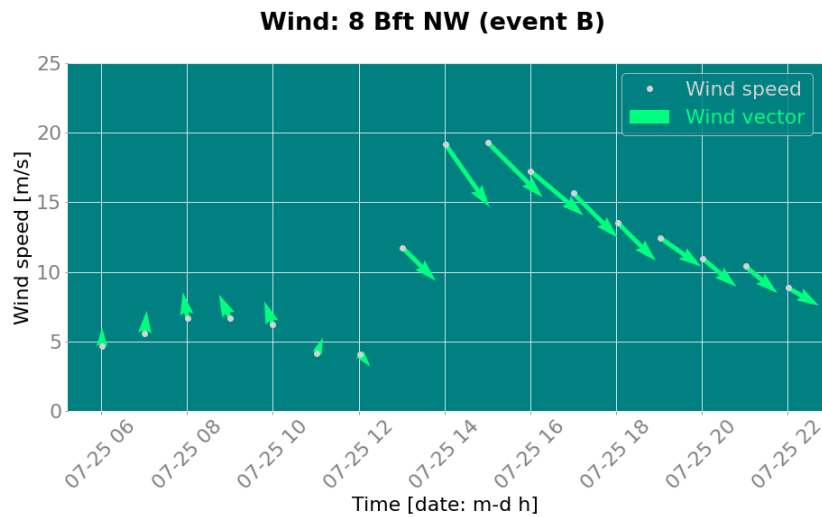
Wind: 8 Bft NW (event B)

Figure B.22: Wind velocity time series: 8 Bft NW (event B)
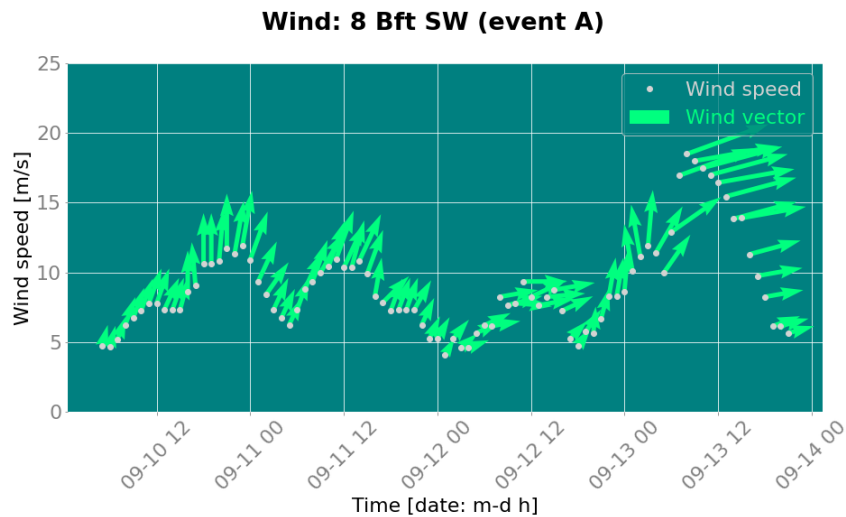
Wind: 8 Bft SW (event A)

Figure B.23: Wind velocity time series: 8 Bft SW (event A)
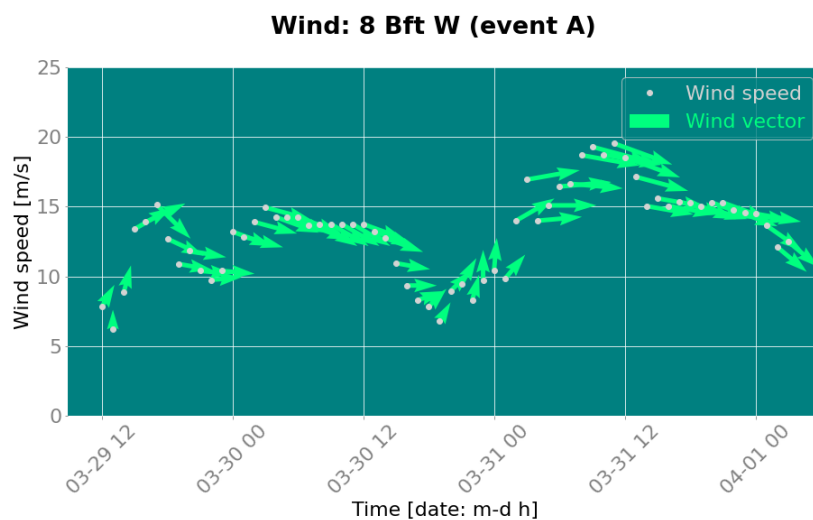
Wind: 8 Bft W (event A)

Figure B.24: Wind velocity time series: 8 Bft W (event A)
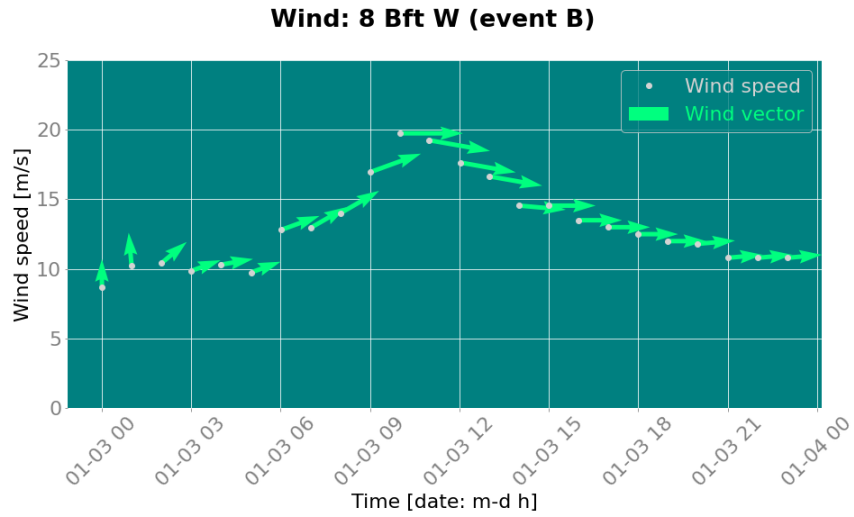
Figure B.25: Wind velocity time series: 8 Bft W (event B)
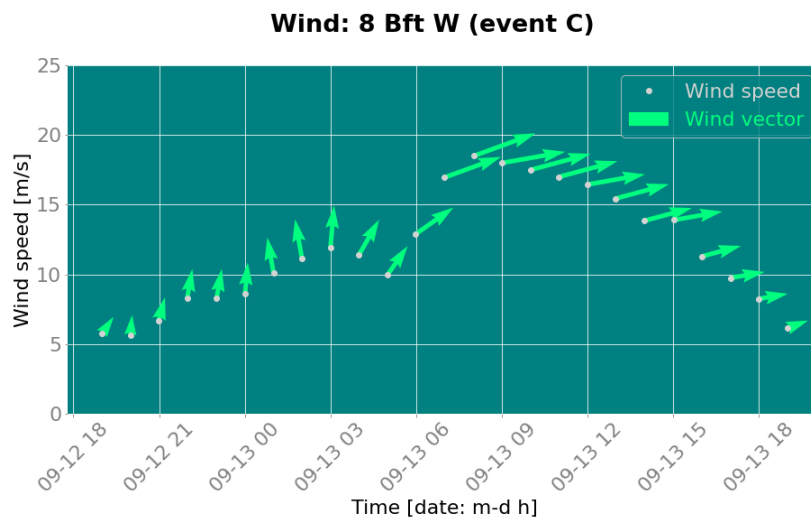
Figure B.26: Wind velocity time series: 8 Bft W (event C)
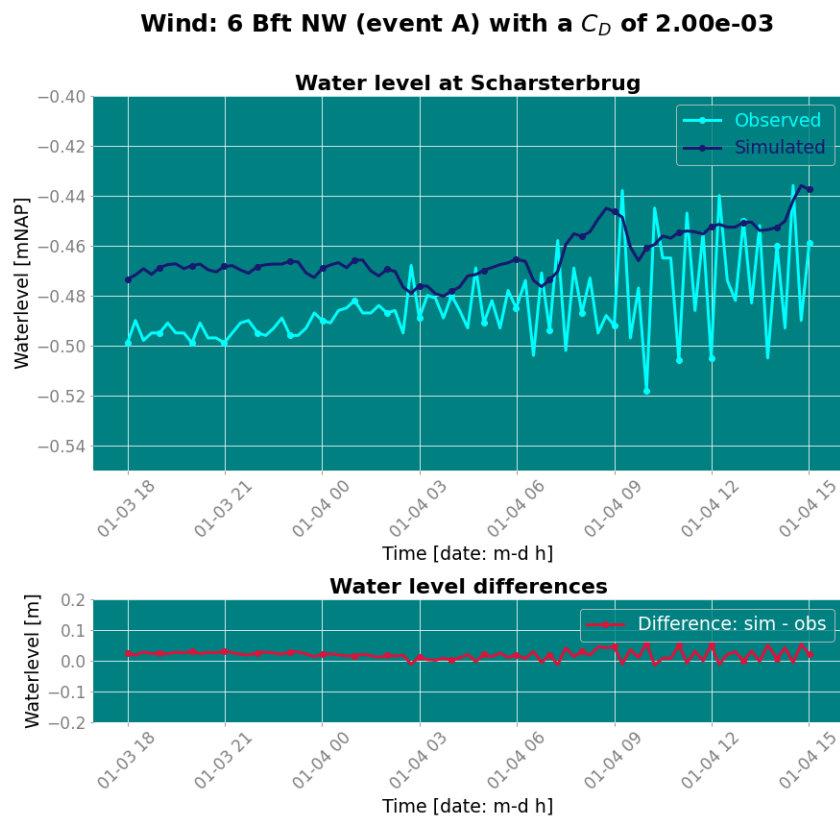
Figure B.27: Water levels at Scharsterbrug during event 6 Bft NW (A) at a C_D of $2 \times 10^{-3}[-]$ and a
KGE of 0.08

Wind: 6 Bft S (event B) with a C_D of 2.05e-03 and 1.25e-03
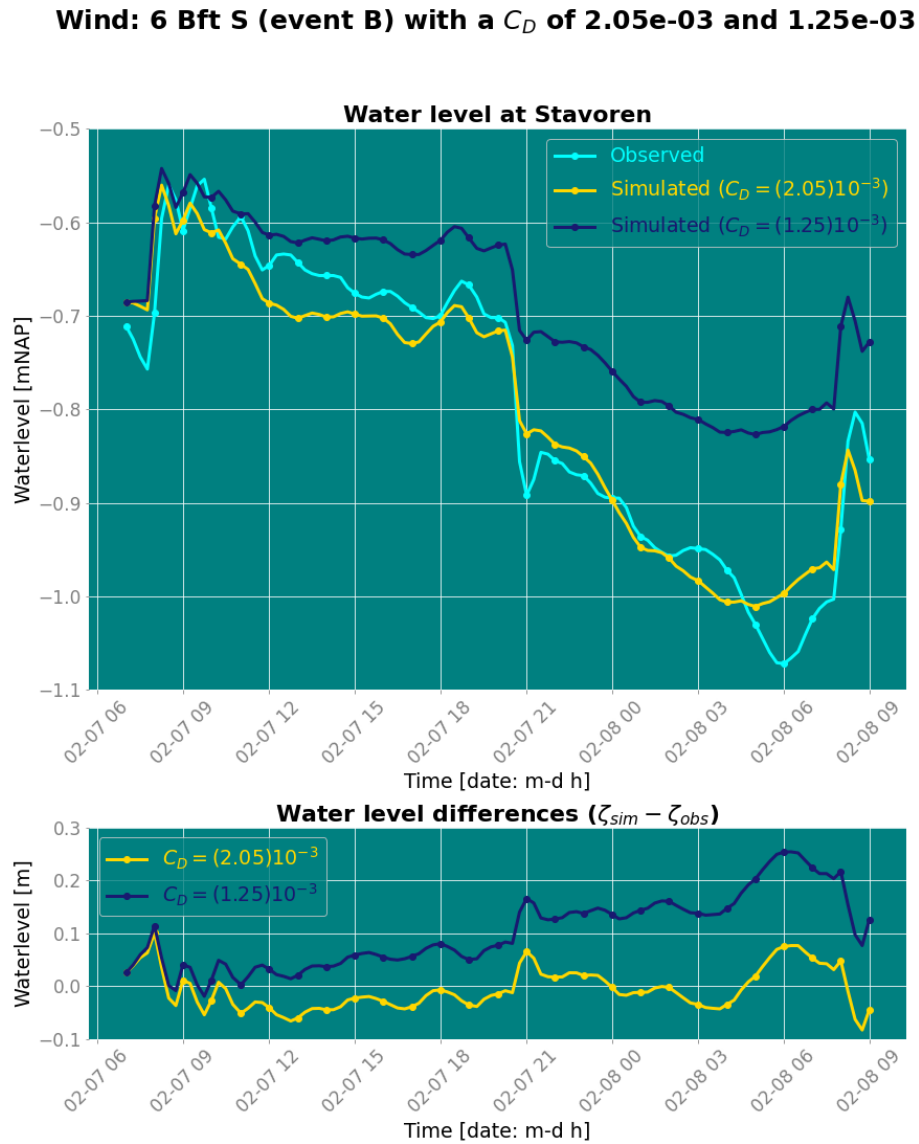
Figure B.28: Water levels at Stavoren during event 6 Bft S (B) at a local optimal C_D of $2.05 \times 10^{-3}[-]$ (KGE$= 0.88$) in comparison to the uniform optimal C_D of $1.25 \times 10^{-3}[-]$ (KGE$= 0.29$)

Wind: 6 Bft W (event A) with a C_D of 1.35e-03 and 1.25e-03
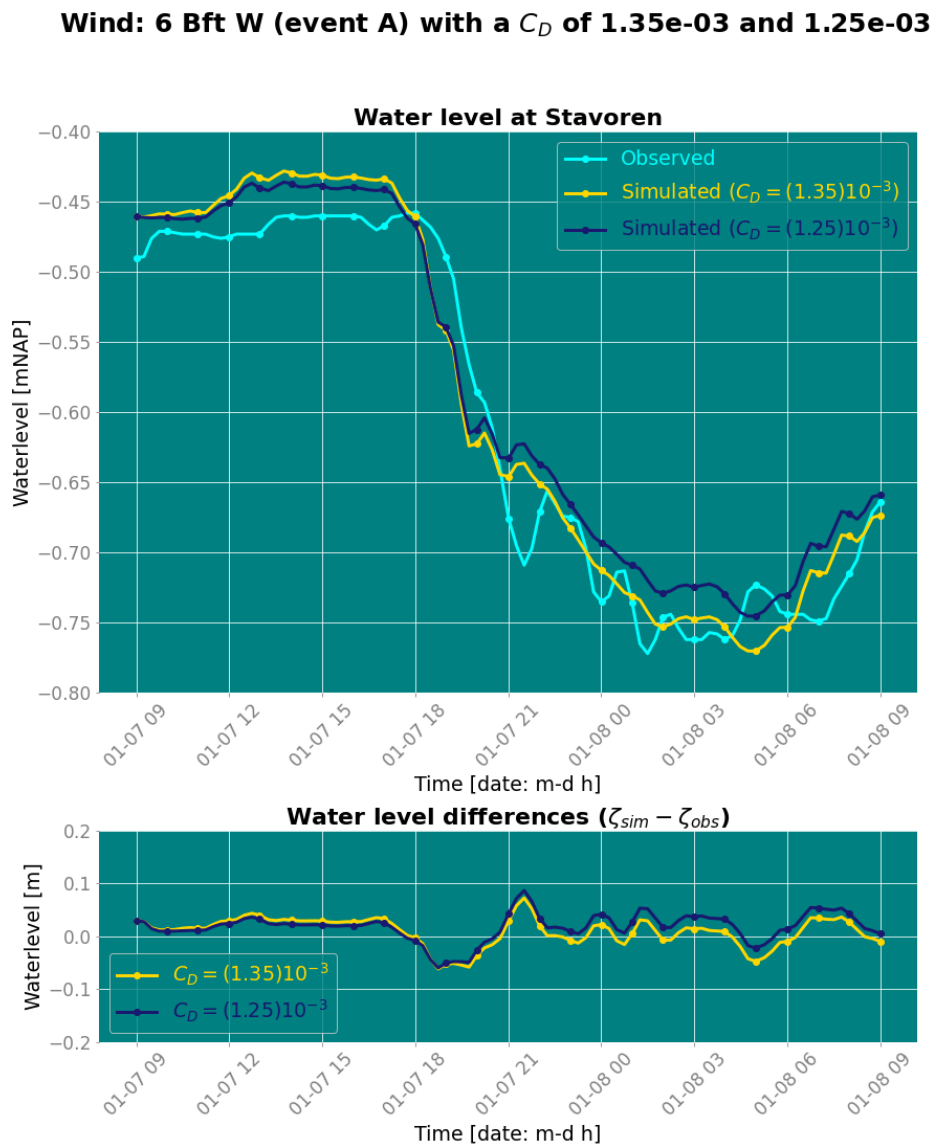
Figure B.29: Water levels at Stavoren during event 6 Bft W (A) at a local optimal C_D of $1.35 \times 10^{-3}[-]$ (KGE$= 0.95$) in comparison to the uniform optimal C_D of $1.25 \times 10^{-3}[-]$ (KGE$= 0.94$)
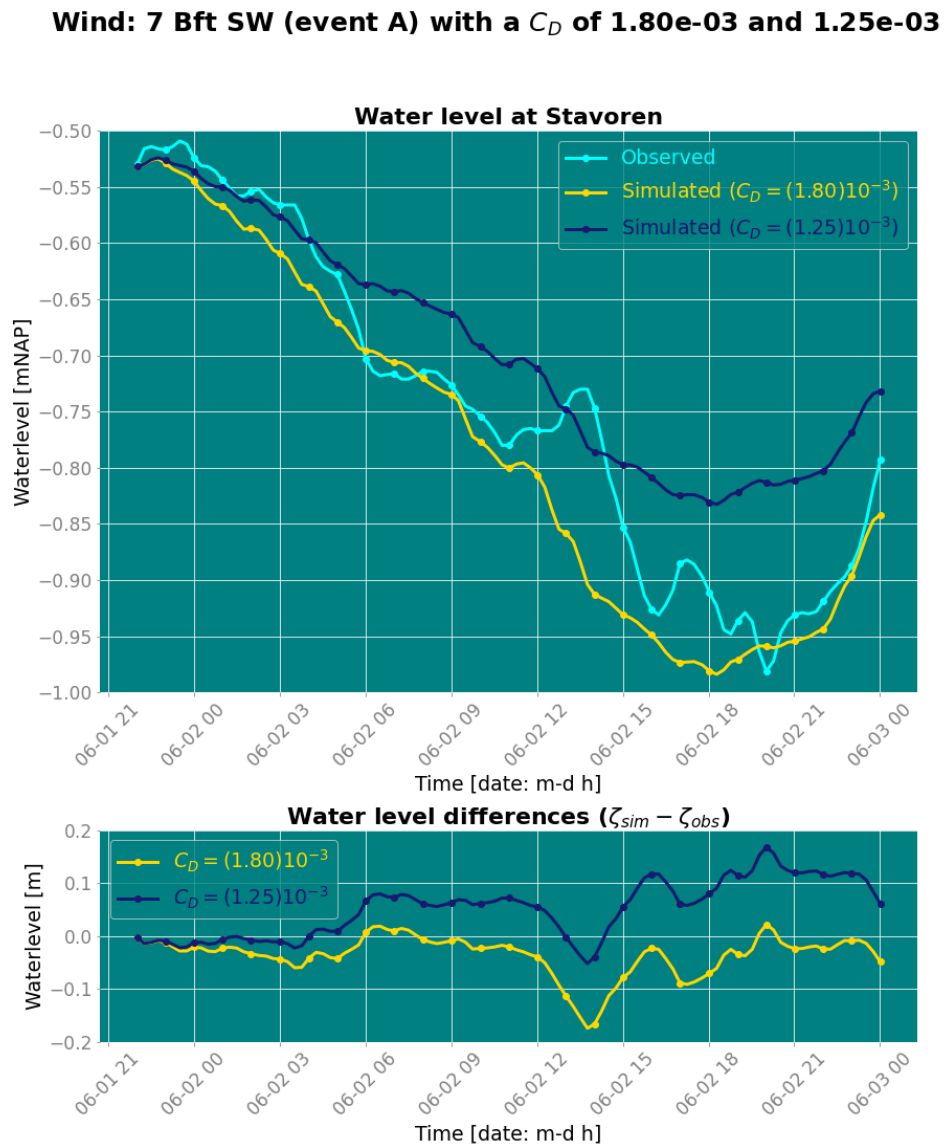
Figure B.30: Water levels at Stavoren during event 7 Bft SW (A) at a local optimal C_D of $1.80 \times 10^{-3}[-]$ (KGE$= 0.93$) in comparison to the uniform optimal C_D of $1.25 \times 10^{-3}[-]$ (KGE$= 0.63$)

Wind: 8 Bft SW (event A) with a C_D of 1.80e-03 and 1.25e-03
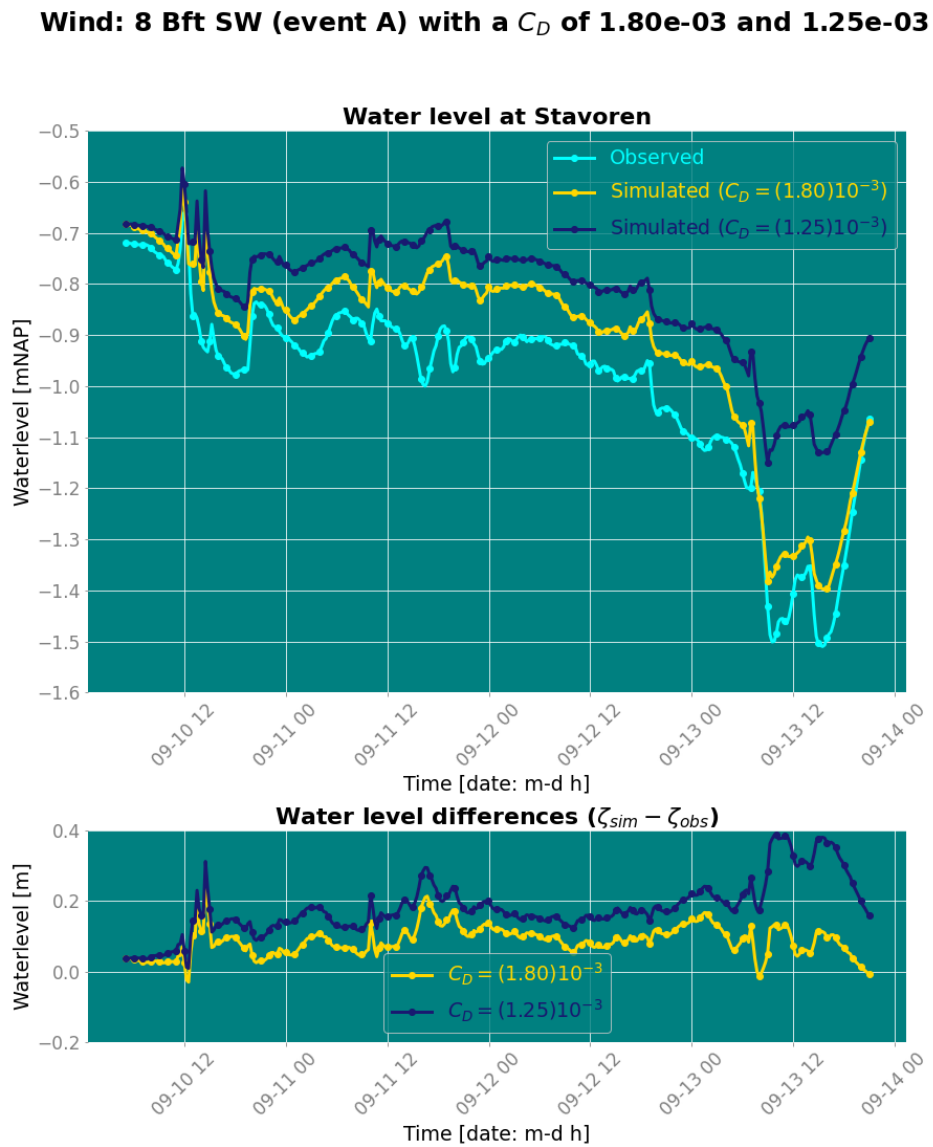
Figure B.31: Water levels at Stavoren during event 8 Bft SW (A) at a local optimal C_D of $1.80 \times 10^{-3}[-]$ (KGE$= 0.90$) in comparison to the uniform optimal C_D of $1.25 \times 10^{-3}[-]$ (KGE$= 0.49$)

Wind: 8 Bft W (event A) with a C_D of 1.80e-03 and 1.25e-03
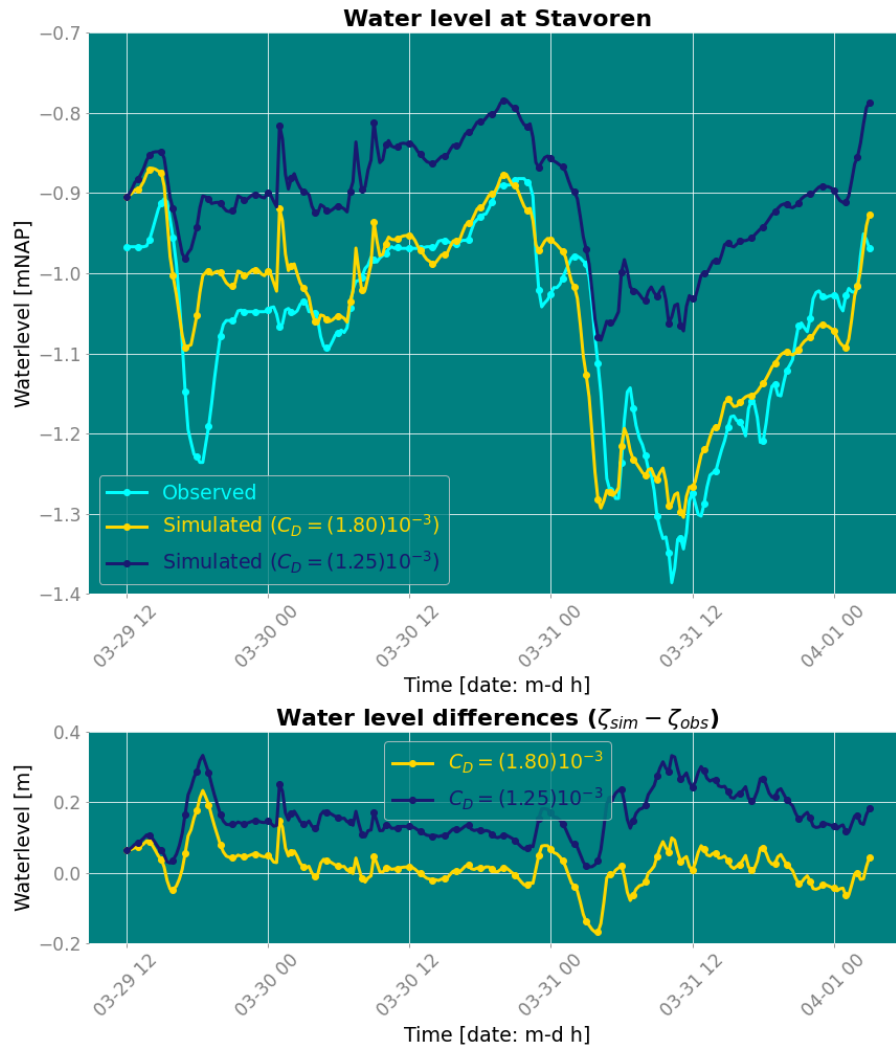
Figure B.32: Water levels at Stavoren during event 8 Bft W (A) at a local optimal C_D of $1.80 \times 10^{-3}[-]$ (KGE$= 0.88$) in comparison to the uniform optimal C_D of $1.25 \times 10^{-3}[-]$ (KGE$= 0.36$)

Wind: 6 Bft S (event B) with a C_D of 2.00e-03 and 1.25e-03

Figure B.33: Water levels at Lemmer during event 6 Bft S (B) at a local optimal C_D of $2.00 \times 10^{-3}[-]$ (KGE$= 0.91$) in comparison to the uniform optimal C_D of $1.25 \times 10^{-3}[-]$ (KGE$= 0.26$)

Wind: 6 Bft W (event A) with a C_D of 8.00e-04 and 1.25e-03

Figure B.34: Water levels at Lemmer during event 6 Bft S (B) at a local optimal C_D of $0.80 \times 10^{-3}[-]$ (KGE$= 0.83$) in comparison to the uniform optimal C_D of $1.25 \times 10^{-3}[-]$ (KGE$= 0.54$)

Wind: 7 Bft SW (event A) with a C_D of 1.40e-03 and 1.25e-03
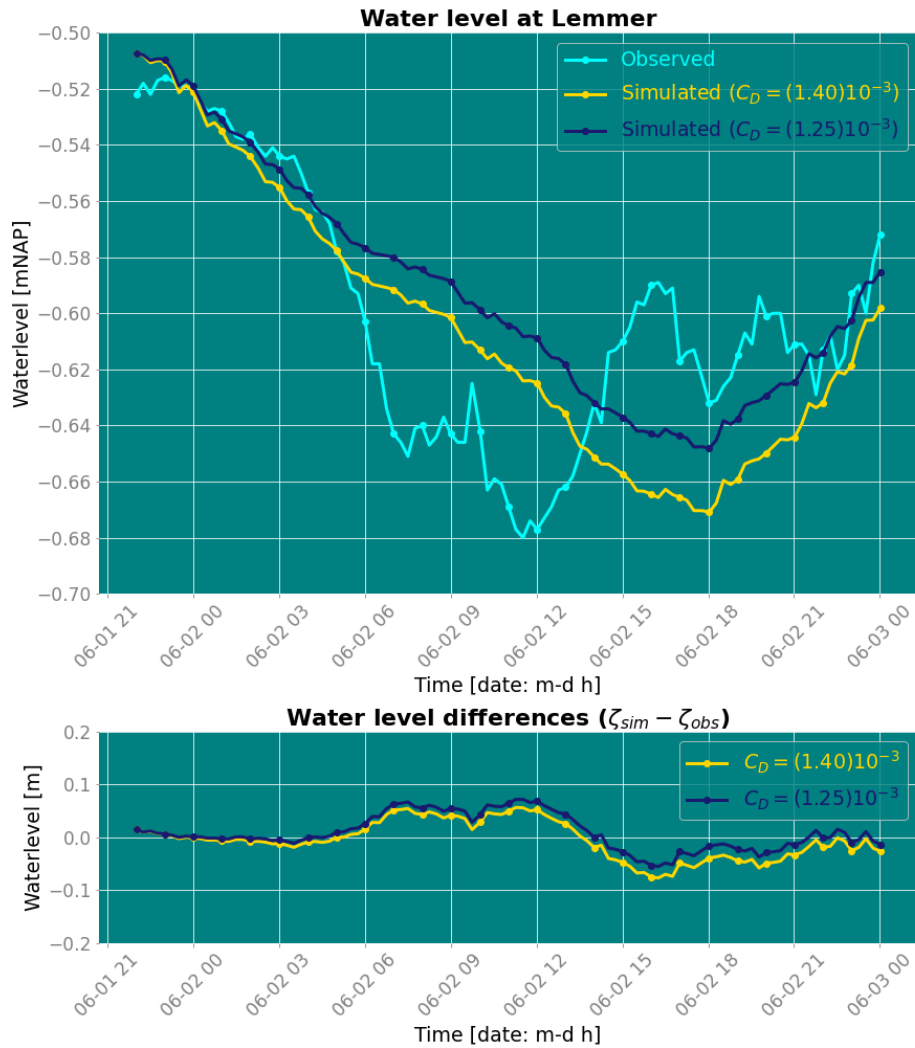
Figure B.35: Water levels at Lemmer during event 6 Bft S (B) at a local optimal C_D of $1.40 \times 10^{-3}[-]$ (KGE$= 0.72$) in comparison to the uniform optimal C_D of $1.25 \times 10^{-3}[-]$ (KGE$= 0.71$)

Wind: 8 Bft SW (event A) with a C_D of 1.50e-03 and 1.25e-03
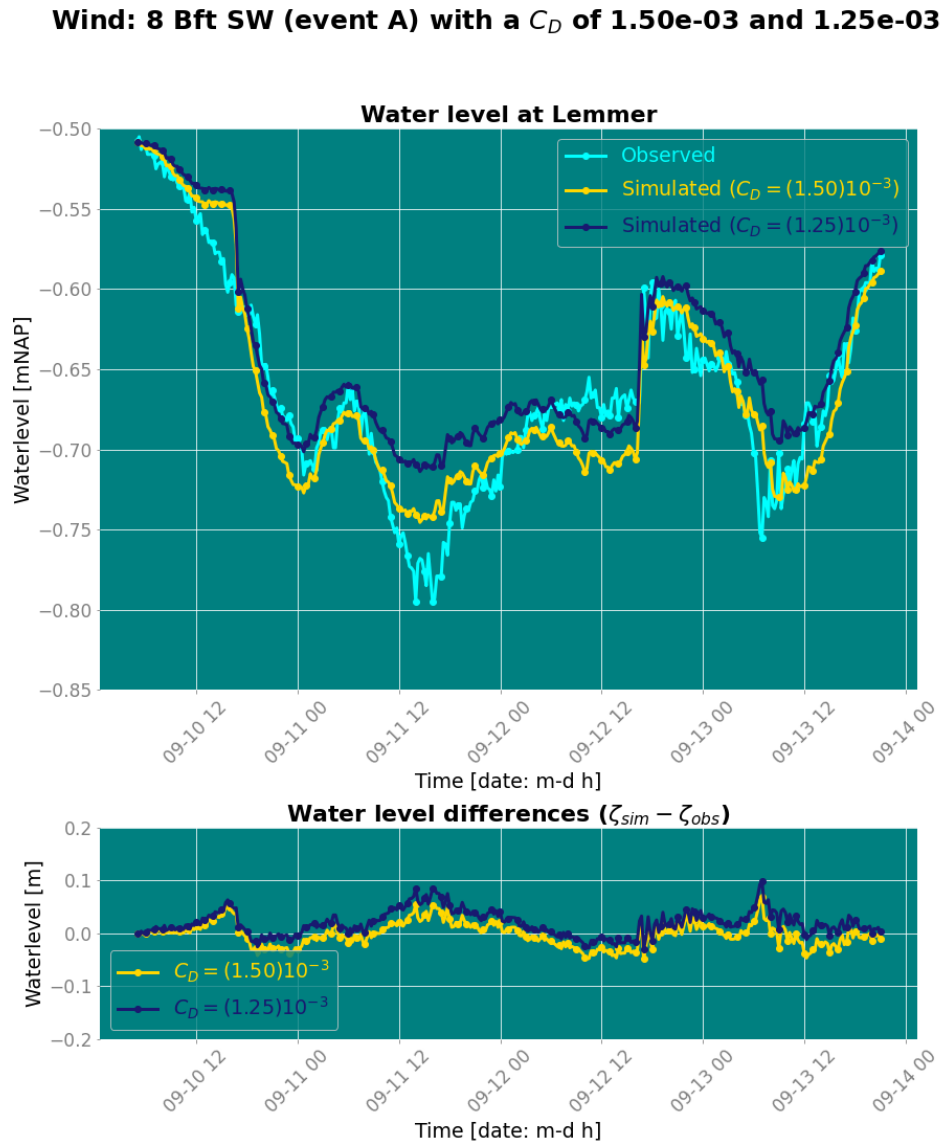
Figure B.36: Water levels at Lemmer during event 6 Bft S (B) at a local optimal C_D of $1.50 \times 10^{-3}[-]$ (KGE$= 0.94$) in comparison to the uniform optimal C_D of $1.25 \times 10^{-3}[-]$ (KGE$= 0.88$)

Wind: 8 Bft W (event A) with a C_D of 2.00e-03 and 1.25e-03
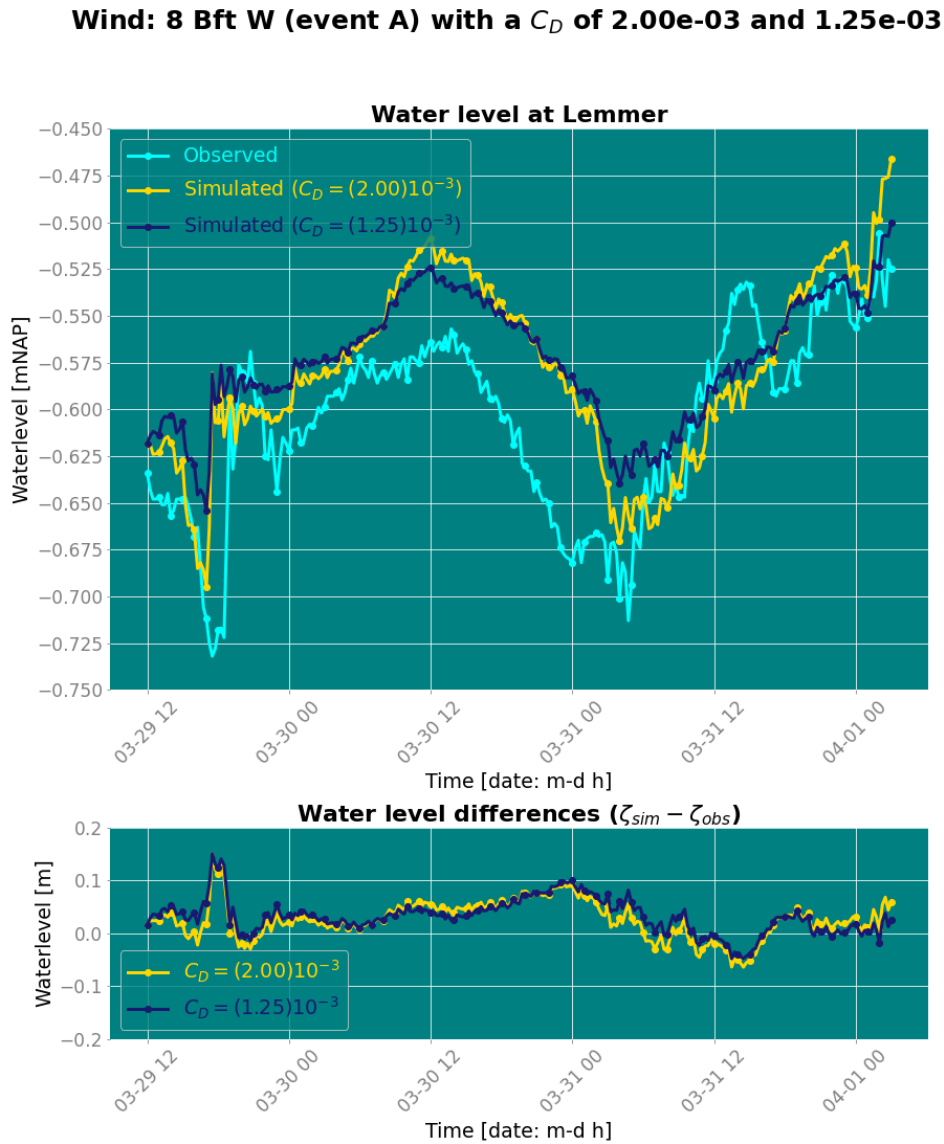
Figure B.37: Water levels at Lemmer during event 6 Bft S (B) at a local optimal C_D of $2.00 \times 10^{-3}[-]$ (KGE= 0.72) in comparison to the uniform optimal C_D of $1.25 \times 10^{-3}[-]$ (KGE= 0.47)
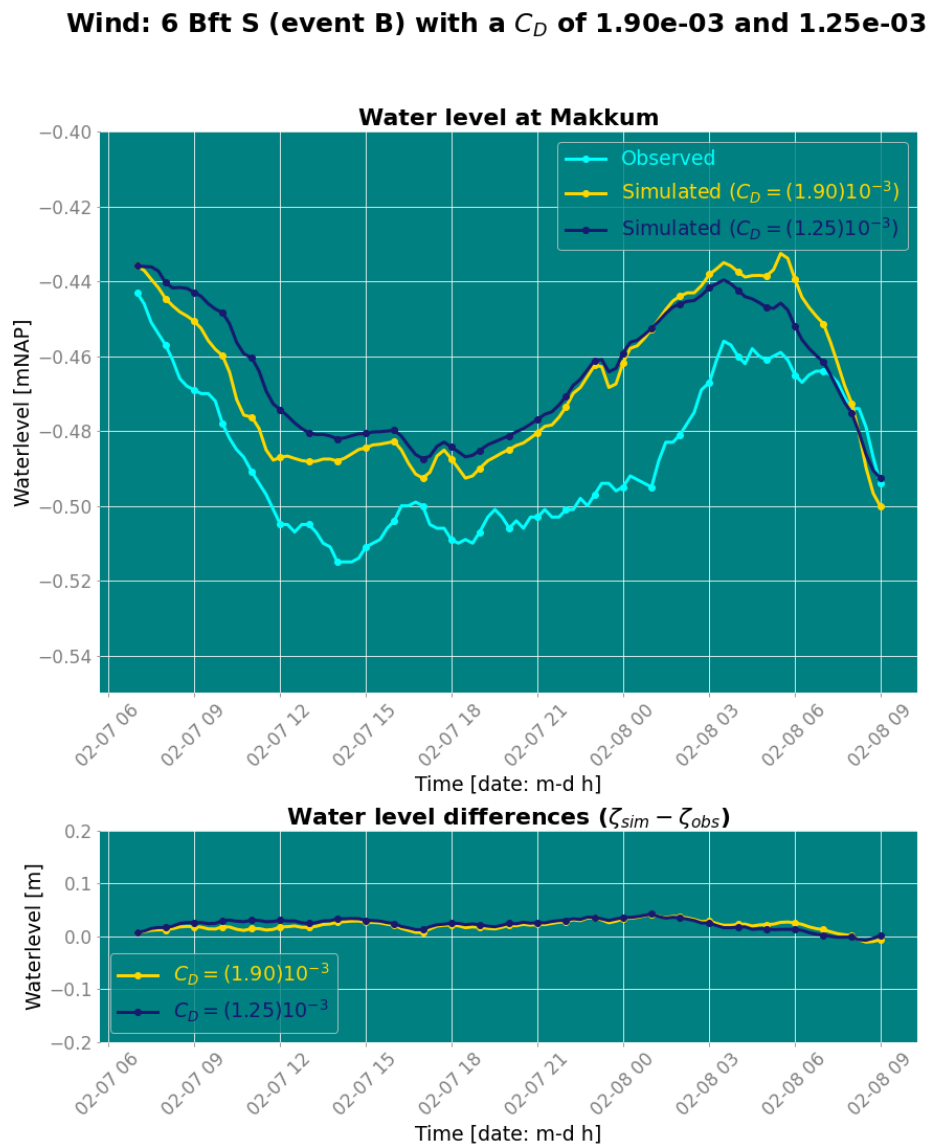
Figure B.38: Water levels at Makkum during event 6 Bft S (B) at a local optimal C_D of $1.90 \times 10^{-3}[-]$ (KGE$= 0.86$) in comparison to the uniform optimal C_D of $1.25 \times 10^{-3}[-]$ (KGE$= 0.78$)

Wind: 6 Bft W (event A) with a C_D of 8.00e-04 and 1.25e-03
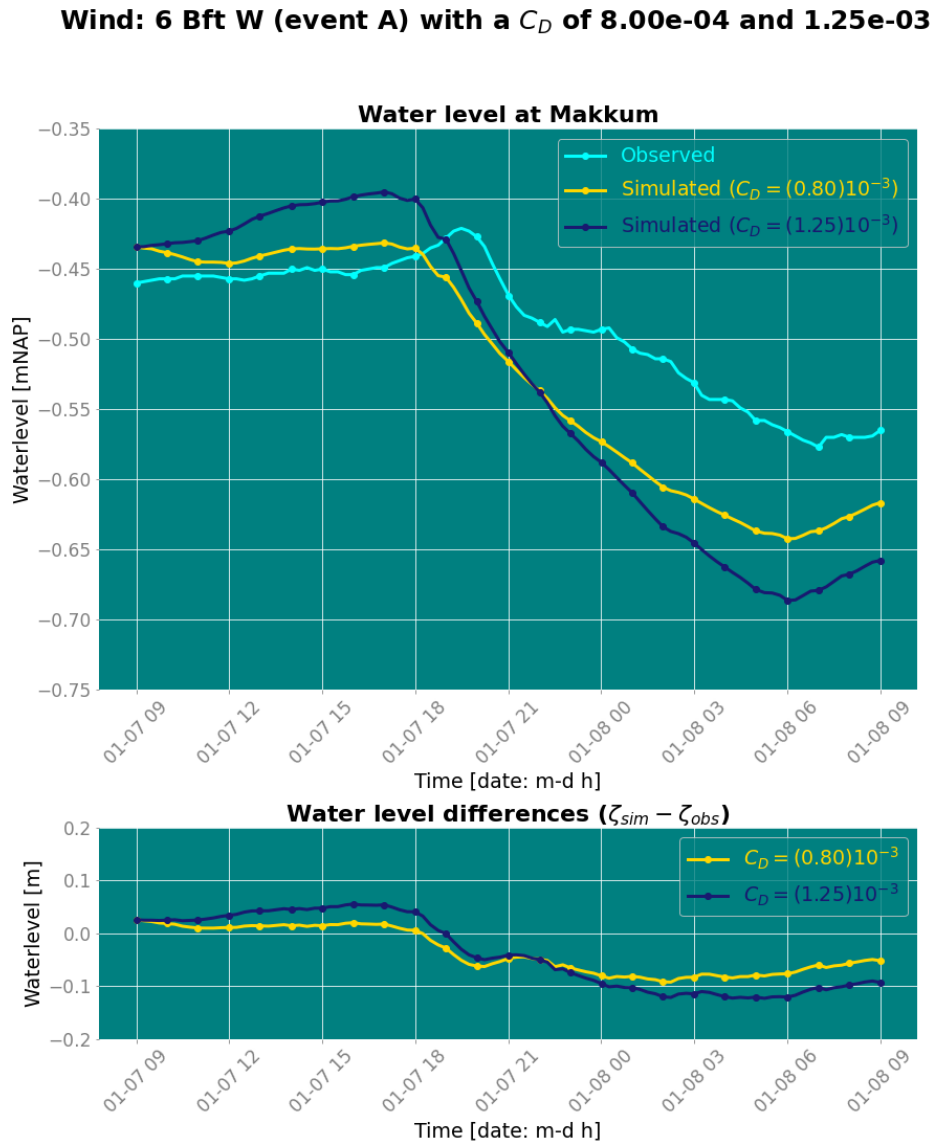
Figure B.39: Water levels at Makkum during event 6 Bft S (B) at a local optimal C_D of $0.80 \times 10^{-3}[-]$ (KGE$= 0.57$) in comparison to the uniform optimal C_D of $1.25 \times 10^{-3}[-]$ (KGE$= 0.42$)
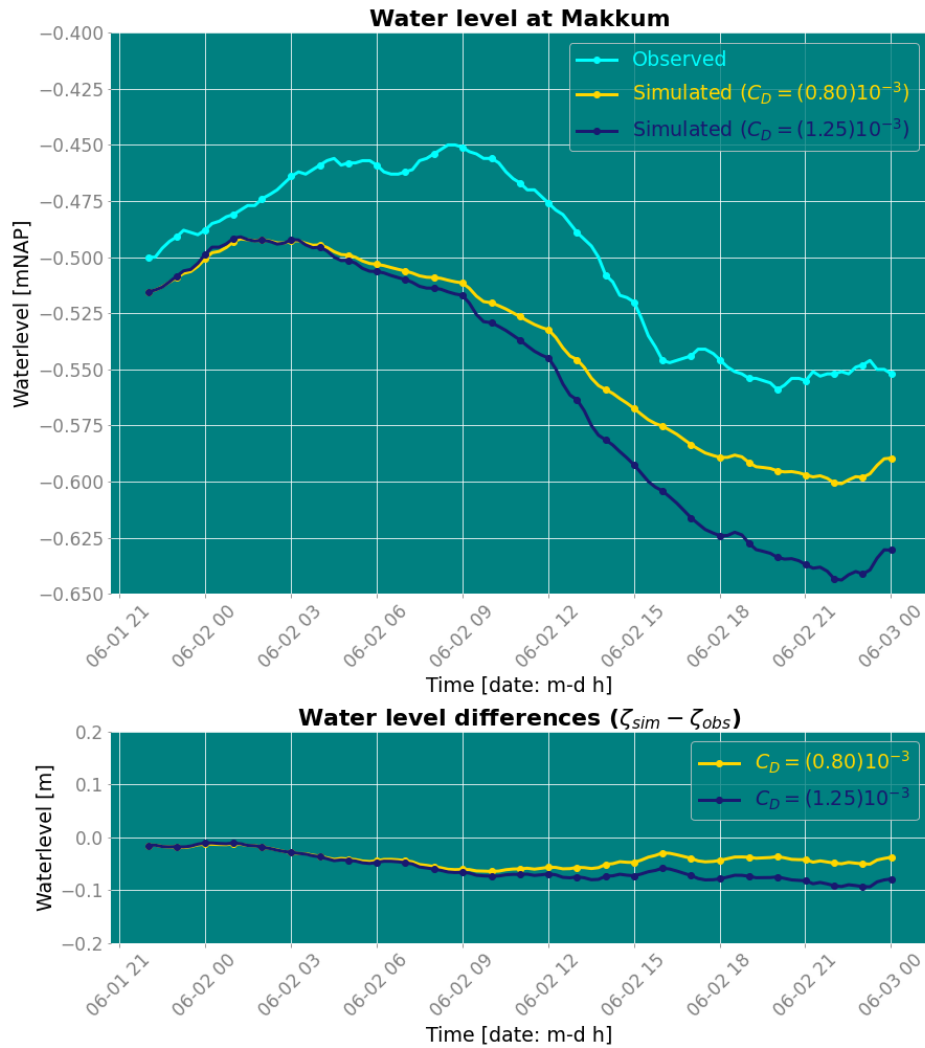
Figure B.40: Water levels at Makkum during event 6 Bft S (B) at a local optimal C_D of $0.80 \times 10^{-3}[-]$ (KGE$= 0.89$) in comparison to the uniform optimal C_D of $1.25 \times 10^{-3}[-]$ (KGE$= 0.65$)

Wind: 8 Bft SW (event A) with a C_D of 1.00e-03 and 1.25e-03
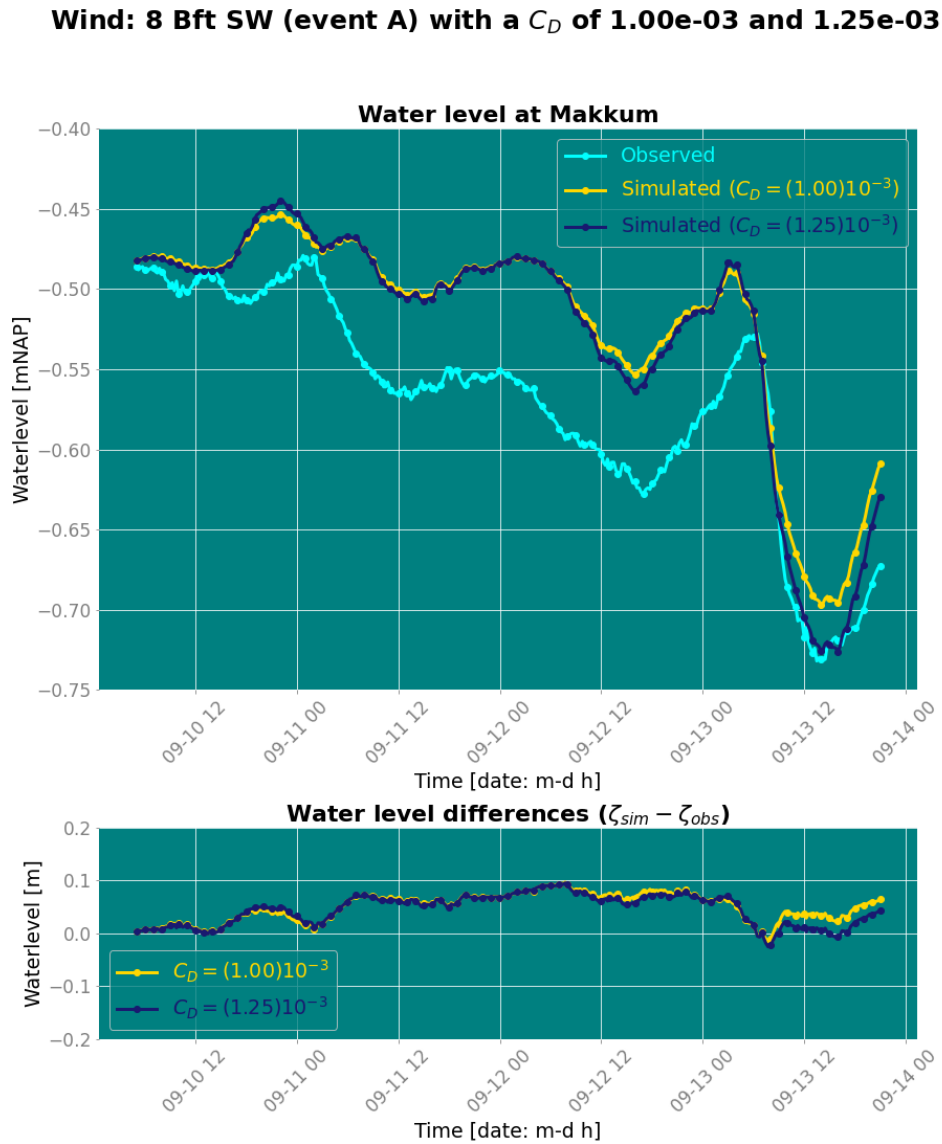
Figure B.41: Water levels at Makkum during event 6 Bft S (B) at a local optimal C_D of $1.00 \times 10^{-3}[-]$ (KGE$= 0.87$) in comparison to the uniform optimal C_D of $1.25 \times 10^{-3}[-]$ (KGE$= 0.84$)

Wind: 6 Bft W (event A) with a C_D of 1.80e-03 and 1.25e-03
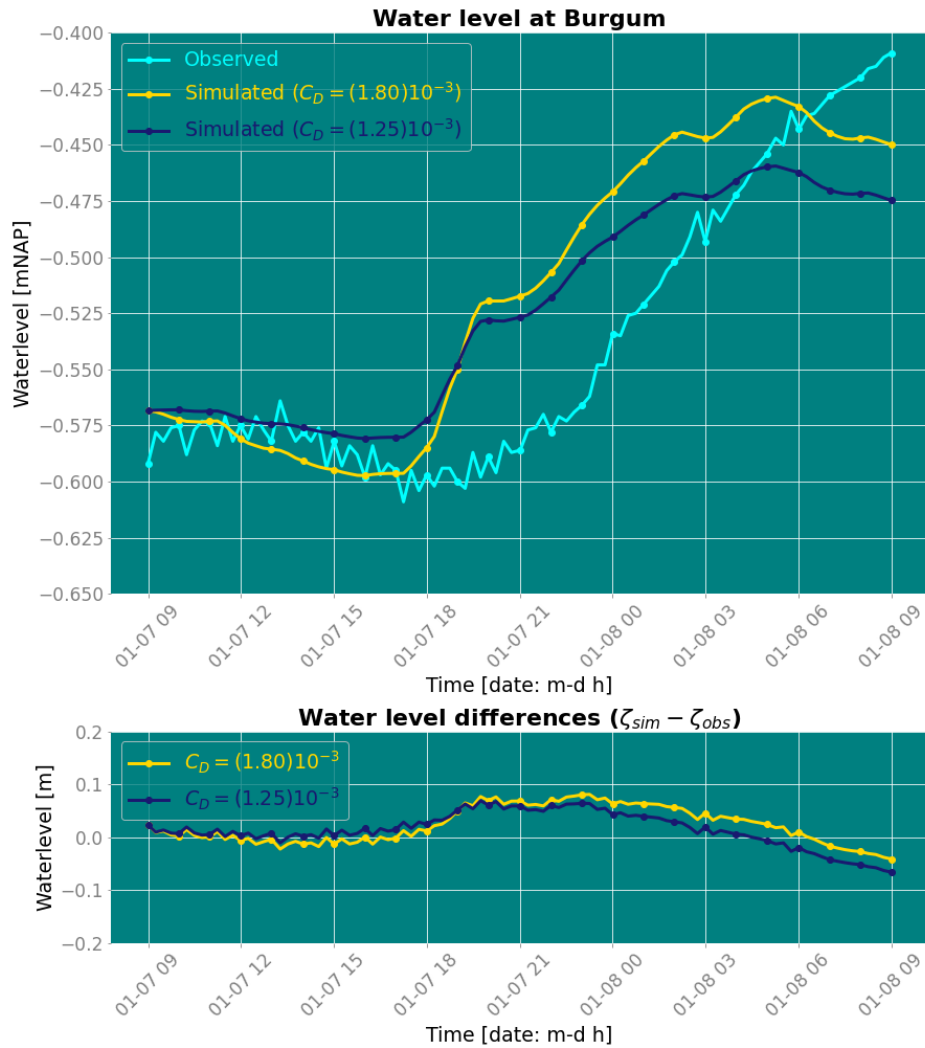
Figure B.42: Water levels at Burgum during event 6 Bft S (B) at a local optimal C_D of $1.80 \times 10^{-3}[-]$ (KGE$= 0.84$) in comparison to the uniform optimal C_D of $1.25 \times 10^{-3}[-]$ (KGE$= 0.65$)

Wind: 7 Bft SW (event A) with a C_D of 1.10e-03 and 1.25e-03

Figure B.43: Water levels at Burgum during event 6 Bft S (B) at a local optimal C_D of $1.10 \times 10^{-3}[-]$ (KGE$= 0.87$) in comparison to the uniform optimal C_D of $1.25 \times 10^{-3}[-]$ (KGE$= 0.84$)

Wind: 8 Bft W (event A) with a C_D of 1.80e-03 and 1.25e-03

Figure B.44: Water levels at Burgum during event 6 Bft S (B) at a local optimal C_D of $1.80 \times 10^{-3}[-]$ (KGE$= 0.84$) in comparison to the uniform optimal C_D of $1.25 \times 10^{-3}[-]$ (KGE$= 0.24$)

Wind: 6 Bft S (event B) with a C_D of 1.00e-03 and 1.25e-03
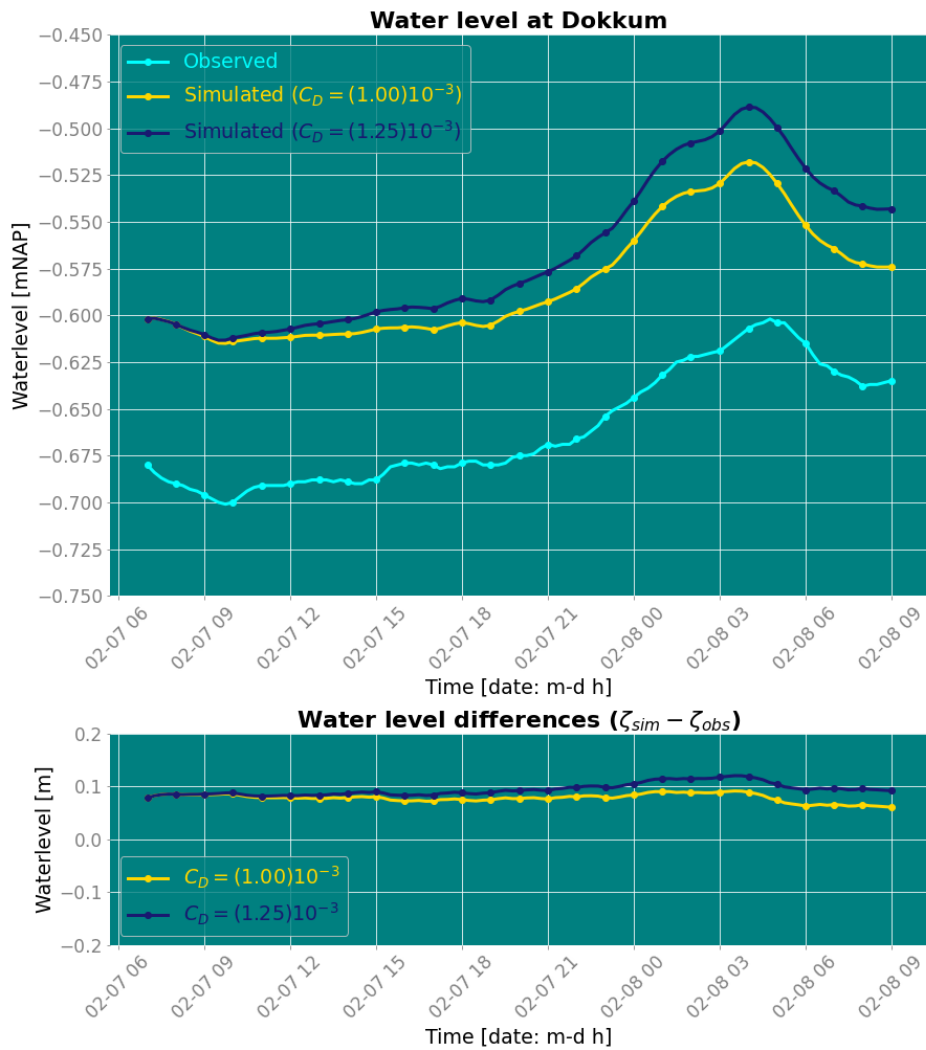
Figure B.45: Water levels at Dokkum during event 6 Bft S (B) at a local optimal C_D of $1.00 \times 10^{-3}[-]$ (KGE$= 0.86$) in comparison to the uniform optimal C_D of $1.25 \times 10^{-3}[-]$ (KGE$= 0.68$)

Wind: 7 Bft SW (event A) with a C_D of 1.15e-03 and 1.25e-03
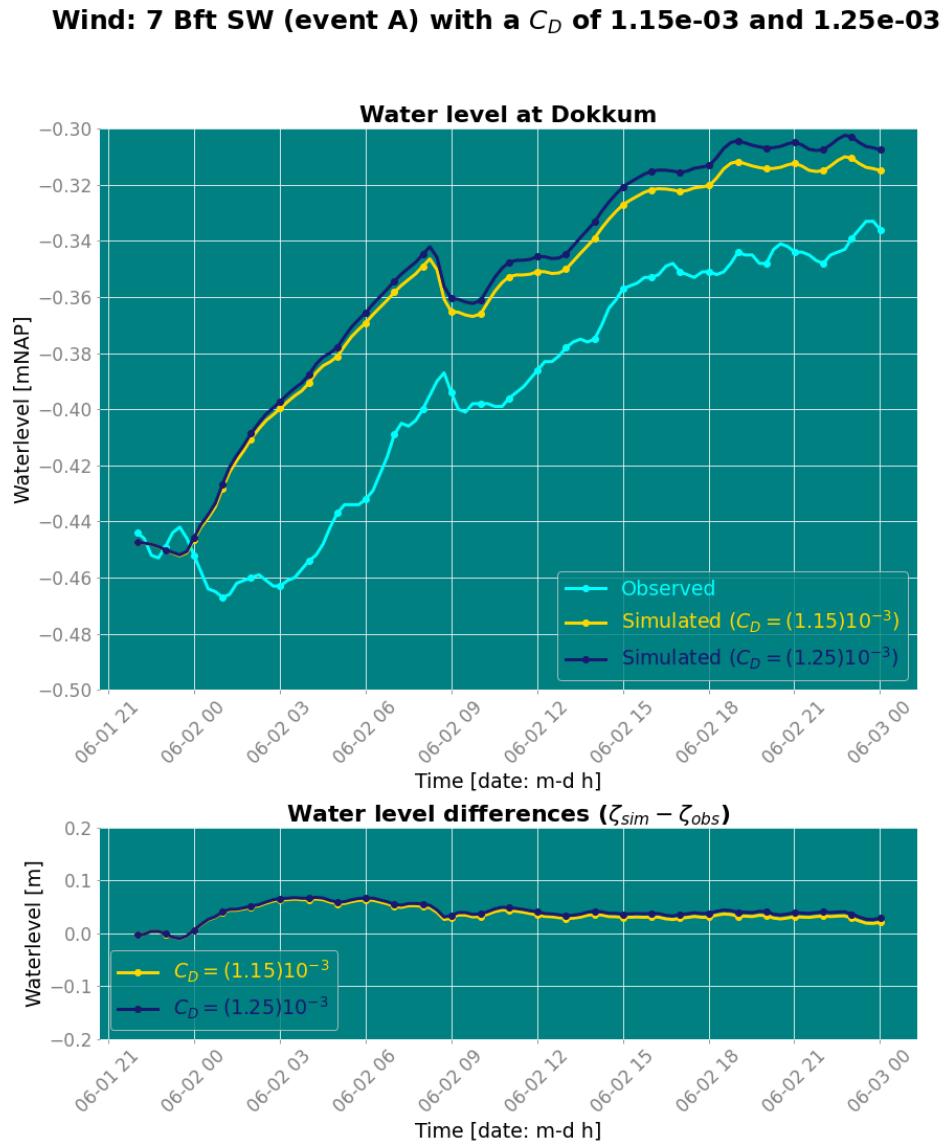
Figure B.46: Water levels at Dokkum during event 6 Bft S (B) at a local optimal C_D of $1.15 \times 10^{-3} [-]$ (KGE$= 0.87$) in comparison to the uniform optimal C_D of $1.25 \times 10^{-3} [-]$ (KGE$= 0.84$)

Wind: 8 Bft SW (event A) with a C_D of 1.55e-03 and 1.25e-03
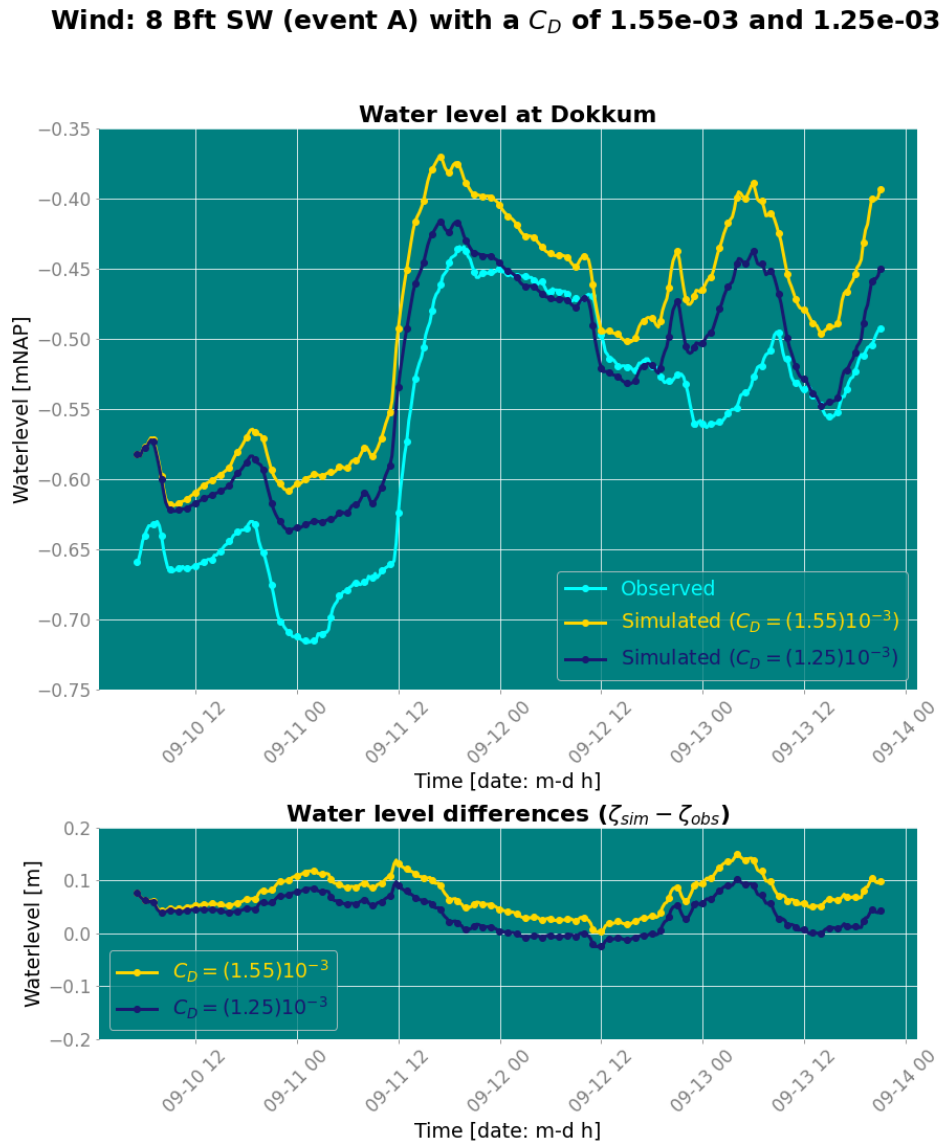
Figure B.47: Water levels at Dokkum during event 6 Bft S (B) at a local optimal C_D of $1.55 \times 10^{-3}[-]$ (KGE= 0.81) in comparison to the uniform optimal C_D of $1.25 \times 10^{-3}[-]$ (KGE= 0.76)

Wind: 8 Bft W (event A) with a C_D of 1.35e-03 and 1.25e-03
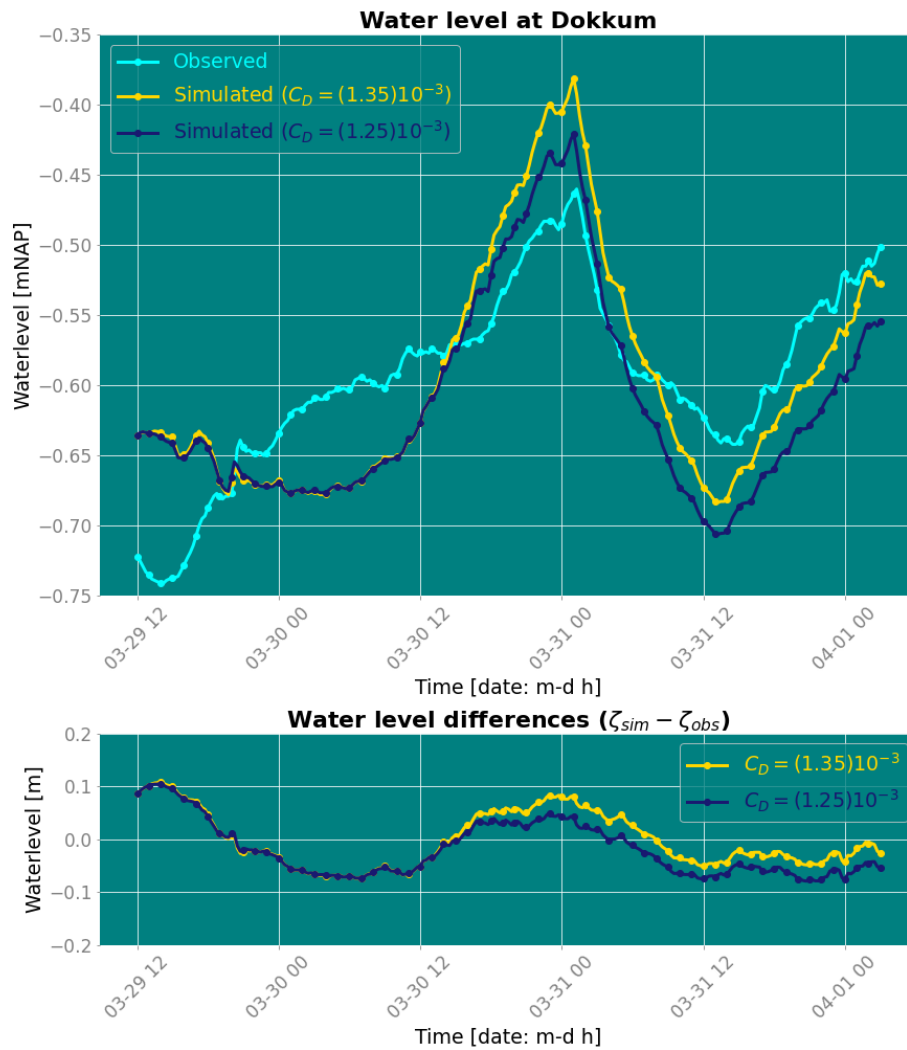
Figure B.48: Water levels at Dokkum during event 6 Bft S (B) at a local optimal C_D of $1.35 \times 10^{-3} [-]$ (KGE$= 0.71$) in comparison to the uniform optimal C_D of $1.25 \times 10^{-3} [-]$ (KGE$= 0.71$)

Appendix C

Model settings

Section 4.1.2 elaborated on the 3Di hydrodynamic model and the matter in which it was set up. However, the actual model settings were not specified. A number of these model settings are defined in Table C.1. Other settings were kept at their standard value. These can be found in the 3Di documentation. Some of the defined settings in Table C.1 require further explanation.

The grid resolution and time step were determined by optimizing the computational time in combination with the model accuracy. A simple assessment was performed, based on the comparison of simulated water levels with observations. This assessment resulted in computational cells ranging from 40 m up to 160 m. The coarsest cells were located in the lakes, while the smaller cells were located within canals and around lake island. The optimal time step was found at 20 seconds, since larger time steps gave significantly less realistic results.

Moreover, the bottom friction coefficient was defined. In this case the Manning coefficient was used, which was standard input for 3Di models. No information on the bottom friction could be provided for this study site by experts. The coefficient was specified based on a number of model results with varying Manning values between 0.03 and 0.04 $s/m^{1/3}$. This assessment was also based on the simulated water levels and the value which gave the most realistic results was 0.035 $s/m^{1/3}$. The interval between 0.03 and 0.04 $s/m^{1/3}$ was chosen, based on standard Manning coefficient for natural streams (clean and straight: 0.030, major rivers: 0.035 and sluggish with deep pools 0.040 (Engineering ToolBox, 2004)).

The friction velocity compares the flow velocity in a stream to a velocity that relates shear between layers of flow. A general rule of thumb is that the friction velocity is 10% of the mean flow velocity (Holmes, 2015). The minimum friction velocity was based on the smallest simulated velocities in big lakes, which were approximately 0.05 m/s. Therefore, the minimum friction velocity was specified at 0.005 m/s.

Table C.1: Model settings

Setting	Value	Unit	Comment
Grid space	40	m	Size of smallest grid cell in quadtree, $k = 1$.
k_{max}	3	-	Maximum multitude of smallest grid size in quadtree. Grid size increases according to $2^{k-1} \times$ grid space.
Friction coefficient	0.035	$s/m^{1/3}$	Constant Manning friction coefficient
Simulation time step	20	s	-
Output time step	900	s	Timestep written in output file.
Use 2D flow	Yes	-	-
Use advection 2D	Yes	-	-
Flooding threshold	1×10^{-6}	m	Water depth threshold for flow between 2D cells.
Min. friction velocity	0.005	m/s	-

Appendix D

Highlighted: Event 8 Bft W (A)

Event 8 Bft W (A) is highlighted, as it is one of the most intense events. This event is accompanied with high wind speeds directed from the west over a long period (Figure B.24). The analysis of the results of this event gives insightful information on the dependencies of the wind drag coefficient. This event took place in 2015, starting at the 29th of March at 12:00.

Calibration

The calibration results are provided for every step along the calibration process, matching the steps defined in the methodology.

Ⓘ Data collection

In the first step, the data of the measurements, water levels, discharges and wind, were collected. The wind velocities are provided in Figure D.1 and the discharges of the inlets and outlets in Figure D.2. Discharges going out the bosom into external water bodies are displayed as negative discharges. During this event only water was discharged from the bosom to external water and not the other way around. Logically, outlet Dokkumer Nieuwe Zijlen and Zoutkamp (see Figure 4.2 for their locations) were used to relieve the northeastern side of the bosom of high water levels due to the wind set-up. Outlet Hoogkamp was also deployed to relieve the southwestern part of the bosom of some water. During the wind event, approximately 22 mm precipitation was observed in Fryslân over the 2,5 days (average of measurement stations Stavoren and Leeuwarden). This precipitation could have contributed to the decision to deploy outlet Hoogkamp. Besides these discharges to external water, the polder pump discharges have been computed automatically. The constant discharge of the 694 polder pumps amounted to $0.13 m^3/s$.

Additionally, the weights for the intermediate assessment between the two stages of the calibration were computed. This was done based on the absolute value of the observed set-up. The weights are provided in Table D.1. Most locations had higher weights due to the intensity of this wind event. The locations with a weight of 3 were all located at outer edges of the bosom (see Figure 4.3), where wind set up is naturally more perceptible.
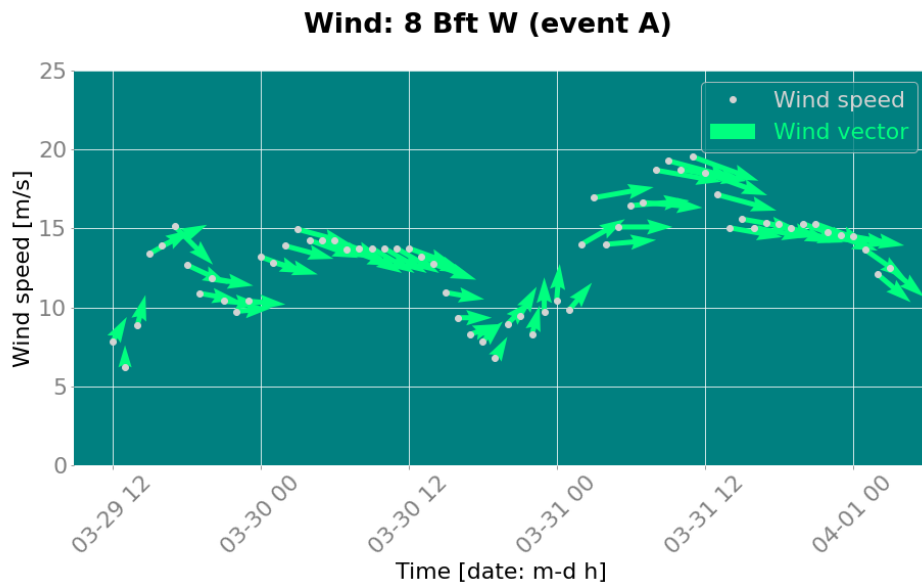
Figure D.1: Wind velocity time series: 8 Bft W (event A)

Table D.1: Applied weights event 8 Bft W (A)

| Location | Weight | | |
	3	2	1
	Stavoren	Scharsterbrug	Woudsend
	Workum	Nesserzijl	Sneek
	Dokkumer NZ	Lemmer	
	Zoutkamp	Wijns	
	Harlingen	Burgum	
	Makkum	Eibersburen	
		Dokkum	
		Arum	

II ▷ Model initialisation

The first simulation initialised the model by gaining a saved state of the water levels at the end of the initialisation period. During this period, no strong winds had taken place. The wind drag coefficient was not varied, it was taken at a constant value of 1.3×10^{-3}. This simulation started at the 28th of March, 2015 at 12:00 and lasted 24 hours.

III ▷ Calibration stage 1

After the model initialisation, calibration stage 1 took place. Seven simulations were run, varying the wind drag coefficient with steps of 0.2×10^{-3} between 0.8×10^{-3} and $2 \times 10^{-3}[-]$.

IV ▷ Interim assessment

Every simulation had a particular wind drag coefficient and per simulation the KGE values are retrieved locally as well as an domain-wide averaged value. The wind drag coefficient and corresponding KGE values per location are provided in Table D.2. The KGE and its sub-components for the domain-wide averaged results are provided in Table D.3.
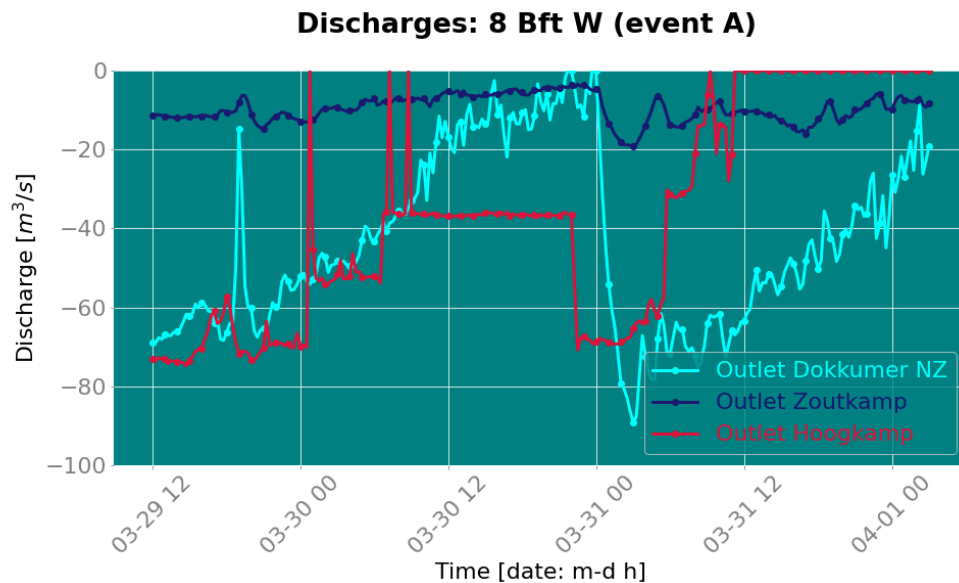
Figure D.2: Discharge time series: 8 Bft W (event A)

The weights were included in the computation of these (domain-wide) averages. Four locations were discarded in this process, namely Elahuizen, Terherne, Leeuwarden and Tacozijl. Their maximum KGE value during stage 1 were the lowest, with respectively: -0.87, -0.14, 0.28 and 0.39. This revealed that the model performed poorly for all wind drag coefficient values at these locations. Lesser performing locations can be caused by a number of reasons, and it was hard to pinpoint the exact cause. These reasons were further discussed in Section 6.1. Next, the automatic calibration script recognised that drag coefficients values 1.4×10^{-3} and $1.6 \times 10^{-3}[-]$ gave the most realistic results. This was input for calibration stage 2.

Ⅴ   Interval refinement

The search interval was redefined between 1.35×10^{-3} and $1.65 \times 10^{-3}[-]$ with steps of 0.05×10^{-3}.

Ⅵ   Calibration stage 2

After the interval refinement, calibration stage 2 took place. Five simulations were run.

Ⅶ   Final assessment

The wind drag coefficient and corresponding KGE values per location are given in Table D.4. The KGE and sub-components of KGE for the domain-wide averaged results are given in Table D.5. From Table D.5 it can be derived that a wind drag coefficient of $1.5 \times 10^{-3}[-]$ is the optimal domain-wide value, resulting in a fairly accurate representation of the observed water levels with a KGE of 0.67.

Table D.2: KGE values per location per wind drag coefficient during calibration stage 1, with in green the highest KGE value

	Wind drag coefficient C_D ($\times 10^{-3}$)						
Location	**0.8**	**1.0**	**1.2**	**1.4**	**1.6**	**1.8**	**2.0**
Makkum	0.45	0.75	0.93	0.89	0.78	0.69	0.61
Workum	0.01	0.44	0.72	0.91	0.93	0.82	0.73
Dokkumer Nieuwe Zijlen	0.81	0.87	0.92	0.92	0.87	0.80	0.72
Stavoren	-0.34	-0.04	0.28	0.55	0.76	0.88	0.84
Eibersburen	0.17	0.72	0.88	0.69	0.50	0.29	0.02
Arum	0.87	0.78	0.68	0.59	0.53	0.47	0.42
Harlingen	0.75	0.87	0.81	0.72	0.63	0.56	0.50
Burgum	-0.72	-0.24	0.21	0.55	0.77	0.84	0.76
Nesserzijl	0.26	0.50	0.67	0.78	0.81	0.78	0.72
Lemmer	-0.04	0.25	0.45	0.58	0.66	0.71	0.72
Dokkum	0.64	0.69	0.71	0.71	0.69	0.65	0.61
Woudsend	-0.96	-0.19	0.28	0.52	0.62	0.62	0.59
Sneek	0.46	0.58	0.58	0.54	0.49	0.45	0.41
Zoutkamp	-0.33	0.12	0.43	0.56	0.50	0.32	0.07
Scharsterbrug	-1.28	-0.62	-0.18	0.10	0.30	0.43	0.50
Wijns	0.29	0.35	0.39	0.41	0.43	0.43	0.43

Table D.3: Mean domain-wide KGE values with its sub-components during calibration stage 1, with in green the highest KGE value

	Wind drag coefficient C_D ($\times 10^{-3}$)						
Location	**0.8**	**1.0**	**1.2**	**1.4**	**1.6**	**1.8**	**2.0**
KGE	0.11	0.40	0.58	0.65	0.66	0.62	0.55
Correlation coefficient, R	0.74	0.79	0.81	0.82	0.83	0.83	0.83
Variability ratio, α	1.77	1.47	1.24	1.07	0.94	0.84	0.76
Bias ratio, β	1.02	1.02	1.02	1.03	1.05	1.07	1.11

Table D.4: KGE values per location per wind drag coefficient during calibration stage 2, with in green the highest KGE value

Location	: Wind drag coefficient C_D ($\times 10^{-3}$)						
	1.35	1.4	1.45	1.50	1.55	1.60	1.65
Workum	0.87	0.91	0.95	0.97	0.96	0.93	0.90
Dokkumer Nieuwe Zijlen	0.93	0.92	0.91	0.90	0.89	0.87	0.85
Makkum	0.91	0.89	0.86	0.83	0.80	0.78	0.75
Nesserzijl	0.76	0.78	0.80	0.81	0.81	0.81	0.81
Burgum	0.48	0.55	0.62	0.68	0.72	0.77	0.81
Stavoren	0.49	0.55	0.61	0.67	0.72	0.76	0.80
Eibersburen	0.74	0.69	0.64	0.60	0.55	0.50	0.45
Harlingen	0.74	0.72	0.69	0.67	0.65	0.63	0.61
Dokkum	0.71	0.71	0.70	0.70	0.69	0.69	0.68
Lemmer	0.55	0.58	0.60	0.62	0.64	0.66	0.67
Woudsend	0.48	0.52	0.56	0.59	0.61	0.62	0.63
Arum	0.61	0.59	0.58	0.56	0.54	0.53	0.51
Zoutkamp	0.54	0.56	0.56	0.55	0.53	0.50	0.46
Sneek	0.55	0.54	0.53	0.52	0.51	0.49	0.48
Wijns	0.41	0.41	0.42	0.42	0.42	0.43	0.43
Scharsterbrug	0.04	0.10	0.16	0.21	0.26	0.30	0.34

Table D.5: Mean domain-wide KGE values with its sub-components during calibration stage 2, with in green the highest KGE value

Location	: Wind drag coefficient C_D ($\times 10^{-3}$)						
	1.35	1.4	1.45	1.50	1.55	1.60	1.65
KGE	0.64	0.65	0.66	0.67	0.67	0.66	0.66
Correlation coefficient, R	0.82	0.82	0.83	0.83	0.83	0.83	0.83
Variability ratio, α	1.11	1.07	1.04	1.01	0.97	0.94	0.92
Bias ratio, β	1.03	1.03	1.04	1.04	1.05	1.05	1.06

Validation

Before analysing these results, validation was required to secure the reliability of the results. An independent wind event was used. This event was categorized based on the same wind direction and wind speed. Wind event 8 Bft W (C) was used as validation event, see Figure B.26 for the wind time series of this event. This event was categorized based on the same wind direction and wind speed as the calibration event. However, the event length deviated from the calibration event. This event was 1,5 day shorter than the calibration event. Additionally, small deviations in the wind direction and/ or wind speed within the classification interval were observed. The peak wind velocities of the validation event were directed more towards the north. The optimal domain-wide value of $1.5 \times 10^{-3}[-]$ (derived during calibration) was specified as wind drag coefficient during this validation run. This simulation resulted in a averaged domain-wide KGE value of 0.60, which is, similar to the calibration, a fairly accurate result.

In-depth analysis

Based on this one wind event, no information on wind-directional and/ or wind speed dependencies could be retrieved. Nevertheless, with this individual event it was possible to provide an indication of the spatial dependency of the wind drag coefficient.

Spatial dependency

To provide insightful information of the model results, on top of the KGE values, the water level time series were examined. Figure D.4 provides the water levels at Workum at its local optimal C_D of $1.5 \times 10^{-3}[-]$, which is also the domain-wide optimal drag coefficient. Figure D.5 presents the water levels at Makkum at its local optimal C_D of $1.2 \times 10^{-3}[-]$, compared to the water levels at the domain-wide optimal C_D of $1.5 \times 10^{-3}[-]$. The simulation with the domain-wide drag coefficient resulted in an overestimation of the wind set-down. The momentum transmission of the wind was therefore overestimated at this location at this domain-wide optimal wind drag coefficient. So, this provides insight into the spatial variability of the drag coefficient.

Moreover, Table D.2 provides a overview and it seems that the spatial variation is an evident phenomenon. Local optimums vary over the entire initial search interval. The water levels at location Arum seemed to be very sensitive to overestimation of the wind momentum transmission, as its local optimum is a C_D of 0.8×10^{-3}. The time series with its local optimal drag coefficient is provided in Figure D.3. This measurement station is situated in a small canal, surrounded by small canals without neighbouring lakes (Figure 4.3). Also, the geometry of the canals are not in line with the western wind direction, see Figure D.6. Wind shielding might be a dominant factor here, explaining why only a small amount of wind momentum was transmitted to the water surface.
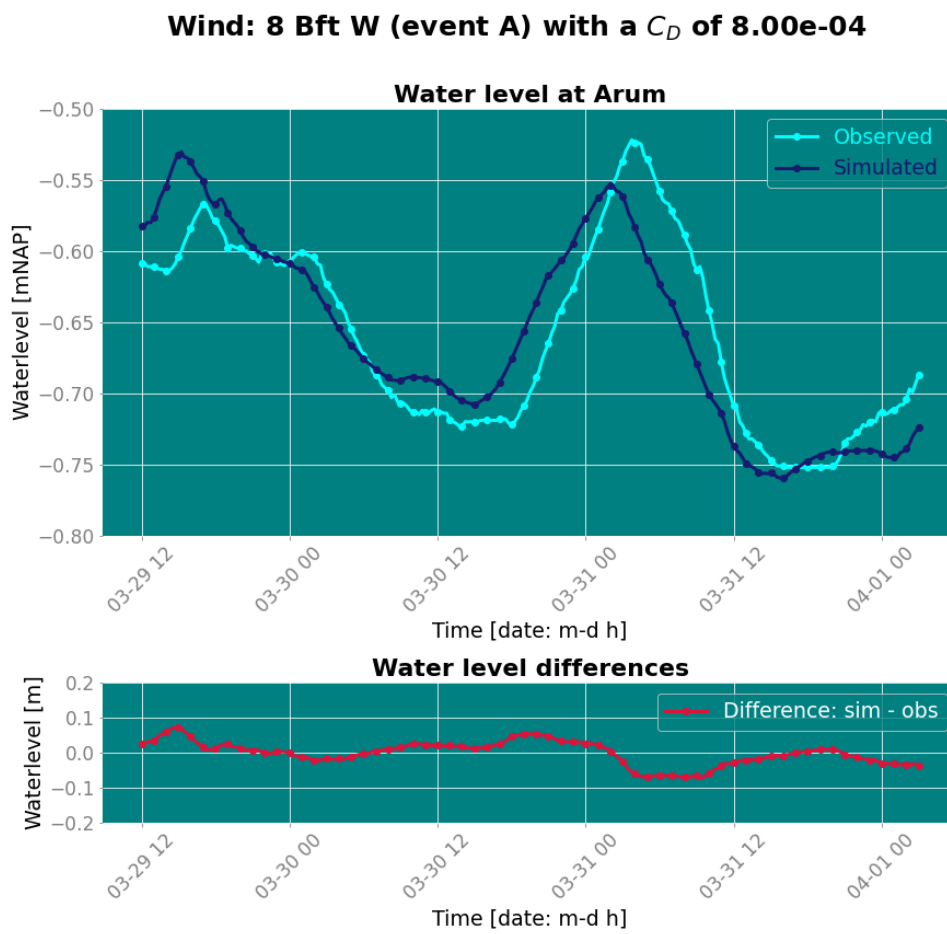
Figure D.3: Water level simulation at location Arum with a C_D of $0.8 \times 10^{-3}[-]$ and a KGE of 0.87
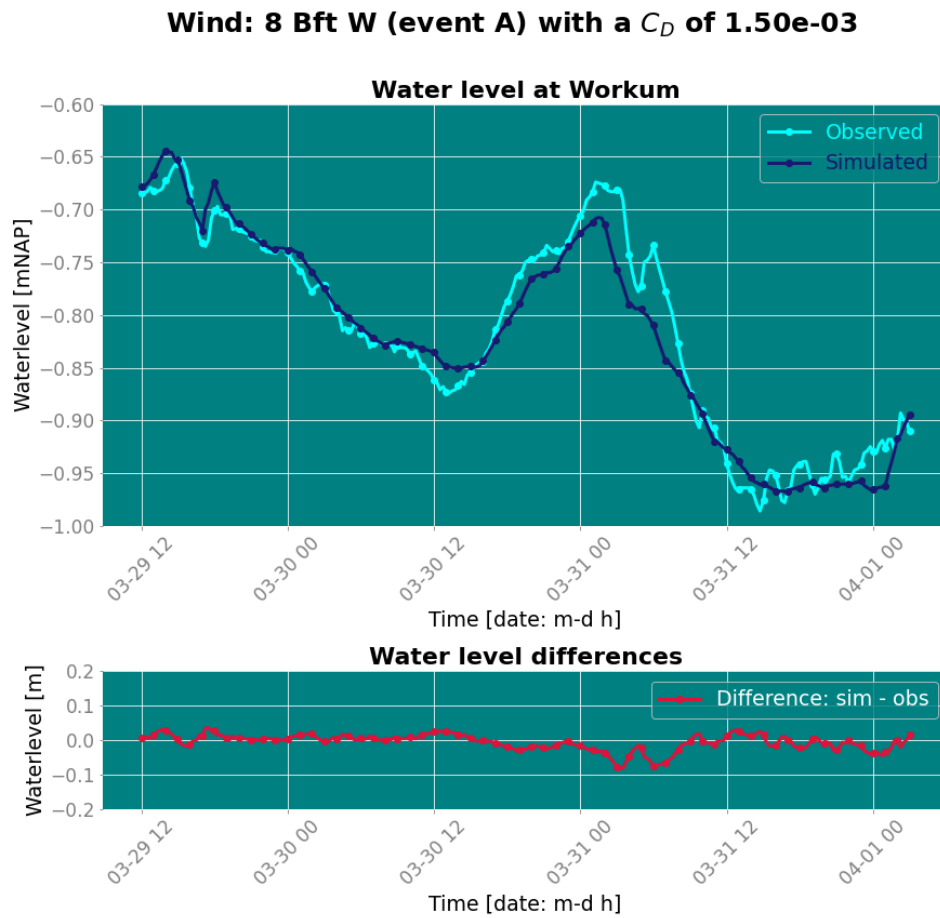
Figure D.4: Water level simulation at location Workum with a C_D of $1.5 \times 10^{-3}[-]$ and a KGE of 0.97

Wind: 8 Bft W (event A) with a C_D of 1.50e-03 and 1.20e-03
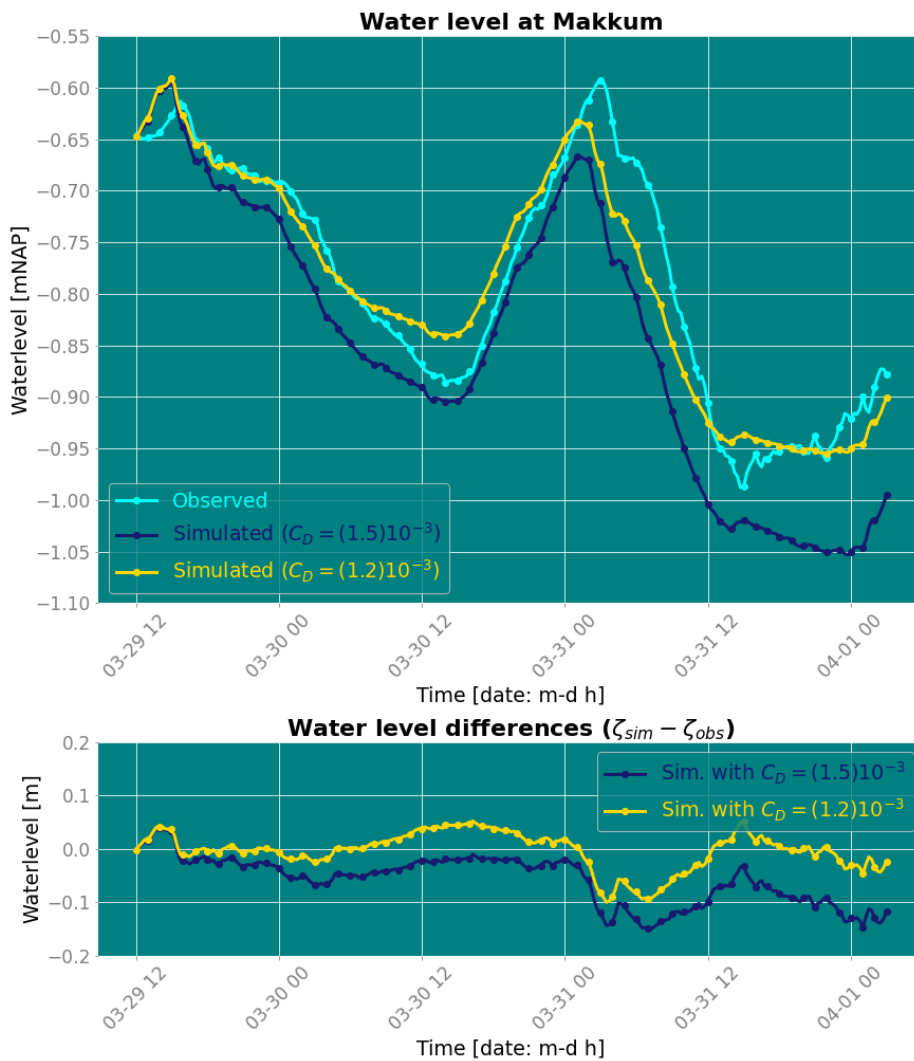
Figure D.5: Water level simulations at location Makkum during wind event 8 Bft W (A) with a local optimal C_D of $1.2 \times 10^{-3}[-]$ (KGE$= 0.93$), compared to water levels at Makkum at the domain-wide optimal C_D of $1.5 \times 10^{-3}[-]$ (KGE$= 0.83$)

Figure D.6: Geometry around measurement station Arum

To compare this to another location, measurement station Burgum was examined. Station Burgum is situated more to the northeastern part of the bosom (Figure 4.3). So, instead of wind set-down, wind set-up was observed. Figure D.7 presents the water levels at Burgum at its optimal C_D of $1.8 \times 10^{-3}[-]$. A small vibration is observed, which was probably caused by a small insecurity of the measurement instrument. However, this had only a small effect on the objective function value. The initialisation of this event resulted in a water level difference at the beginning of this simulation. This cannot always be prevented, as the initialisation is not calibrated. The wind set-up is small here, but the trend is captured quite good. The KGE value for this simulation was 0.84. As an aside, comparing the water levels with the NSE objective function would lead to a significantly lower value. This would be unjustified, as in practice with the right initialisation this model could accurately simulate the wind set-up at Burgum.

In contrary to at Arum, at Burgum, the accuracy of simulations of this location benefited from a higher wind drag coefficient, of 1.8×10^{-3}. This measurement location is situated in a wider canal in-line with the western wind direction. So, all locations differ in water body dimension and/ or in surrounding objects causing wind shielding, leading to a large spatial variation in optimal wind drag coefficient values. In this way the different locations can all be analysed individually based on their wind drag dependencies.

Figure D.7: Water level simulation at location Burgum with a C_D of $1.8 \times 10^{-3}[-]$ and a KGE of 0.84

Appendix E

Additional validation

In this appendix the choice for including three additional validation events is elaborated. This is shortly mentioned in the methodology (Chapter 4. Furthermore, a short introduction to cross-validation is provided. In follow-up researches this method of cross-validation can be applied.

Additional validation events

Three wind events were discarded for validation purposes, cause these events were modelled poorly despite the wind drag coefficient value. Therefore, these events could not be relied on for information on the optimal wind drag coefficient value of that wind class. Additional wind events belonging to these classes were available, and denoted with a letter C. It was found that these wind events could be modelled with sufficient accuracy.

Underlying reasons for the inaccurate model results of the three original events were difficult to specify. Wind event 8 Bft W is highlighted to illustrate this. Firstly, wind event B was used for validation (Figure B.25). This event is 1,5 day shorter than the calibration event, however the peak wind velocities are similar. The optimal domain wide C_D of $1.5 \times 10^{-3}[-]$ resulted in a domain-wide KGE value of 0.42. Further investigation revealed that this wind event was modelled poorly despite the wind drag coefficient value. A maximum domain-wide KGE value of 0.47 was achieved at a C_D of $1.75 \times 10^{-3}[-]$.

Since this wind event was modelled poorly despite the drag coefficient value, this event was not used for validation. The model initialisation displayed great inaccuracies at multiple locations in the northeastern part of the bosom (Dokkum, Dokkumer Nieuwe Zijlen and Zoutkamp). The observed water levels were up to 25 cm lower than the simulated water levels at the beginning of the event. This could indicate that the discharges of pumping stations Dokkumer Nieuwe Zijlen and/ or Zoutkamp were not accurately represented by the measurement data. The water board could have lowered the water levels in the northeastern part of the bosom, in the prospect of an high wind speed event from western direction, as significant wind set-up could be expected. Also, the initialisation was not calibrated and can therefore have led to inaccuracies.

Table E.1: The bundled results of calibration, validation and the extra validation: the optimal domain-wide drag coefficient with the KGE values. With in green the optimal results

Wind event	Calibration		Validation		Extra validation	
	$C_D \times 10^{-3}$	KGE	$C_D \times 10^{-3}$	KGE	$C_D \times 10^{-3}$	KGE
6 Bft E	1.60	0.56	1.60	0.39	1.00	0.52
6 Bft N	1.25	0.48	1.25	0.65	1.00	0.72
6 Bft NW	0.95	0.64	0.95	0.54	1.25	0.50
6 Bft S	1.85	0.69	1.85	0.73	1.50	0.68
6 Bft SW	1.25	0.82	1.25	0.71	1.00	0.64
					1.50	0.71
6 Bft W	1.55	0.53	1.55	0.54	1.25	0.55
7 Bft NW	1.00	0.74	1.00	0.62	1.25	0.61
7 Bft SW	1.10	0.69	1.10	0.64	1.60	0.73
7 Bft W	1.10	0.61	1.10	0.57	1.40	0.58
8 Bft NW	1.30	0.52	1.30	0.36	1.00	0.29
					1.60	0.36
8 Bft SW	1.45	0.72	-	-	-	-
8 Bft W	1.50	0.67	1.50	0.60	1.25	0.57
					1.75	0.57

Cross-validation

Table E.1 provides an overview of the calibration and validation results, similar to the manner in which this is presented in Section 5.2. However, an additional column is provided named 'Extra validation'. Extra simulations have been performed to find out if the model accuracy during validation could be significantly improved with another wind drag coefficient. This would indicate that the calibrated optimal drag coefficient was not optimal for the validation event.

It was found that the model accuracy of some events benefit from another wind drag coefficient value relative to that of the calibration event. Event 6 Bft E is an good example of this, where the validated optimal C_D differs with 0.6×10^{-3} from the calibrated optimal C_D. Moreover, the model accuracy is rated with a relatively low KGE for both the calibration as the validation. The optimal wind drag coefficient for this event remains quite uncertain for these reasons. The other wind events, that improve with a different wind drag coefficient, show small improvements of their KGE value. As explained in Section 5.2, it cannot be expected that the optimal wind drag coefficient during validation is exactly identical to that of the calibration event for every case.

In follow-up researches this method of cross-validation might be applied. The average value of the optimal wind drag coefficient resulting from this cross-validation can be used per wind class. The advantages of this method are: it results in a better estimate of the model accuracy and it is more efficient as the data of every wind event is used for both calibrating and validating.